DISSERTATION

submitted to the

Combined Faculties for the Natural Sciences and for Mathematics

of the Ruperto-Carola University of Heidelberg, Germany

for the degree of

Doctor of Natural Sciences

Tumor-microenvironment interactions studied by zonal transcriptional profiling of squamous cell lung carcinoma

presented by

Hui Wu

born in Fu'an, P. R. China

Heidelberg 2010

Accepted by the Combined Faculties for the Natural Sciences and for Mathematics of the Ruperto-Carola University of Heidelberg, Germany: September 14th, 2010

Referees:

Priv.-Doz. Dr. Karsten Rippe

Prof. Dr. Peter Lichter

Day of the oral examination: October 26th, 2010

The investigations of this dissertation were performed from April 2006 to August 2010 under the supervision of Prof. Dr. Peter Lichter, Prof. Dr. Stefan Joos, Dr. Armin Pscherer and PD. Dr. Michael A. Rogers in the Division of Molecular Genetics at the German Cancer Research Center (DKFZ), Heidelberg, Germany.

Publication

Wu H, Haag D, Muley T, Warth A, Zapatka M, Toedt G, Roger MA, Pscherer A, Joos S, Müller-Decker K, Hahn M, Rieke RJ, Miester M, Schnabel P, Hoffmann H, Lichter P. Tumor-microenvironment interactions studied by zonal transcriptional profiling of squamous cell lung carcinoma

In preparation…

Declarations

I hereby declare that I have written the submitted dissertation 'Tumor-microenvironment interactions studied by zonal transcriptional profiling of squamous cell lung carcinoma' myself and in this process have used no other sources or materials than those expressly indicated. I hereby declare that I have not applied to be examined at any other institution, nor have I used the dissertation in this or any other form at any other institution as an examination paper, nor submitted it to any other faculty as a dissertation.

_____ _____

(Place, Date) Hui Wu

To A.W.
& my family

Table of Contents

Abbreviations

AB	Antibody
Bp	Base pairs
BSA	Bovine serum albumine
cDNA	Complementary DNA
DAPI	4',6-Diamidino-2'-phenyllindol-dihydrochloride
DIG	Digoxygenine
DNA	Desoxy-ribonucleic acid
dNTP	Desoxy-nucleotide triphosphate
ds	Double stranded
HRP	Horse radish peroxidase
Ig	Immunoglobulin
Kb	Kilo base pairs
mRNA	Messenger RNA
NFκB	Nuclear factor kappa B
NSCLC	Non small cell lung cancer
SCLC	Small cell lung cancer
TLDA	TaqMan Low Density Array
EMT	Epithelial to mesenchymal transition
FISH	Fluorescence in situ hybridization
LCM	Laser capture microdissection
LMPC	Laser microdissection and pressure catapulting
PCR	Polymerase chain reaction
qRT-PCR	Quantitative real-time polymerase chain reaction
rpm	Rounds per minute
RT	Room temperature
TBE	Tris-borate buffer

TSG	Tumor suppressor gene
TNFα	Tumor necrosis factor alpha
H&E	Hematoxylin and eosin
UV	Ultraviolet
V	Variable
V(H)	Variable heavy chain
v/v	Volume per volume
w/v	Weight per volume

Summary

Invasiveness is a critical step in lung tumor progression, and the interaction between tumor cells with their surroundings may play an important role in tumor invasion and metastasis. To better understand the molecular mechanisms of tumor invasion and the interaction of the tumor with the surrounding cellular environment, matched-pair transcriptional profile analyses of inner tumor-, tumor invasion front-, adjacent lung- and normal lung cells from 18 patients with squamous cell lung carcinoma were undertaken to identify novel molecular markers by parallel gene expression profiling using oligonucleotide microarrays and microRNA TaqMan Low Density Arrays. Through "punch aided laser capture microdissection", T7 based RNA amplification and oligonucleotide microarray, 13 genes were identified as being differentially expressed between the tumor invasion front and the inner tumor. In addition to the identification of significant genes in the tumor invasion front, Ingenuity pathway analysis ranked eicosanoid pathway signalling high in tumor cells, with prostaglandin E synthase and F synthase being highly expressed in the tumor cells and the receptors of prostaglandin E being expressed only in lung tissue adjacent to the tumor. CCL19, APLNR and GIMAP7 as well as several proteins associated with prostaglandin formation and signalling, were validated by immunohistochemistry. Prostaglandins E and F may, therefore, be crucial messenger molecules in the interaction of the tumor with its surroundings. In addition to the mRNA gene candidates, several microRNAs were identified as being important in lung cancer. Hsa-mir-196a was indentified as being expressed less in the tumor invasion front than in the inner tumor; hsa-mir-650 was a unique adjacent lung specific microRNA; 66 microRNAs were differentially expressed between tumor and normal lung. The expression patterns of hsa-mir-196a, hsa-mir-650 and hsa-mir-224 were verified by microRNA FISH. Hsa-mir-196a and hsa-mir-650 may, therefore, be crucial microRNAs for tumor-microenvironment interactions.

Zusammenfassung

Invasivität stellt einen wesentlichen Aspekt des Krankheitsverlaufs von Lungenkrebs dar. Wechselwirkungen zwischen Krebszellen und umgebendem Gewebe spielen eine wichtige Rolle bei der invasiven Ausbreitung und Metastasierung von Tumorerkrankungen. Das Erstellen von Genexpressionsprofilen von Lungentumoren und angrenzendem Gewebe, könnte helfen, die molekularen Mechanismen der Invasion von Tumorzellen und deren Interaktionen mit den angrenzenden Zellen zu verstehen. In der vorliegenden Studie wurden Analysen von (1) innerem Tumorgewebe, (2) Tumorinvasionsfront, (3) angrenzendem Lungengewebe sowie (4) normalem Lungengewebe von insgesamt 18 Patienten mit Plattenzellkarzinomen der Lunge durchgeführt. Hierbei wurden im Wesentlichen die Unterschiede in der Genexpression der verschiedenen Areale pro Patient ermittelt. Ziel war es, mittels Oligonukleotidmicroarray-basierter paralleler Transkriptmessung und dem TaqMan Low Density Array-Format zur semiquantitativen Bestimmung von MicroRNAs, neue molekulare Marker zu identifizieren. Besonderes Interesse galt hierbei dem invasiven Prozess von Krebszellen, sowie der Reaktion des angerenzenden Gewebes. Unter Verwendung von lasergestützter Mikrodissection, sowie einem Protokoll zur linearen Amplifikation von Gentranskripten (T7-basierend) und Oligonukleotidmicroarrays, wurden 13 Gene identifiziert, die eine differentielle Expression zwischen invasiver Tumorfront und innerem Tumorbereich zeigen. Eine zusätzliche Auswertung zu zellulären Signalwegen durch die Ingenuity® Software, ergab eine Überrepräsentation der Eikosanoid-Signalkaskade. Dies beinhaltete eine erhöhte Genexpression von Prostaglandin E Synthase und Prostaglandin F Synthase in Tumorarealen, sowie die erhöhte Genexpression von korrespondierenden Rezeptoren in ausschließlich tumorbenachbartem Lungengewebe. Die Proteine CCL19, APLNR und GIMAP7, nebst weiteren Proteinen zur Synthese und Signalverarbeitung von

Prostaglandinen, wurden durch immunhistochemische Methoden validiert. Demnach könnten Prostaglandin E und F entscheidende Signalmoleküle für die Wechselwirkungen zwischen Krebszellen und umliegendem Gewebe sein. Neben diesen Kandidatengenen wurden in dieser Studie auch verschiedene MicroRNAs im Zusammenhang mit Lungenkrebs identifiziert. Hsa-mir-196a war hierbei in invasiver Tumorfront vergleichsweise geringer exprimiert als in inneren Tumorbereichen. Des Weiteren war Hsa-mir-650 als einzige MicroRNA spezifisch für Lungengewebe, welches dem Tumor angrenzt. Zudem zeigten insgesamt 66 MicroRNAs eine differentielle Expression zwischen Tumor und normaler Lunge. Die Expressionsmuster von Hsa-mir-196a, Hsa-mir-650 und Hsa-mir-224 wurden durch MicroRNA-FISH verifiziert. Folglich könnten Hsa-mir196a und Hsa-mir650 eine entscheidende Rolle bei der Interaktion zwischen Tumor und Mikroenvironment spielen.

1 Introduction

1.1 Cancer

Cancer accounted for about 23% of all deaths, ranking second only to heart disease in the world (Jemal et al., 2006). Almost all cancers are caused by genetic alteration in somatic cells, which generally demonstrate uncontrolled cell division, invasion and metastasis. Cancer has been, and is, an increasingly huge global challenge to human health (Vogelstein and Kinzler, 2002).

Incidence of cancer varies dramatically between geographic regions (Figure 1); as some cancers are more common in the developed world (for example, breast and prostate); others occur more frequently in people, who live in developing countries (for example, cervical and stomach). Cancers of the lung have high incidence in both developed countries and areas undergoing economic development such as China (Parkin et al., 2002). Although these regional differences might be explained by genetic and epigenetic differences among populations, variations in lifestyles, environmental exposures and medical practices such as screening are also important to determine cancer risk (Ferlay et al., 2001) .

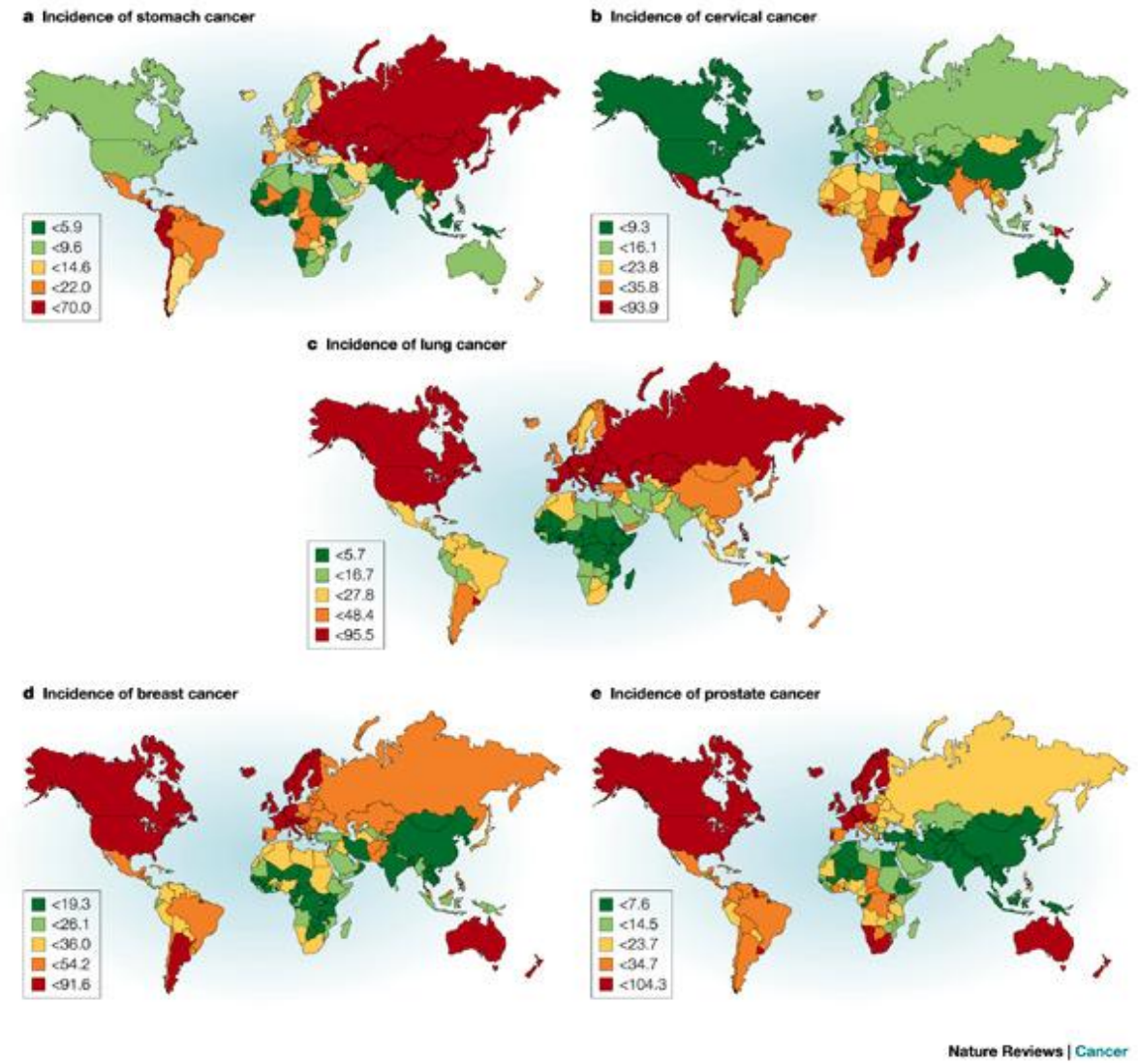

Figure 1. Global variations in cancer incidence for specific cancers. There is substantial global variability in cancer incidence (measured as age-standardized rates) occurring in people living in developing countries (a–c) and those in developed nations (d,e). a. The incidence of stomach cancer for men of all ages is highest (orange and red) in developing countries such as Asia and South America, and lowest (light and dark green) in North America, parts of Africa, India and Australia. b. The incidence of cervical cancer is also high in developing regions of the world including Latin America, Africa and India, and is low (green) in North America, Europe and Australia. c. Lung cancer incidence is currently high in developed countries as well as those countries undergoing economic transition, such as China (d,e). Cancers with the highest incidence in developed countries include breast and prostate cancer, which occur most commonly in North America, Europe and Australia, and with much lower incidence in Asia and Africa. These differences highlight the role that environmental and lifestyle factors such as diet have in cancer development. (Ferlay et al., 2001).

1.2. Lung cancer

Lung cancer is a malignant neoplasm of uncontrolled cell growth in lung tissue and bronchus. This uncontrolled cell growth can lead to tumor cell invasion into normal lung tissue and metastasis to other organs. Lung cancer is the most common cause of cancer-related death in men (31%) and the second most common in women (25%) (Jemal et al., 2002). Lung cancer is classified into two main types, small cell lung carcinoma and non-small cell lung carcinoma. While the small cell type is sensitive to chemotherapy and radiation, the non-small cell type is mainly treated by surgical resection (Vaporciyan et al., 2000). 50% of the NSCLCs and 80% of the SCLCs are metastatic at diagnosis,see Table 1.

Table 1. Frequency of histological types of lung cancer (Travis et al., 1995)

Histological type	Frequency (%)
Non-small cell lung carcinoma	80.4
Small cell lung carcinoma	16.8
Cardinoid	0.8
Sarcoma	0.1
Unspecified lung cancer	1.9

1.2.1 Small cell lung carcinoma

The SCLCs, also named oat cell carcinoma, are mainly centrally located in the lung, presenting in the main stem or lobular bronchii. Arising in the peribronchial tissues, they infiltrate the bronchial sub-mucosa. Pathological studies show that they arise from basal neuroendocrine or Kulchitsky cells, which are rarely found in the adult lung, but common

in the fetal lung (Weitberg et al., 2002). Since the 19th century, SCLC has been known as "*Bergkrankheit*", a disease of miners which was discovered originally in the uranium and pitchblende mines in the area of Bohemia and Saxony (Meyer et al., 1980). Initially, SCLC was not recognized as a carcinoma, but rather a sarcoma, until Barnard identified this tumor entity in 1926 (Barnard, 1926). In 1973, the United State Working Party for the Therapy of Lung Cancer classified the SCLC as two main sub-types: oat cell carcinoma and intermediate carcinoma (Matthews, 1973). The morphological separation of these two subtypes was difficult., However, the WHO adopted this classification in 1981 and defined oat cell carcinoma as "a malignant tumor composed of uniform small cells, generally larger than lymphocytes, having dense round or oval nuclei, diffuse nuclei, and very sparse cytoplasm" and SCLC of intermediate type as "a malignant tumor composed of small cells, with nuclear characteristics similar to the oat cell, but with more abundant cytoplasm. The cells may be polygonal or fusiform and are less regular in appearance than those of the oat cell carcinoma" (Hess et al., 1981). As other types of lung cancer, SCLC is also of male predominance, but in recent years, female SCLC has been increasing. In some areas, the number of women with SCLC even exceeds that of men (Curnen, 1983). Only 16.8% of lung cancers are small cell lung carcinoma. It is clinically aggressive and associated with early extra-thoracic metastases. At the stage of initial diagnosis, 66% of the SCLC patients already show metastases in one or more sites, for example in bone, liver, central nervous system, lymph nodes, subcutaneous tissue, and pleura (Elliott et al., 1987). Small cell lung carcinoma cells grow fast and typically contain dense neurosecretory granules, secreting various mitogenic neuropeptides, which could be used as biomarkers for this tumor type (Driscoll et al., 2003). The etiology of SCLC is strongly associated to cigarette smoking (Barbone et al., 1997).

1.2.2 Non-small cell lung carcinoma

Non-small cell lung cancer is the most common type of lung cancer, comprising about 80% of all cases. . There are three main subtype of this carcinoma: squamous cell lung carcinoma, adenocarcinoma, and carcinoid (Table 2).

Table 2 Sub-types of non-small cell lung cancer in smokers and never-smokers (Bryant and Cerfolio, 2007)

Histological subtypes		Frequency of non-small cell lung cancers (%)	
		Smokers	Never-smokers
Squamous cell lung carcinoma		42	33
Adenocarcinoma	Adenocarcinoma (not otherwise specified)	39	35
	Bronchioloalveolar carcinoma	4	10
Carcinoid		7	16
Other		8	6

Adenocarcinoma accounts for about 40% of the non small cell lung cancers (Travis, 2002). In Western and developed countries, adenocarcinoma are normally found in peripheral lung parenchyma and associate with peripheral scar or honeycombing (Terasaki et al., 2003), whereas in India, 50% of the adenocarcinomas are located more centrally (Shields et al., 1970). The majority of adenocarcinomas are between 2.0 and 5.0 cm in diameter with mixed cell types, while tumors smaller than 1.5 cm are usually of one cell type. Adenocarcinoma cells grow slower than squamous cell lung carcinoma, and usually show a vascular invasion phenotype (Miettinen et al., 2003). Most cases of adenocarcinoma are related to smoking; however, among the never smoking population, adenocarcinoma is the most common type in lung cancer (Subramanian et al., 2007). As a common cause of lung cancer, occupation is also a key risk factor in adenocarcinoma development. A study in Missouri, USA, shows that carpenters, furniture makers, plumbers, printers, and welders are, a priori, high-risk occupations for adenocarcinoma (Zahm et al., 1989). The WHO classification divides adenocarcinomas into four subtypes:

acinar adenocarcinoma, papillary adenocarcinoma, bronchoalveolar carcinoma, and solid adenocarcinoma with mucin production (World Health Organization, 1982).

Accounting for 25% of all lung cancers (Travis et al., 2002), squamous cell lung carcinomas arise in sub-segmental or larger bronchi, where the tumor shows both endobronchial and invasive growth into the peribronchial soft tissue, lung parenchyma, and nearby lymph nodes, often compressing the pulmonary arteries and veins. Mucin-containing cells, which are normally found in adenocinoma, are frequently seen in squamous cell carcinoma of lung, especially in peripheral tumors. More than 50% of the peripheral squamous cell lung carcinomas are actually adeno-squamous carcinomas (Stephen et al., 1994). Most squamous cell lung carcinomas are between 3.0 and 5.0 cm in size when they are detected. In the center of the tumor, necrosis and hollow cavities generated by the necroses are commonly found. Well-differentiated squamous cell lung cancers are usually more slowly growing than other types of cancers (Vaporciyan et al., 2000).

1.3 Molecular genetics of cancer

Cancer is caused by alterations of oncogenes, tumor-suppressor genes, and non protein coding genes (Croce, 2008). Most cancers originate from a single cell, and this cell and its descendants accumulate sufficient mutations in several genes before turning into cancer (Nowell, 1976). The mutations of the hundreds of genes that could possibly contribute to the causation of cancer are called cancer-critical genes and can be classified into two main groups: The genes which undergo gain-of-function mutations, which result in deregulation of normal cellular proliferation and differentiation, are called oncogenes. The genes which undergo loss-of-function mutations resulting in a loss of feedback inhibition are called tumor suppressor genes. Cancer is assumed to be a genetic disease that is either initiated by activating specific oncogenes, or inactivating specific tumor suppressor genes. Those two gene modifications are caused either by direct mutation or by chromosomal aberrations in the respective tissue (Alberts et al.,

2002). In addition to genetic changes, cancer is also a disease driven by 'epigenetic changes' — modifiers of gene expression that are regulated by mechanisms that do not affect the basic structure of the DNA sequence. DNA methylation and histone modifications are two epigenetic processes that appear to regulate cancer-critical gene expression in many types of tumors (Weinhold, 2006). Furthermore, microRNAs, noncoding short sequence RNAs, also play an important role in the modification of cancer-critical gene expression and, at the same time, the expression of microRNAs itself can also be modified by other epiginetic factors (Chuang and Jones, 2007).

1.3.1 Oncogenes

An oncogene is able to stimulate cellular growth and transformation. When this kind of gene is mutated or over-expressed, it can contribute to transform a normal cell into a tumor cell. Most somatic cells possess the ability to undergo apoptosis (programmed cell death). Activated oncogenes can assist cells to avoid these cellular death programs leading to increased proliferation and survival. The activation of most oncogenes requires an additional step, such as mutations in another gene, or environmental factors such as viral infection, in order to cause cancer (Croce, 2008). In 1982, the first oncogene was discovered in bladder carcinoma cell lines in the laboratories of Robert Weinberg, Michael Wigler and Mariano Barbacid (Shih and Weinberg, 1982, Pulciani et al., 1982 and Parada et al., 1982). The cloned cellular gene had the same transforming properties as the oncogene from the v-ras containing Harvey Murine Sarcoma Virus. (Parada et al., 1982). Oncogenes can be switched on by structural alterations causing by gene fusion or mutation (Konopka et al., 1985), by gene amplification, or by gene rearrangement resulting in the juxtaposition of genes to enhancer sequences (Tsujimoto et al., 1985). Translocations and mutations can occur during tumor initiation or progression, while amplification usually occurs during progression (Finger et al., 1986). The protein products of oncogenes are classified into six groups: transcription factors, chromatin remodelers, growth factors, growth factor receptors, signal transducers, and apoptosis regulators

(Croce et al., 2008). The oncogenes most relevant to human solid malignancies, their mechanism of activation, biochemical function, and the tumor types most often affected by each are summarized in Table 3.

Table 3. Representative oncogenes mutated in human tumors.

Oncogene	Location	Mutation	Function	Tumor
ABL1	9q34.1	Translocation	Signal Transduction (tyrosine kinase)	CML, other hematological neoplasms
BCL2	18q21.3	Translocation	Anti-apoptosis	B cell lymphoma
CCND1	11q13	Amplification Translocation	Cell cycle regulation	Breast and other carcinomas, B cell lymphoma
CDK4	12q14	Amplification point mutation	Cell cycle regulation	Sarcoma, familial melanoma
ERBB family	N/A	Amplification	Growth factor	Glioma, squamous cell carcinoma, carcinoma
FOS	14q24.3	Amplification	Transcription factor	Osteosarcoma
HRAS	11q15.1	Point mutation	Signal transduction	Bladder carcinoma, thyroid cancer
HST	11q13.3	Amplification	Growth factor	Stomach carcinoma
INT2	11p13	Amplification	Growth factor family	Oesophagus cancer, breast cancer, glioma
KRAS	12p12.1	Point mutation	Signal transduction	Pancreas-, colon-, lung-adenocarcinoma, endometrium- other carcinoma, melanoma
KIT	4q11-21	Constitutive activation, point mutation	Receptor tyrosine kinase	(hereditary) GIST, ANLL, testis cancer
MET	7q31	Point mutation	Receptor tyrosine kinase	(hereditary) papillary kidney tumor
MYC (C-MYC)	8q24	Amplification Translocation	Transcription factor	Lymphoma, carcinomas
MYCN	2p24	Amplification	Transcription factor	Neuroblastoma, SCLC
NRAS	1p13.2	Point mutation	Signal transduction	Thyroid cancer,melanoma
PIM1	6p21	Constitutive activation	Signal transduction	T cell lymphoma
RAF1	3p25	Translocation	Signal transduction	Stomach carcinoma
RET	10q11	Translocation Point mutation	Receptor tyrosine kinase	Thyroid cancer

1.3.2 Tumor Suppressor Genes

The discovery of oncogenes appeared to explain cancer cell progression and proliferation in a very simple and direct way. However, in the 1970s and early 1980s, our accumulated knowledge about oncogenes turned was unable to explain all aspects of cancer cell genetics, which hinted that other genes existed that regulate growth control and operate to suppress cell proliferation. These antigrowth genes were called tumor suppressor genes (Weinberg, 2007). In the 1980s, Webster Cavanee and colleagues in Raymond White's lab found that the retinoblastoma gene (RB; also known as RB1) located in chromosome 13, had homozygous mutations at the RB loci in inherited and sporadic retinoblastoma, thereby confirming the two hit hypothesis (also known as allelic-hit hypothesis) (Cavenee et al., 1983). In 1989, Bert Vogelstein's group found cancer-associated deletions of the TP53 gene on chromosome 17p, and showed that one copy was mutated and the other deleted in colorectal cancers. Similar to RB, the tumor suppressor function of TP53 was confirmed by mutation of TP53 to inhibit carcinoma cells growth. Table 4 summarizes the most common tumor-suppressor genes, their chromosomal locations, suspected biochemical functions, and the hereditary and sporadic tumors with which they are most commonly associated.

Table 4. Tumor suppressor genes and their roles in hereditary cancer syndromes

Gene	Location	Syndrome	Function	Tumor
CDH1	16q22	Regulator of cell adhesion	Regulator of cell adhesion	Stomach carcinoma
APC	5q21- q22	Familial adenomatous polyposis and its variants	β-catenin binding, Wnt signal pathway, transcription factor	Gastrointestinal tumor, brain, thyroid carcinoma, retina lesions
PTCH	9q22	Gorlin syndrome/ Neviod basal cell carcinoma	Sonic hedgehog pathway receptor	Skin basel cell carcinoma, medulloblastoma
SMAD4	18q21	Juvenile polyposis	SMAD4: TGF-β signalling	Gastrointestinal tumor
BMPR1A	10q22		BMPR1A: Gatekeeper	
TP53	17q13.1	Li-Fraumeni	Translocation factor, cell cycle, apoptosis, DNA repair etc. regulator	Sarcomas, beast-, brain tumor, Leukaemia, adenocorticoid tumors
MEN1	11q13	Multiplex endocrine neoplasia 1	Inhibit trascription with JunD transcription factor	Insulinoma, Gastroinoma, parathyroid tumors, pituitary adenomas
NF1	17q11	Neurofibramotosis 1(von Reklingenshausen)	GTPase activator	Neurofinbroma, neurofibrosarcoma
NF2	22q12	Neurofibramotosis 2	Role in cell adhesion	Schwannoma, meningioma
BRCA1	17q21	Hereditary breast cancer	Transcription factor, DNA repair	Breast-, ovary-, pancreas-, prostate- cancer
BRCA2	13q13			Male and female breast-, pancreas-, prostate-cancer
CDKN2/ P14/ P16/ P19ARF	9p21	Hereditary melanoma	Cell cycle regulator	Melanoma, pancreas-, prostate, bladder-, esophagus- cancer, leukaemia
MLH1	3p21	Hereditary non polyposis colorectal cancer (HNPCC)	DNA mismatch repair	Gastrointestinal tumor, endometrial, ovarian, heptabiliary and urinary tract cancer, glioblastoma
MSH2	2p22-p21			
MSH6	2p16			
PMS1	2q31-q33			
PMS2	7p22			
TGFBR2	3p22		TGF-β pathway receptor	
RB1	13q14.3	Hereditary retinoblastoma	Transcrition factor, cell cycle regulator	Retinoblastoma, osteosarcoma
VHL	3p25	von Hippel-Lindau	Component of ubiquitin ligase complex, regulator of cell cycle, adhesion	Clear cell kidney cancer, pheaochromocytoma, hemangioblastoma

1.3.3 Oncomirs — microRNAs with a role in cancer gene expression

Gene expression in either normal cells or cancer cells is highly regulated by sophisticated gene regulatory networks. MicroRNAs, single strand RNAs about 21 to 23 nucleotides in length, are a group of small non protein coding RNAs that play a negative regulatory role in such networks. This microRNA negative regulatory mechanism occurs by annealing of a portion of the microRNA to its complementary target mRNA, leading either to degradation of the target mRNA or blockage of its protein translation (Croce, 2008).

In the human genome, the genes encoding microRNAs are much longer than the mature microRNA molecule; microRNAs genes are first transcribed as large RNA precursors, pri-microRNAs with 5' cap and poly-A tails, by RNA polymerase II and then processed to 70 nucleotide -pre-microRNA with stem-loop structures in the cell nucleus by a protein complex of the double-stranded RNA binding protein Pasha and the nuclease Drosha (Denli et al., 2004). These pre-microRNAs are then exported to the cytoplasm and processed to mature microRNAs by the endonuclease Dicer (Bernstein et al., 2001). Although either strand of the mature microRNA may potentially act as a functional molecule, only one strand is usually incorporated into the RNA-induced silencing complex (RISC) where the microRNA and its mRNA target interact. Both the sense and antisense strand of genomic DNA can function as templates to generate microRNAs (Stark et al., 2008).

Just as other cancer critical genes in cancer cells, microRNAs may locate in chromosomal regions, where amplifications, deletions, rearrangements and mutations occur (Calin et al., 2004). MicroRNA profiling studies have shown that microRNA expression patterns are associated with cancer progression, staging, classification, diagnosis and prognosis, as well as response to therapy (Calin and Croce., 2006, 2005, Yanaihara et al., 2006).

MicroRNA can be up or down regulated in cancer cells (Volinia et al., 2006). In specific tissues, microRNAs, due to their regulatory functions, may play roles similar to that of oncogene or tumor suppressor genes. (Zhang et al., 2007, see Figure 2). One example for such an oncogene mimicking function is mir-17–92. The mir-17–92 cluster is located on chromosome 13q31, a region that is amplified in lung cancer and in some lymphomas, for example in diffuses large B-cell lymphoma (Hayashita et al., 2005; He et al., 2005). The mir-17–92 is highly expressed in lung cancer and lymphomas when compared to normal tissue. The miR-17–92 cluster also contributes to lung cancer cell growth (Hayashita et al., 2005). In mir-17–92 overexpressing transgenic mice, mir-17–92 significantly increases the formation of B-cell lymphomas (He et al., 2005). Let-7 is an example of a microRNA with a tumor supressor mimicking function. let-7 was originally identified in C. elegans. It is highly conserved in animals, from nematodes to humans (Pasquinelli et al., 2000), and the expression of let-7 is dependent on the stage of development (Johnson et al., 2003; Johnston and Hobert, 2003; Miska et al., 2004; Thomson et al., 2004). Let-7 directly targets the RAS oncogene and negatively regulates RAS gene expression by binding to the 3′ UTR of RAS mRNA, leading to translational repression. In lung cancer, tumor cells often display a significantly increased expression of RAS protein and a significantly reduced expression of let-7 compared to normal lung tissue, suggesting that let-7 functions as a tumor suppressor gene in lung cancer by regulating of the RAS pathway (Johnson et al., 2005). These findings suggest that microRNAs can be used as molecular biomarkers for tumor diagnosis, prognosis of disease specific outcomes, and prediction of therapeutic responses (Waldman et al., 2007).

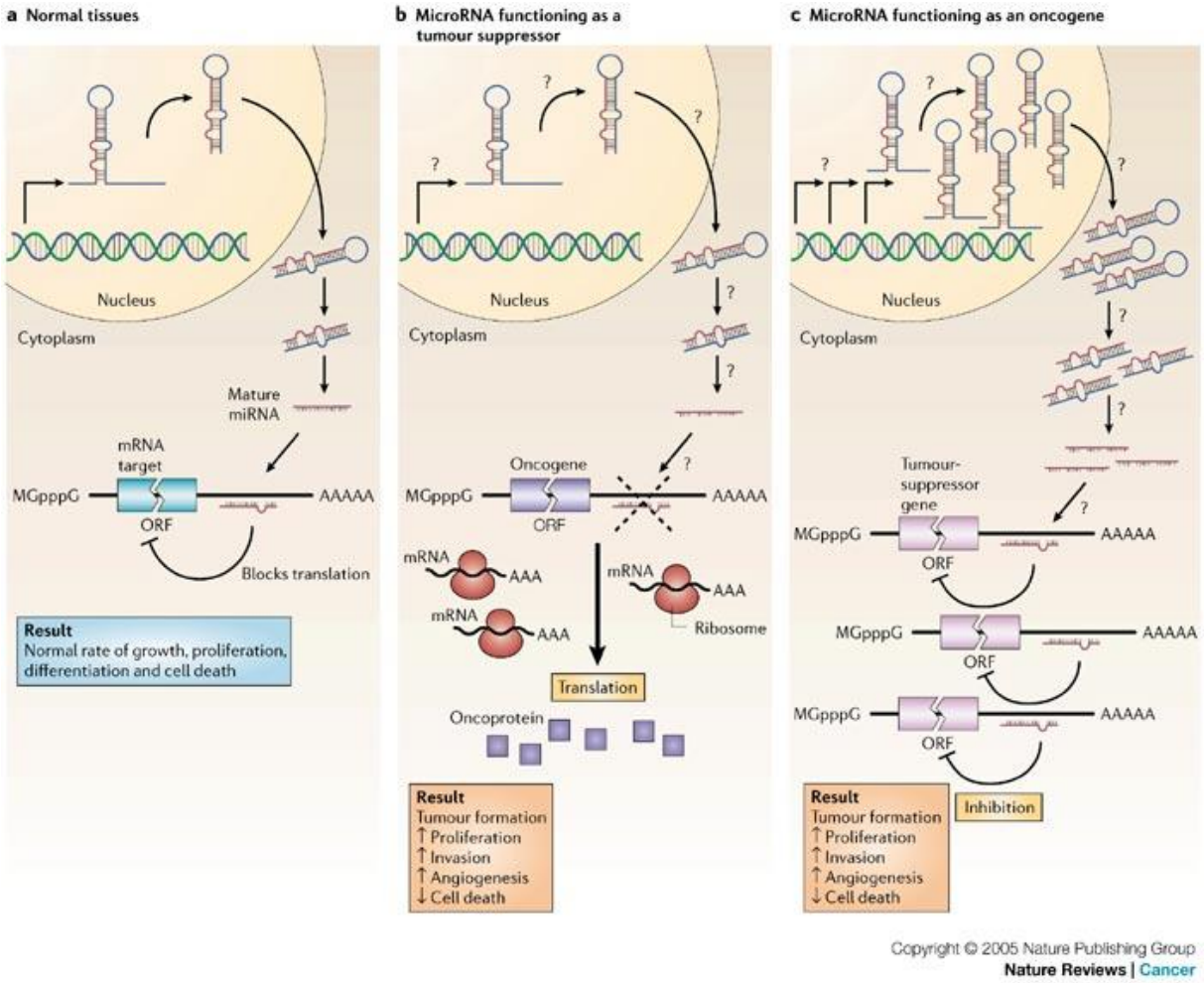

Figure 2. MicroRNAs can function as tumor suppressors and oncogenes.
a.) In normal tissues, proper microRNA transcription, processing and binding to complementary sequences on the target mRNA results in the repression of target-gene expression through a block in protein translation or altered mRNA stability (not shown). The overall result is normal rates of cellular growth, proliferation, differentiation and cell death. b.) The reduction or deletion of a microRNA that functions as a tumor suppressor leads to tumor formation. A reduction in or elimination of mature microRNA levels can occur because of defects at any stage of microRNA biogenesis (indicated by question marks) and ultimately leads to the inappropriate expression of the microRNA-target oncoprotein (purple squares). The overall outcome might involve increased proliferation, invasiveness or angiogenesis, decreased levels of apoptosis, or undifferentiated or de-differentiated tissue, ultimately leading to tumor formation. c.) The amplification or overexpression of a microRNA that has an oncogenic role would also result in tumor formation. In this situation, increased amounts of a microRNA, which might be produced at inappropriate times or in the wrong tissues, would eliminate the expression of a microRNA-target tumor-suppressor gene (pink) and lead to cancer progression. Increased levels of mature microRNA might occur because of amplification of the microRNA gene, a constitutively active promoter, increased efficiency in microRNA processing or increased stability of the microRNA (indicated by question marks). ORF, open reading frame. (Figures are from Esquela-Kerscher and Slack, 2006)

1.3.4 Molecular Genetics of Lung Cancer

Lung cancer oncogenesis conforms to the multistep model of tumorigenesis (Fearon et al., 1985). Similar to other tumor entities, activation of oncogenes and inactivation of tumor-suppressor genes are the basic events underlying lung tumorigenesis (Zochbauer-Müller et al. 2002).

1.3.4.1 Activation of oncogenes in human lung cancer

The *RAS* genes (*HRAS*, *KRAS*, and *NRAS*) encode GTPase proteins that play a role in transducing growth-promoting and survival signals from membrane-bound receptor tyrosine kinases (RTK)s. The *RAS* oncogenes acquire their transforming capacity by G-T transversal point mutations that are detected in 20%-30% of lung adenocarcinomas and in 20% of all NSCLCs (Slebos et al. 1989; Rodenhuis and Slebos 1992). Most of those point mutations are found in codon 12, followed by mutations in codons 13 and 61 (Rodenhuis et al. 1988), and correlate with smoking (Slebos et al. 1989). About 90% of the mutations are found in *RAS* in lung adenocarcinomas, whereas no RAS mutations have been detected in SCLC. The *RAS* mutations relate to poor prognosis for any stage of NSCLC (van Zandwijk et al. 1995; Graziano et al. 1999). The *MYC* proto-oncogenes, *MYCL*, *MYCN*, and *MYC*, encode basic helix-loop-helix transcription factors that regulate the expression of genes involved in DNA synthesis, RNA metabolism, and cell cycle regulation (Oster et al. 2002). Activation of *MYC* genes occurs by amplification or loss of transcriptional control, which results in *MYC* protein overexpression. In SCLC, *MYCN*, *MYCL* or *MYC* are often amplified and aberrantly expressed, whereas in NSCLC, exclusively *MYC* is affected and only in a fraction of the tumors. *MYC* amplification occurs in 15%-30% SCLCs and 5%-10% NSCLCs (Richardson and Johnson 1993). *MYC*

amplification could therefore be indicative for poor prognosis (Johnson et al. 1996). A member of the *NOTCH* gene family, *NOTCH3*, was found to be overexpressed in NSCLCs on chromosome 19p translocation (Dang et al. 2000). *NOTCH3* is involved in differentiation and neoplasia (Campese et al. 2003) and likely influences differentiation of lung cancer cells (Dang et al. 2003). Finally, overexpression of the proto-oncogene *BCL2* is often found in lung cancer (Pezzella et al. 1993; Kaiser et al. 1996). *BCL2* is an antiapoptotic protein and is expressed in 75%-95% of SCLCs (Jiang et al. 1995), whereas it is expressed in 25%-30% of the squamous cell carcinomas and ~10% of adenocarcinomas (Pezzella et al. 1993). *BCL2* counteracts *BAX*, a proapoptotic protein and a downstream target of *TP53*. High *BCL2* and low *BAX* expression are frequently found in SCLCs that are p53-deficient (Brambilla et al. 1996). Interestingly, SCLCs with high *BCL2* expression levels are mostly very sensitive to chemotherapy (Pakunlu et al., 2004). Moreover, *BCL2* expression in NSCLC is believed to be a favorable prognostic factor, while *BCL2* expression does not influence survival in SCLCs (Maitra et al. 1999; Martin et al. 2003).

1.3.4.2 Inactivation of tumor suppressor genes in human lung cancer

Tumor-suppressor genes are frequently inactivated in lung cancer. One of the most commonly found aberrations is mutation or deletion of *TP53*. *TP53* is critical for maintaining genomic integrity after DNA damage inflicted by γ and UV irradiation or carcinogen exposure (Khanna and Jackson, 2001; Hanawalt et al., 2003). Cellular stress such as DNA damage or hypoxia causes up-regulation of *TP53*, which then acts as a transcription factor driving expression of a range of genes such as *TP21*, controlling G1/S cell cycle transition, or *GADD45*, involved in the G2/M DNA damage checkpoint. Apoptosis can be induced through *TP53* by activating *BAX*, *PERP* (Ihrie et al., 2003), and

other genes (Mori et al., 2004). Loss of *TP53* function in lung cancer often occurs through mis-sense mutations and rarely by deletions and is found in ≥75% and ~50% of SCLCs and NSCLCs, respectively (Toyooka et al., 2003a). The *TP53* mutations in lung tumors, mostly G-T transversions, are due to smoking (Lewis and Parry, 2004). Normally, expression levels of *TP53* are kept low through an autoregulatory feedback loop with *MDM2*, which itself is transcriptionally controlled by *TP53*. MDM2-p53 binding enhances the proteasome-dependent degradation and, therefore, keeps TP53 levels in check. Overexpression of *MDM2* is found in 25% of NSCLCs (Higashiyama et al., 1997).

The p16INK4A (CDKN2A)-cyclin D1 (*CCND1*)-CDK4-RB pathway is critical in controlling the G1/S cell cycle transition, and one of its components is invariably mutated or functionally altered in lung cancer. Allelic loss, mutations, or promoter hypermethylation of *CDKN2A* occur frequently in NSCLC but rarely in SCLC (Fong et al., 2003). Between 30%-50% of primary NSCLCs do not express *CDKN2A*. p16INK4A (CDKN2A) functions by binding to cyclin-dependent protein kinase 4 (CDK4), inhibiting the ability of CDK4 to interact withCCND1. The CCND1-associated CDK4 phosphorylates RB, thereby releasing the cell from RB-mediated cell cycle arrest (Malumbres et al., 2003). *CDK4* as well as *CCND1* overexpression have been found in NSCLCs (Borczuk et al., 2003; Ratschiller et al., 2003) and are correlated with a poor prognosis (Caputi et al., 1997). The key component of this pathway, the *RB* gene, can be inactivated by point mutations, alternative splicing, or deletions. Abnormalities in the RB protein have been found in >90% of SCLCs and 15%-30% of NSCLCs (Reissmann et al., 1993; Dosaka-Akita et al., 1997). As would be expected from proteins acting in the same pathway, mutations of both *RB* and *CDKN2A* are rarely found in the same lung tumor. Interestingly, in spite of the mutual exclusiveness of mutations in *CCND1*, *CDK4/6*, *CDKN2A*, and *RB*, alterations in *CDKN2A-CCND1-CDK4* are most commonly seen in NSCLC, whereas *RB* gene

inactivation is a typical feature for SCLCs (Zochbauer-Müller et al., 2002). In the case of the other members of the *RB* family, *RBL1* and *RBL2*, only *RBL2* is found mutated or expressed at a low level in both NSCLCs (Claudio et al., 2000) and SCLCs (Helin et al., 1997). The alternative reading frame product protein p14ARF encoded by the *CDKN2A* locus, was inactivated in 65% of SCLCs (Gazzeri et al., 1998), whereas *CDKN2A* mutations were found in ~20% of NSCLCs (Nicholson et al., 2001). Since p14ARF interacts with MDM2 and thus prevents p53 degradation, it is an integral member of the p53-MDM2-p14ARF pathway (Fong et al., 2003). There remains, however, a possibility that p14ARF acts also through a yet unknown pathway (Weber et al., 2000) in lung cancer, since loss of p14ARF can be found independent from *CDKN2A* and concurrent with *TP53* mutations in both NSCLC and SCLC (Gazzeri et al., 1998; Nicholson et al., 2001). Also, other tumor-suppressor genes are of importance as is evident by recurrent chromosomal losses found in this cancer type. Several candidate tumor suppressor genes were identified in the chromosome 3p region that frequently show *LOH* in lung cancer (Wistuba et al., 2001). One candidate is *FHIT* in region 3p14.2, showing aberrant transcripts in 80% of SCLC and 40% of NSCLCs, while no FHIT protein is seen in 50% of all lung cancers (Sozzi et al., 1996; Zochbauer-Müller et al., 2001). Other candidate tumor-suppressor genes from the 3p region include *RASSF1* (Dammann et al., 2000; Burbee et al., 2001), *SEMA3B* (Sekido et al., 1996), *FUS1* (Kondo et al., 2001), and *RARB* (Virmani et al., 2000).

An alternative way for inactivating tumor-suppressor genes in lung cancer is hypermethylation of promoter regions resulting in transcriptional inactivation of one allele while the remaining allele is lost via *LOH*. This epigenetic inactivation is often found in both NSCLC and SCLC (Zochbauer-Müller et al., 2002) but can also be detected in early preneoplastic lesions of smokers. Methylated promoter regions of the individual

genes TIMP3, *CDKN2A*, *CDKN2A*, *CDH13* (*H-Cadherin*), *CDH1* (*E-Cadherin*), *DAPK*, *GSTP1* (Zochbauer-Müller et al., 2002), and the genes of the chromosome 3p region (*RASSF1*, *SEMA3B*, *RARB*, and *FHIT*) have been reported (Kuroki et al., 2003). Several regional hypermethylation spots at chromosomal regions 4q, 10q, and 17p are present in both NSCLC and SCLC, but so far no adjacent candidate tumor-suppressor genes have been identified in these regions (Fong et al., 2003).

1.3.4.3 microRNA and human lung cancer

Numerous publications have reported aberrant expression of microRNAs in cancer (Landgraf et al., 2007). In solid cancers, one of the largest studies of microRNAs expression was performed by the group of Carlo M. Croce (Volinia et al., 2006). The authors analyzed the "microRNome" of 363 tumors (breast, lung, pancreas, stomach, colon and prostate) versus 177 healthy tissues and identified a solid cancer microRNA signature composed of a large portion of overexpressed microRNAs, such as mir-21, mir-191 and mir-17-5p. Comparison of 123 lung cancers and 123 corresponding normal lungs led to the detection of 38 microRNAs with abnormal expression (some members of the let-7 family, mir-16-2, mir-21, mir-191, mir-17-5p and mir-155). A specific microRNA signature in lung cancers was confirmed in the study from the Curtis C. Harris lab (Yanaihara et al., 2006). The authors performed a microarray analysis in 104 non squamous cell lung carcinoma (NSCLC) and corresponding non-cancerous lung tissues and identified 43 differentially expressed microRNAs: 15 upregulated (including mir-21, mir-191, mir-155, mir-17-3p) and 28 downregulated (including let-7-a2 and mir-125a). These findings have supported the concept of a specific microRNAs signature in solid cancers, opening a large field of research.

1.4 Invasion and metastasis of cancer

Approximately 90% of cancer-associated deaths are caused by invasion and metastasis (Sporn, 1996), which consists of a complicated series of sequential, interrelated steps. Initially, the primary tumor cells invade adjacent host tissues and enter the blood vessels or the lymphatic system. These cells then flow through the vasculature, arrest in tissue capillaries away from the primary tumor, then escape out of the blood vessel walls, invade into the surrounding tissue and finally proliferate from microscopic growths to macroscopic secondary tumors (Fidler, 2003).

In 1889, a British physician Stephen Paget enunciated the "seed and soil" hypothesis which still holds forth today. "When a plant goes to seed, its seeds are carried in all directions," he wrote. "But they can only live and grow if they fall on congenial soil" (Paget, 1889). This idea was a prevalent theory at that time, which stated that disseminating cancer cells, having been spread through the body into the blood or lymph "in all directions", could colonize in some tissues and transform the adjacent cells to grow in a similar way. However the "seed and soil" theory could not explain the metastatic pattern of all types of human cancer. Sugarbakeer and Kinsey challenged Paget's hypothesis by ectopically transplanting various organ tissues in *DBA/2* syngeneic mice and injecting them from different routes using the melanoma S91 Cloudman strain. They reported that tumor cells specifically metastasized to lungs but not any other transplanted organs (Sugarbaker, 1952; Kinsey, 1960).

Epithelial to mesenchymal transition or transformation (EMT) is a program of development of biological cells characterized by loss of cell adhesion, repression of E-cadherin expression, and increased cell mobility. EMT is essential for numerous developmental processes including mesoderm formation and neural tube formation.

Epithelial to mesenchymal transition (EMT) was first described as a distinct embryogenesis process by Garry Greenburg and Elisabeth Hay in 1982 (Greenburg and Hay, 1982), although it had been studied for more than a century previously. As a highly conserved and fundamental cellular program occurring during critical stages of animal embryonic development, EMT had been proposed to promote the cancer phenotype of invasion and metastasis during the past ten years (Tepass et al., 1996). Loss of *E-cadherin* (*CDH1*) expression is a key step involved in EMT. E-cadherin is a protein that functions in cell-cell adherence and is crucial for formation of the embryonic epithelia. E-cadherin loss of function studies shows the EMT phenotype in embryogenesis as well as in tumor invasion and metastatic processes. (Tepass et al., 1996; Edelman et al., 1983; Berx et al., 1995; Becker et al., 1994; Guilford et al., 1998). During embryonic development, *E-cadherin* is tanscriptionally repressed by several E-Box binding zinc-finger proteins such as twist, snail, slug and sip1 (Figure 3). Moreover, investigators found that *SNAIL* is highly expressed in human breast carcinoma and also in lymph-node-positive tumors; Furthermore, *E-cadherin* and *SNAIL* expression levels have an inverse correlation in breast- (Blanco et al., 2002) and oral squamous cell carcinoma (Yokoyama et al., 2001). *SNAIL* and *SIP1* share partly overlapping binding sites and are normally co-expressed in E-cadherin-negative carcinomas (Comijn et al., 2001). *SIP1* expression is controlled both by tyrosine kinase receptor and TGF-ß signalling which also regulates *SNAIL* expression (Comijn et al., 2001). NF-κB was identified as an important mediator of EMT in breast cancer progression, and the E-cadherin repressors Twist and Snail are downstream targets of NF-κB (Huber et al., 2004). As a key regulator of the EMT process, E-cadherin mutation might be a risk factor for oncogenesis. Parry Guilford and colleages found E-cadherin germ-line mutations in some families in New Zealand, whose members have a high probability of developing diffuse gastric cancer (Guilford et al., 1998).

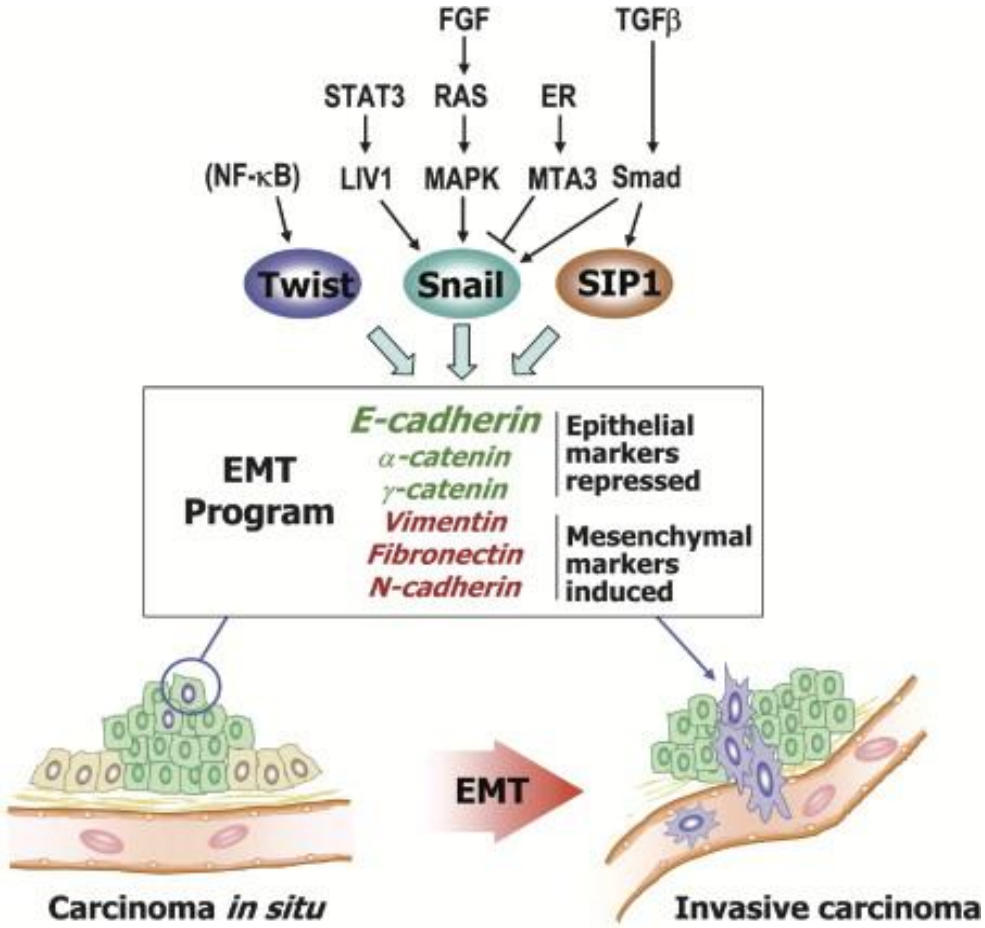

Figure 3. Drivers and mediators of EMT. Early stage tumor cells (green) maintain epithelial properties similar to the neighboring normal epithelium (brown). The overexpression of master regulators of EMT, such as twist, snail, and sip1, in cancer cells (shown with purple nuclei) leads to dramatic changes in gene expression profile and cellular behavior. Twist, Snail, and Sip1 repress the expression of *E-cadherin* via E boxes in its promoter and trigger expression of an entire EMT transcriptional program through as yet unknown mechanisms. Several pathways are known to regulate *TWIST*, *SNAL*, and *SIP1* expression in tumor cells while others (shown in parentheses) do so at least in developmental contexts. (Figure from, Kang and Massagué, 2004)

1.5 Tumor-Microenvironment Interactions

There are two compartments of tissue immediately associated with each other in tumors. The first compartment is the malignant tissue with its tumor cells. The second is the tumor microenvironment, which is composed of different types of cells, for example, resident fibroblasts, endothelial cells, and other nonmalignant cells, infiltrating fibroblasts, lymphocytes, macrophages, extracellular matrix, growth factors, cytokines, chemokines, antibodies, proteases, other types of enzymes, and various metabolites. All of these

molecules may be excreted from the malignant tumor cells or from the nonmalignant cells in the tissue complex (Witz et al., 2008a). The tumor microenvironment functions as an active “educational, inductive, selection” niche, where the tumor is directed into possible cellular signalling pathways by microenvironmental factors. However, the interaction between microenvironment and malignant tumor cells is bidirectional: Tumor cells and their secreted extracellular factors are also able to regulate gene expression in non-tumor cells residing in, or infiltrating into, the microenvironment, which then might alter their phenotypes (Witz et al., 2008b).

It is widely accepted that how the tumor interacts with the components of the associated microenvironment is crucial for cell fate, whether malignant cells grow, invade and metastasize, or become dormant or even regress completely. These interactions influence cellular processes that promote or suppress oncogenesis: invasion, metastasis, angiogenesis, inflammation, motility, chemotaxis and protective immunity, Although additional mechanisms of interaction probably still have to be uncovered, and the significance of other known interactions has still to be elucidated, it is safe to tentatively conclude that many, if not most, of these interactions constitute dangerous liaisons: They promote tumor progression and metastasis (Witz et al., 2008b).

The physiological conditions within the tumor microenvironment are considerably different from those in normal tissue. Hypoxia, low pH and glucose levels are common in the tumor microenviroment. Moreover, massive cell death occurs, releasing proteins and small molecules into the surrounding regions. These factors may prevent or promote tumor growth (Witz and Levy-Nissenbaum, 2006). Hypoxia in the tumor microenvironment may cause the generation of oxygen free radicals, which can lead to DNA damage (mutation). Under hypoxic conditions, repairing DNA damage is not efficient. The result is an increase in the mutation rate and variations in the malignant tumor cell populations.

Another result is that only those mutated cells which can survive in this microenvironment will continue to grow and contribute to the tumor (Laconi, 2007).

Furthermore, the conditions within the tumor microenvironment do not only affect malignant tumor cells. The adjacent cells surrounding a tumor demonstrate altered characteristics compared to corresponding cells in normal tissue. These cells in adjacent tissue also develop mutations, and the tissue itself is often disorganized compared to normal tissue (Zalatnai, 2006). These abnormal alterations might arise in two ways: the hypoxia and low pH in tumor microenvironment may induce mutations, or soluble products (growth factors, cytokines, or other metabolic products) released from the malignant tumor cells may alter the genes expression in the stoma cells (Witz and Levy-Nissenbaum, 2006). Interestingly, mutations were reported in the non-cancerous stroma tissue from breast cancer patients, suggesting that the genetic alterations in the stroma may play a crucial role in tumor initiation (Laconi, 2007).

1.6 Eicosanoid signalling and cancer

Human epidemiological and animal model studies proved that a high-fat diet is associated with risk of cancer, especially in colorectal, breast, pancreatic and prostate cancer (Woutersen et al., 1999). Arachidonic acid has a crucial role in chronic inflammation and cancer. It is one of the major ingredients of animal fats and many biologically active lipids (prostaglandins, leukotrienes, thromboxins etc.) are derived from this substrate. By involvement of the cyclooxygenase (COX), lipoxygenase (LOX) and P450 epoxygenase pathways, the metabolism of arachidonic acid generates different types of eicosanoids, including prostanoids, leukotrienes, epoxyeicosatrienoic acids (EETs), hydroxyeicosatetraenoic acids (HETEs) and hydroperoxyeicosatetraenoic acids (HPETEs) (Wang and DuBois, 2010).

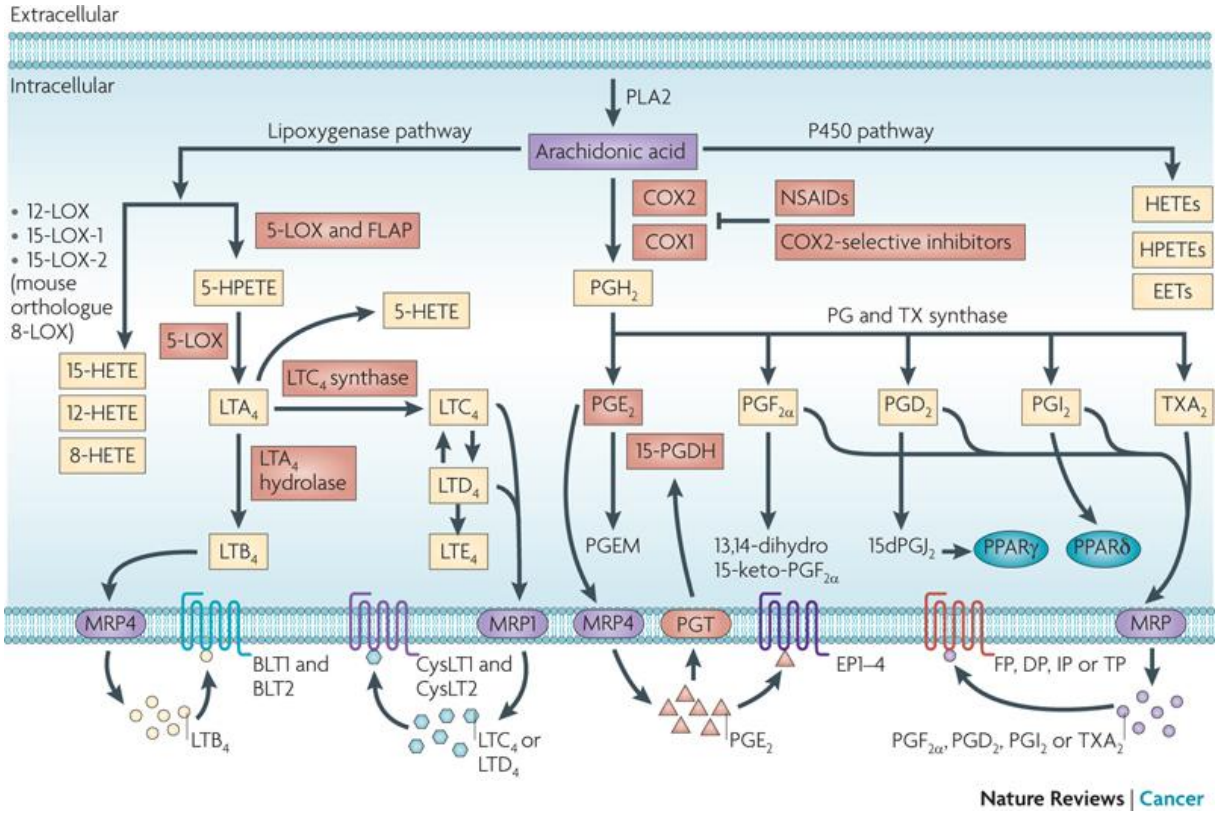

Figure 4. An overview of eicosanoid synthesis pathways. Arachidonic acid is set free from the cellular membranes by cytoplasmic phospholipase A2 (PLA2). Free arachidonic acid can be metabolized to eicosanoids through three major pathways: the cyclooxygenase (COX), the lipoxygenase (LOX) and the cytochrome P450 monooxygenase pathways. The prostaglandin E, F, D and I are synthesized through COX pathway. In the COX pathway, the key step is to enzymaticly convert arachidonic acid to the intermediate prostaglandin G2 (PGG2), which is then reduced to an intermediate form of PGH2 by the COX peroxidase activity. Each of the prostaglandins and leukotrienes exerts its biological effects by binding to its receptor, kind of G protein-coupled receptor. PGH2 can be metabolized to PGE, PGF, PGD and PHI by their specific synthases. Hydroxyprostaglandin dehydrogenase 15-(NAD) (15-PGDH) mainly metabolizes intracellular PGE2 and PGF2α to a stable 13,14-dihydro-15-keto-PGE2 and 13,14-dihydro-15-keto-PGF2α (Wang and DuBois, 2010).

Among the prostanoids involved in eicosanoid signalling, pro-inflammatory PGE2 plays a crucial role in promoting tumor growth. PGE2 is the most common prostaglandin found in different human cancers, including lung, colon, breast, and head and neck cancer, and is associated with a poor prognosis. (Rigas et al., 1993; Wang et al., 2004; McLemore et al., 1988; Hambek et al., 2007). 15-PGDH, an inactivator of eicosanoids, is expressed more highly in normal tissues than in corresponding human lung, colon, gastric and breast malignant tumors (Backlund et al., 2005; Wolf et al., 2006; Hughes et al., 2008; Thiel et

al., 2009). Low expression level of 15-PGDH in these tumors results in increasing endogenous PGE2 concentration. A recent study show direct evidence that PGE2 promotes tumor growth, PGE2 treatment strikingly increase intestinal adenoma burden in ApcMin/+ mice and significantly promotes azoxymethane (AOM)-induced colon tumor progression (Wang et al.,2004; Kawamori et al., 2003). On the other hand, inhibition of endogenous PGE2 can suppresses intestinal tumorigenesis in ApcMin/+ and AOM models26 by the genetic knock out of prostaglandin E synthase (Ptges). The role that PGE2 plays in colorectal tumorigenesis has been confirmed by investigating mice with a homozygous deletion of individual PGE2 receptors (Watanabe et al., 1999; Mutoh et al., 2002; Sonoshita et al., 2001). Limited information is available regarding the role of PGE2 signalling in animal models of other cancers. By the overexpression of COX2 and PTGES, increasing PGE2 levels results in gastric oncogenesis in keratin 19 driven CRE/Wnt1-transgenic mice (Oshima et al., 2006). Deletion of the EP2 receptor suppresses lung tumorigenesis in a chemical carcinogen mouse model. (Keith et al., 2006) and inhibits COX2-induced mammary hyperplasia in mice (Chang et al., 2005). Similarly, an EP1 antagonist inhibits chemically induced breast cancer development in rats (Kawamori et al., 2001). Above all, these studies demonstrate that PGE2 is a crucial small molecule in cancer progression.

The role of other prostaglandins in tumor animal models is not well studied. Function loss of TBXA2R, FP or IP receptors does not affect colon tumor formation in the AOM mouse model (Mutoh et al., 2002), suggesting that the three receptors are not important in colon cancer progression. PGF2α can enhance carcinogen-induced transformation of fibroblasts in vitro by inducing COX2 (Wolfle et al., 2003). Activation of PPARδ promote intestinal tumor growth in ApcMin/+ mice (Wang et al., 2006), suggesting that PGI2 may accelerate colon tumor progression through this receptor.

1.7 Aim of this work

The aim of the present work was to identify genes and microRNAs involved in tumor invasion and tumor microenvironment interaction in squamous cell lung carcinoma. First after the isolating of four target cell populations (tumor center, tumor front, adjacent lung front and normal lung) by laser capture microdissetion and the assurance of high RNA intergrity, a novel method, punch aided laser microdissection, was developed to investigate these four cell populations in human lung tumor sections. T7 based RNA linear amplification was used to amplified total RNA for oligonucleotide microarray experiments and then used to identify candidate genes and canonical pathways with functions on tumor invasion and tumor microenvironment interactions. Second, in parallel, microRNAs expression in the four cell compartments were analyzed using TaqMan Low Density Arrays to explore differences in the zonal expression microRNAs, which might alter tumor invasion and the microenvironment. Third, integrative bioinformatic analysis of the crosstalk between microRNA and mRNA expression was carried out in order to find the regulatory role that microRNAs could play in tumor microenvironment and invasion. The respective candidate genes discovered by these two array techniques are possible targets for diagnosis and anti-cancer therapies.

2 Materials and Methods

2.1 Materials

2.1.1 Chemicals and Biochemicals

2-mercaptoethanol	Sigma-Aldrich, Munich, Germany
Acetic anhydride	Sigma-Aldrich, Munich, Germany
Alexa Fluor 594, goat anti-mouse IgG	Invitrogen, Kalsruhe, Germany
Aminoallyl-dUTP	Fermentas, St. Leon-Rot, Germany
Ammonium acetate solution, 7.5 M	Sigma-Aldrich, Munich, Germany
Antibody Diluent, Background Reducing	Dako, Glostrup, Danmark
Cot-human DNA	Invitrogen, Kalsruhe, Germany
Chloroform, pro analysis	Merck, Darmstat, Germany
Cyanin 3-dUTP	Amersham Bioscience,Freriburg, Germany
Cyanin 5-dUTP	Amersham Bioscience,Freriburg, Germany
Cy5-Streptavidin	Invitrogen, Camarillo, Germany
Deoxynucleotide set, 100 mM solution	Fermentas, St. Leon-Rot, Germany
DEPC (diethylpyrocarbonate)-treated water	Ambion, Austin, USA
Diaminoethane tetraacetic acid	Sigma-Aldrich, Munich, Germany
Eosin	Sigma-Aldrich, Munich, Germany
Ethanol, pro analysis	Sigma-Aldrich, Munich, Germany
Ethanolamine	Sigma-Aldrich, Munich, Germany
Ethidiumbromide	Sigma-Aldrich, Munich, Germany
Eukitt quick-hardening mounting medium	Sigma-Aldrich, Munich, Germany
FITC-Streptavidin	Invitrogen, Camarillo, Germany
Formaldehyde solution	Sigma-Aldrich, Munich, Germany
Formamide, pro analysis	Merck, Darmstat, Germany
Glycine	Sigma-Aldrich, Munich, Germany
Goat serum	Abcam, Cambridge, UK
Hematoxylin	Sigma-Aldrich, Munich, Germany
Human Universal Reference RNA	Stratagene, La Jolla, USA
Hydrochloric acid	Sigma-Aldrich, Munich, Germany
Jung Tissue Freezing Medium	Leica, Bensheim, Germany
Linear polyacrylamide (LPA), 5µg/µl	Ambion, Austin, USA
M-MuLV Reverse Transcription Buffer	Fermentas, St. Leon-Rot, Germany

miRCURY LNA microRNA Detection Probes. (hsa-mir-220, hsa-mir-196a, hsa-mir-650, 6U, Scramble-mir)	Exiqon, Vedbaek, Denmark
Nuclease-free water (not DEPC treated)	Ambion, Austin, USA
Oligo T7 (dT) 21 Primer	BioSpring, Frankfurt am Main, Germany
PCR nucleotide mix, 10mM	GE Healthcare, Buckinghamshire, UK
Pdn6 random primers	Roche Diagnostics, Mannheim, Germany
Phenol-chloroform-isoamylalcohol 25:24:1,	Sigma-Aldrich, Munich, Germany
QIAzol Lysis Reagent	Qiagen, Hilden, Germany
Ribonucleic Acid (tRNA)	Sigma-Aldrich, Munich, Germany
RNaseZap	Ambion, Austin, USA
RNasin Ribonuclease Inhibitor	Promega, Madison, USA
Roti-Histol	Carl Roth GmbH, Kalsruhe, Germany
Second strand buffer	Invitrogen, Kalsruhe, Germany
SSC solution (20X)	Ambion, Austin, USA
Tris(hydroxymethyl) aminomethane	Sigma-Aldrich, Munich, Germany
Tween-20	Sigma-Aldrich, Munich, Germany
Universal Human Reference RNA	Stratagene, La Jolla, USA
Vectashield mouting medium (Dapi)	Vector, Burlingame, USA
Xylene	Sigma-Aldrich, Munich, Germany

2.1.2 Enzymes

DNA ligase	USB, Cleveland, USA
DNA polymerase I	Promega, Madison, USA
Proteinase K	Qiagen, Hilden, Germany
RevertAid M-MuLV Reverse Transcriptase	Fermentas, St. Leon-Rot, Germany
Ribonuclease H	Epicentre, Madison, USA
T4 DNA polymerase	NEB,Frankfurt am Main, Germany
T4 Gene 32 protein (cloned), 500 µg	USB, Cleveland, USA

2.1.3 Antibodies

Anti AKR1C3 antibody	Abcam, Cambridge, UK
Anti Apelin Receptor antibody	Novus, Littleton, USA
Anti CD11b antibody	Abcam, Cambridge, UK
Anti CD45 antibody	Abcam, Cambridge, UK
Anti GIMAP7 antibody	Sigma-Aldrich, Munich, Germany
Anti Macrophage Inflammatory Protein 3 ß (CCL19) antibody	Abcam, Cambridge, UK
Anti- mouse IgG	Chemicon International, Temecula, USA
Anti Prostaglandin E Synthase-1 antibody	Cayman Chemical, Ann Arbor USA
Anti Prostaglandin E Receptor 1 antibody	Cayman Chemical, Ann Arbor USA
Anti Prostaglandin E Receptor 2 antibody	Cayman Chemical, Ann Arbor USA
Anti Prostaglandin F Receptor antibody	Cayman Chemical, Ann Arbor USA
Anti- rabbit IgG	Chemicon International, Temecula, USA
Biotinylated Anti-mouse IgG (H+L)	VECTOR, Burlingame, USA
Biotinylated Anti-rabbit IgG (H+L)	VECTOR, Burlingame, USA

2.1.4 Kits

BioPrime Array CGH Genomic Labeling System	Invitrogen, Kalsruhe, Germany
Dako Cytomation Biotin Blocking System	Dako, Glostrup, Danmark
Dako REAL Detection Systems	Dako, Glostrup, Danmark
RNA 6000 Nano Chip kit	Agilent, Santa Clara, USA
RNA 6000 Pico Chip kit	Agilent, Santa Clara, USA
RNeasy Mini Kit (with RNase-Free DNase Set)	Qiagen, Hilden, Germany
RNeasy Micro Kit (with RNase-Free DNase Set)	Qiagen, Hilden, Germany
RiboMAX Large Scale RNA Production System - T7	Promega, Madison, USA
TaqMan Low Density Array Human MicroRNA Panel v1.0 (including 8 microRNA RT pools)	Applied Biosystems, Foster City, USA
TaqMan MicroRNA Reverse Transcription Kit	Applied Biosystems, Foster City, USA
TaqMan Universal PCR Master Mix	Applied Biosystems, Foster City, USA
MiRNeasy mini kit (with RNase-Free DNase Set)	Qiagen, Hilden, Germany

2.1.5 Other Materials

AdhesiveCap 500 opaque	Carl Zeiss, Munich, Germany
Cover slides	Menzel-Glaser, Braunschweig, Germany
Homo sapiens AROS V4.0 70mer oligo set for gene expression profiling	Operon Technologies, Cologne, Germany
MembraneSlide NF 1.0 PEN	Carl Zeiss, Munich, Germany
QMT epoxysilane coated slides	Quantifoil Micro Tools, Jena, Germany
Micro Bio-Spin chromatography columns (P6)	Bio-Rad, Munich, USA
Microcon YM-30 spin-columns	Millipore, Schwalbach, Germany
Phase Lock Gel Heavy	5 PRIME, Hamburg , Germany
RNase-free microfuge tubes	Ambion, Austin, USA
SuperFrost Plus microscope slides	Menzel-Glaser, Braunschweig, Germany

2.1.6 Instruments

2100 Bioanalyzer	Agilent, Foster City, USA
7900HT Fast Real-Time PCR System	Applied Biosystem, Foster City, USA
Biofuge Fresco	Heraeus Instruments, Osterode, Germany
Cryostat CM1850	Leica Microsystems, Wetzlar, Germany
SureHyb chambers	Agilent, Foster City, USA
Manual Rotary Microtome RM2235	Leica Microsystems, Wetzlar, Germany
Microarray Scanner G2565BA	Agilent, Santa Clara, USA
Multifuge 3S	Heraeus Instruments, Osterode, Germany
MultiGourmet steamer	Braun, Kronberg, Germany
Nanodrop ND -1000 spectrometer	Thermo Fisher Scientific,Wilmington, USA
OmniGrid Microarrayer	Gene Machines, San Carlos, USA
P.A.L.M. MicroBeam	Zeiss Instruments, Munich, Germany
Precision hotplates with separate controller	Harry Gestigkeit, Dusseldorf, Germany
Stratalinker Model 2400 UV illuminator	Stratagene, La Jolla, USA
Thermomixer R Thermal Block	Eppendorf, Hamburg, Germany
Vortexer for Agilent Bioanalyzer	IKA Werke GmbH, Staufen, Germany
Wasserbad Julabo Shake Temp SW 22	Julabo Labortechnik, Seelbach, Germany

2.1.7 Software

ChipYard	DKFZ, Heidelberg Germany
GenePix Pro 6.1	Molecular Devices, Union City, USA
Ingenuity Pathway Analysis	Ingenuity System, Redwood City, USA
PALM Robo V4.	Zeiss Instruments, Munich, Germany
SDS 2.2.2	ABI, Foster City, USA
R 2.9.2	R Foundation, Viana, Austria

2.1.8 Solutions

2.1.8.1 Standard Solutions

Name	Compositions
SSC (20x)	3M NaCl, 0.3 M Sodium citrate, pH 7.0
PBS (10x)	137 mM NaCl 27 mM KCl 100 mM NaH_2PO_4 17 mM KH_2PO_4
TBS-T	20 mM Tris-Base 137 mM NaCl 3.8 ml 1M HCl 0.1% (v/v) Tween-20
SDS (10%)	10% SDS (w/v) dissolve in ddH_20
Tris (1M)	1M Tris base 1000ml ddH_20 pH 7.5
TE Buffer	10 mM Tris-Cl, 1 mM EDTA, pH 7.5

2.1.8.2 Microarray Solutions

Name	Compositions	
Blocking Mix (1X) (for blocking of unspecific hybridization)	Cot-1 DNA (1µg/µl) PolyA RNA (5µg/µ tRNA (10µg/µl)	12.5 µl 2.5 µl 3.75 µl
Slide blocking buffer	Ethanolamine 10% SDS 1M Tris (pH 9.0) H_2O	1.5 ml 5.0 ml 50.0 ml 448.5 ml
FBNC spotting buffer	Formamide 20 g/l nitrocellulose in DMSO 2.5 M betaine hydrochloride dd H_2O	2.50 ml 0.25 ml 2.00 ml 5.25 ml
Chip hybridization buffer	Formamide SSC (20X) SDS (10%) H_2O	25.0 ml 10.0 ml 10.0 ml 5.0 ml
Medium stringency washing buffer	SSC (20X) SDS (10%) dd H_2O	25.0 ml 10.0 ml 965.0 ml
High Stringency Washing Buffer	SSC (20X) SDS (10%) dd H_2O	2.5 ml 10.0 ml 987.5 ml
Post-wash buffer	SSC (20X) dd H_2O	2.5 ml 997.5 ml
Post-wash buffer/Tween	SSC (20X) Tween-20 dd H_2O	2.5 ml 0.5 ml 997.0 ml

2.1.8.3 Histology solutions for microRNA FISH and immunohistochemistry

Name	Compositions	
Hybridization buffer	Formamide	2.50 ml
	SSC (20X)	1.25 ml
	Denhards (50X)	0.10 ml
	Yeast tRNA(20 mg/ml)	0.05 ml
	Signal strand salmon	0.25 ml
	sperm DNA (10 mg/ml)	
	dd H_2O	1.10 ml
Pre-hybridization buffer	Formamide	25.0 ml
	SSC (20X)	2.5 ml
	dd H_2O	22.5 ml
Acetylation buffer	Acetic anhydride	0.450 ml
	HCl (12N)	0.375 ml
	dd H_2O	72.00 ml
Wash solution-1	SSC (20X)	7.00 ml
	Tween-20	0.07 ml
	dd H_2O	62.93 ml
Blocking buffer B1	1M Tris	100 ml
	NaCl	8.77 g
	dd H_2O	900 ml
Blocking buffer B1 plus	1M Tris	100 ml
	NaCl	8.77 g
	dd H_2O	900 ml
	10% Goat Serum	1.00 ml
	Tween-20	0.005 ml
Citrate buffer (10X)	Tri-sodium citrate	29.4 g
	dd H_2O	1000 ml
	pH 7.5	

2.1.9 Tumor Material and Patient Characteristics

18 human squamous cell lung carcinomas and normal lung tissues were laser capture microdissected and analyzed by gene expression oligonucleotide microarray and microRNA TaqMan Low Density Array analysis. Clinical data of the patients was obtained from the National Center for Tumor Diseases (NCT) in Heidelberg, Germany. The average age of the patients was 66 (range from 41 to 83) and the male/female ratio was 5:4. The use of the samples was approved by the local ethics committees and the diagnoses were evaluated by a pathologist. Clinical information for the tumors is listed in Table 5 and Table 6.

Table 5. Clinical stage of primary tumors in 18 squamous cell lung carcinoma patients.

Gender	
Male	10
Female	8
Average age (range)	66 (41-83)
Clinical stage	
IA	1
IB	8
IIB	3
IIIA	3
IIIB	3

18 squamous cell lung carcinomas collected for further analysis. Tumors were obtained from 8 female and 10 female with average age of 66. Clinical staging is based on AJCC Cancer Staging Manual (Greene et al., 2002)

Table 6. Clinical data of each squamous cell lung carcinoma patient.

Patient No.	TNM	AGE	Gender	Note
1. 1317	pT2N2M0G2R0	58	M	Chemotherapy
2. 2490	pT2N1M0G3R0	72	F	
3. 1316	pT2N0M0G2R0	70	M	
4. 1219	pT2N0M0G3R0	60	F	
5. 1219	pT2N0M0G3R0	60	F	
6. 2496	pT2N0M0G2R0	74	M	
7. 2505	pT3N1M0G2R0	41	M	
8. 1299	pT4N0M0G3R0	64	M	Metastasis
9. 2269	pT4N0M0G3R2	78	F	
10. 1209	pT3N0M0G2R0	48	F	
11. 2275	pT4N1M0G3R1	56	M	
12. 1331	pT2N0M0G3R0	83	F	
13. 1404	pT2N0MxG3	74	M	
14. 1297	pT1N0M0G2R0	69	F	Metastasis
15. 2502	pT3N1M0G3R1	64	M	
16. 2690	pT2N0MxG3R0	70	M	
17. 1417	pT2N0MxG3R0	77	F	
18. 1418	pT2NxMxG3N0	71	M	

The table shows the patients information with patient number, TNM stage, age and gender. The TNM stage is based on AJCC Cancer Staging Manual (Frederick et al., 2002). Primary Tumor (T): TX, Primary tumor cannot be evaluated; T0, No evidence of primary tumor; Tis, carcinoma in situ (early cancer that has not spread to neighboring tissue); T1, T2, T3, T4, Size and/or extent of the primary tumor. Regional lymph nodes (N): NX, Regional lymph nodes cannot be evaluated; N0, No regional lymph node involvement (no cancer found in the lymph nodes); N1, N2, N3, Involvement of regional lymph nodes (number and/or extent of spread). Distant metastasis (M): MX, Distant metastasis cannot be evaluated; M0, No distant metastasis (cancer has not spread to other parts of the body); M1, Distant metastasis (cancer has spread to distant parts of the body). Tumor grade: GX, Grade cannot be assessed (Undetermined grade); G1, Well-differentiated (Low grade); G2, Moderately differentiated (Intermediate grade); G3, Poorly differentiated (High grade); G4, Undifferentiated (High grade). (Greene et al., 2002)

2.2 Methods

2.2.1 Tissues and Serial Slides Preparation

Primary squamous cell lung carcinoma samples were obtained from the Thorax Clinic, affiliated with the University of Heidelberg, Germany. Tissue samples were immediately cryopreserved in a -80°C freezer post-operative. Paraffin-embedded squamous cell lung carcinoma tissues were obtained from the tumor bank of The National Center for Tumor Diseases (NCT) in Heidelberg. All of the 4 µm paraffin tissue sections of squamous cell lung carcinoma for immunohistochemistry and microRNA FISH were prepared by the tumor bank of the National Center for Tumor Diseases (NCT) in Heidelberg. All tissues tissue sections were analyzed histologically and characterized by a pathologist.

Cryopreserved tissues were imbedded into Jung Tissue Freezing Medium using a dry-ice/ethanol bath. Embedded frozen tissue blocks were fixed on the tissue holder and trimmed in order to gain access to the tumor tissue. For test experiments, the tumor tissues were sliced at 15µm using a cryotome. For the actual analysis, tumor tissues were perpendicularly punched three times using a needle, 0.5mm in diameter, beginning at the trimmed surface. Thereafter, these holes were used as physical reference markers for the orientation and re-identification of tumor cells in each individual cryosection. Next, serial sections were cut (Section1: 35µm; Section2: 8µm, Section3: 35µm; Section4: 35µm; Section5: 8µm, Section6: 35µm). The 8 µm slides were used for hematoxylin and eosin staining; the 35 um slides were used to prepare total RNA for microarray and Taqman expression analysis. All of the 35µm sections were treated with ice cold 100% ethanol for 3 minutes, dried for 2 minutes, then tightly sealed and stored in a 50ml Falcon tube at -80°C. Normal lung tissues were cryoperserved in

a similar manner but without hole punching. For test experiments, consecutive 15 µm lung tumor sections were prepared in the same way as normal lung tissues cryosectionsections. All the sections used for laser capture microdissection were attached on Membrane Slides (NF1.0, PEN), all the reference sections were attached on normal glass slides. The procedure for serial cryosectioning is shown in Figure 5.

.

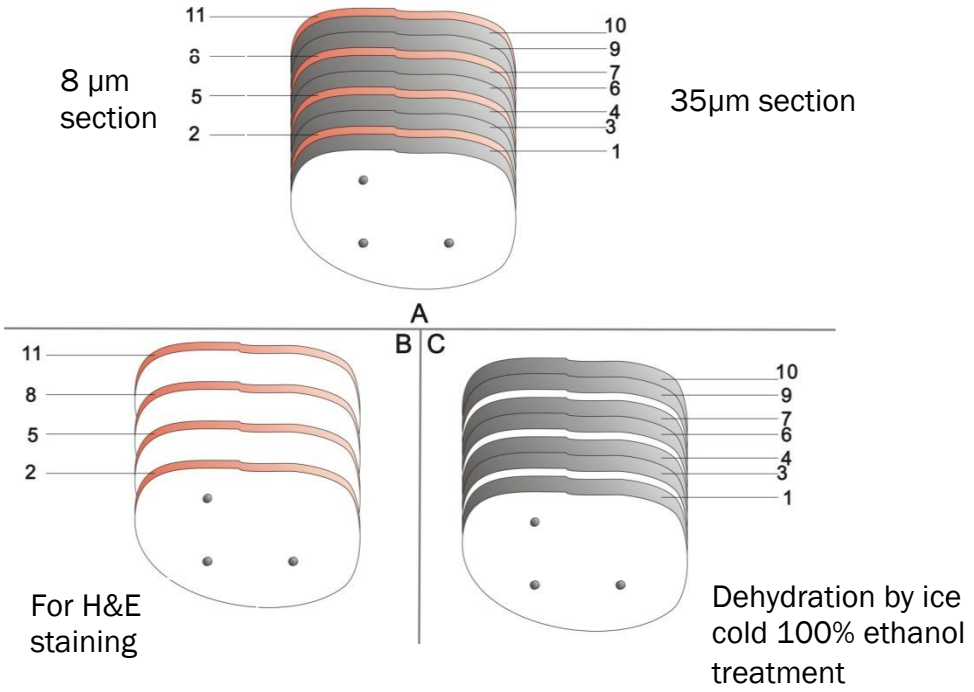

Figure 5. Scheme of serials cryosections. A. Fresh frozen tissue was punched with three holes and serials sections made. B. Sections marked with red color were saved for H&E staining as reference sections. C. Sections marked with black color were treated with 100% ethanol for 3 minutes, then air-dried and stored until use at -80°C.

Normal hematoxylin and eosin staining was performed as described below. The reference tissue sections were first incubated in xylene for 5 minutes, thereafter twice in 100 % ethanol and once in 70% ethanol, both for 1 minute, followed by a tap water rinse for 5 minutes. Thereafter, the tissue sections were stained with hematoxylin for 4 minutes, washed in tap water for 15 minutes, and then counterstained with eosin solution for 1 minute, followed by a 5 minute tap water

washing. In order to dehydrate the sections, the slides were quickly passed through 70% and 100% ethanol and then incubated in 100% ethanol for 2 minutes. Finally, the tissue sections were incubated in xylene for 2 minutes and mounted with cover slips.

In the past, RNA preserved staining protocols have been developed and applied to target cell populations in laser microdissection, but certainly, any staining step might decrease RNA quality. To compare the RNA qualities of microdissected samples from unstained cryosections and RNA preserved hematoxylin and eosin stained cryosections, the two types of slides were prepared for later laser capture microdissection. RNA preserved hematoxylin and eosin staining was performed as following: 15 µm cryosections were cut on the Membrane Slide (NF 1.0 PEN) and then dried for 3 minutes in the cryostat. The slides were then directly transfered to 70% ethanol for 1 minute, hematoxylin for 3 minutes, 70% ethanol three times for 1 minute, eosin staining for 1 minute, then 70%, 90%, and 100% ethanol, each for 1 minute. The previous staining was carried out in an ice bath. After 100% ethanol incubation, the stained slides were air-dried for 3 minutes and placed in a 50 ml Falcon tube by -80°C for future microdissection. The unstained cryosections from the same tumor tissue were cut at 15 µm onto the MembraneSlide (NF 1.0 PEN) and then dried for 3 minutes in the cryostat. The slides were directly put in ice cold 100% ethanol for 3 minutes and then air-dried for 3 minutes at room temperature. The slides were then stored in a 50 ml Falcon tube by -80°C until capture microdissection.

2.2.2 Laser capture microdissection

2.2.2.1 Laser capture microdissection for stained and unstained test cryosections

The Falcon tubes containing the frozen 15µm slides were shortly brought to room temperature just before laser capture micro-dissection. On the PALM Robo V4 laser microdissection program, the cutting energy value was set at 80, speed value was set as 60 and the same regions (about 250,000 μm^2) from unstained cryosetions and RNA preserved hematoxylin and eosin stained cryosections were microdissected and catapulted into different AdhesiveCap 500 opaque tubes by the P.A.L.M. MicroBeam instrument. 30 µl of QIAzol lysis reagent was added to the small pieces of captured tissue and samples were preserved at -80°C.

2.2.2.2 Consecutive test of microdissection

The T7-based RNA-amplified oligonucleotide microarray platform was previously established in our laboratory (Schlingemann et al., 2005), but testing was still needed to see whether this platform was suitable, and reproducible, in combination with laser capture microdissection technology. Therefore, the analysis of 15 µm serial sections of normal tissue was initially performed in order to test the reproducibility and reliability of our laser capture mirodissection and oligonucleotide microarray system. The laser capture microdissection procedure was perform as previously described, but, in this experiment, the same regions of 600X800 µm were microdissected on each of the serials test slides, captured and the consecutive cryosections were given the designations A-F. The dissected tissue from slides A, B, C … (Figure 6) were captured and frozen in a AdhesiveCap 500 opaque tube with QIAzol Lysis Reagent and evaluated by oligonucleotide microarray analysis to determine the reproducibility of the technique.

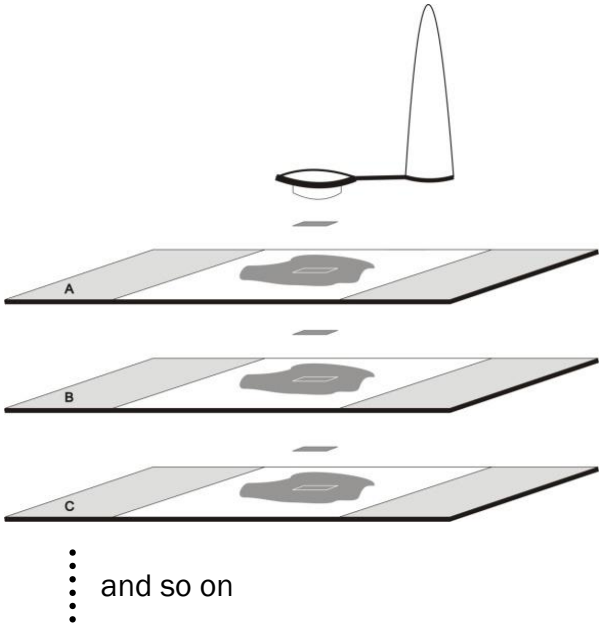

Figure 6. Scheme of consecutive microdissection for testing of reproducibility. Consecutive preserved RNA sections, A, B, C were microdissected from the same regions and harvested for oligonucleotide microarray analysis.

2.2.2.3 Punch aided serial laser capture microdissection

For normal lung, the unstained lung tissue cryosections were randomly cut without punch aided LCM. For dissection of tumor tissue containing adjacent lung tissue, punch aided LCM was carried out as follow: Every second H&E stained reference slide was first placed on the mechanical stage of the microscope and a complete image of the slide was scanned. The tumor and adjacent tissue morphology could easily be assessed on the microscope by H&E staining. Then the three reference points were marked in the middle of the punched circles. Next, three dissection areas, the tumor center (the tumor cell population 1000 µm away from the leading edge of the tumor tissue, toward the middle of the tumor), tumor invasion front (tumor cells located within 500 µm of the leading edge of the tumor tissue, on the tumor tissue side) and adjacent lung tissue (cells located over 500 µm away from the leading edge of the tumor away from the

tumor tissue side) were marked by different cutting elements by the microdissection software. All of the cutting elements and reference points were set to be in one group on the PALM Robo V4 software. Thereafter, the consecutive 35 µm cryosections were shortly incubated at room temperature and then placed on the mechanical stage of the microscope. Using the PALM Robo V4 program, the three reference points were marked as the reference slides and set as a group on the 35 µm cryosections. Finally, by matching the elements from the reference slides with the guide from the three reference points, the cutting elements were oriented on the unstained slides and the tissue areas were captured by Laser Microdissection and Pressure Catapulting (LMPC). The catapulted unstained areas were transferred to AdhesiveCap 500 opaque tubes. The cutting energy value was set as 90; the cutting speed was set as 65. A summary of the procedure is shown in Figure 7.

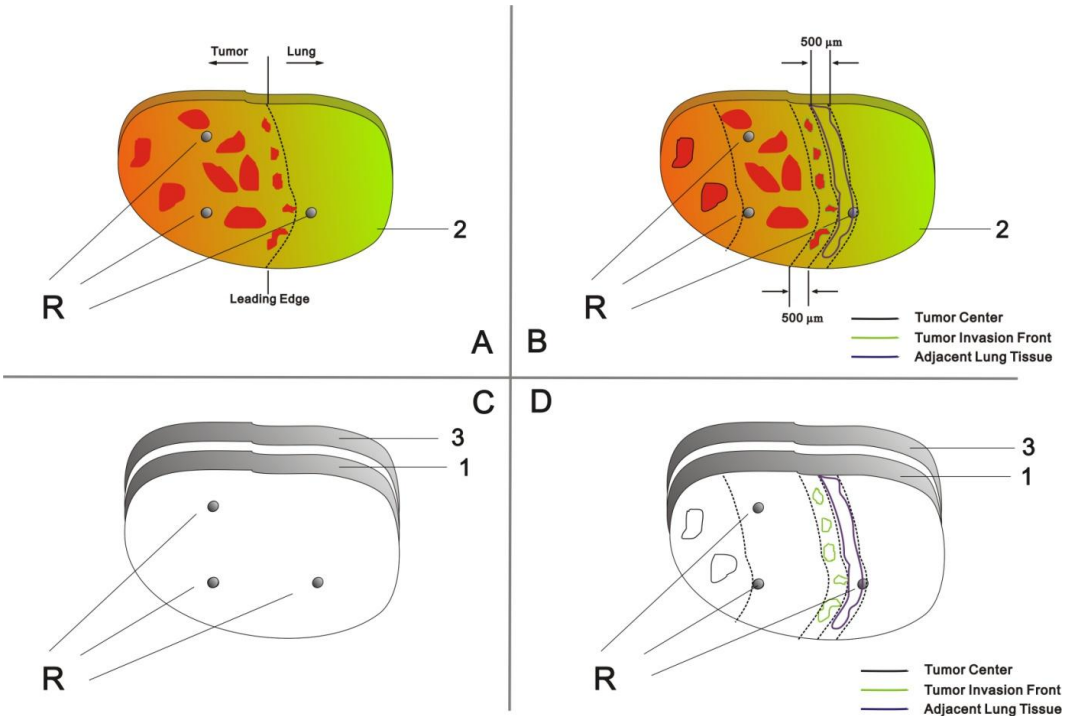

Figure 7. Scheme of punch aided laser microdissection. A. Each reference section was stained as a reference section; the tumor region and the adjacent lung tissue region are visible. The red regions show the tumor cell populations.. B. Marking of the cutting elements on the PALM Robo V4 software. C. Unstained targets of the first and the third sections. Only the reference points are visible. D. In the target sections, the three reference points are matched to the reference sections, and then the target cell populations are excised. R: Reference points; 1, 3: the first and the third target sections; 2: the second section is a reference section.

2.2.3 RNA Extraction from LCM Samples

In order to obtain small amounts of total RNA from microdissected tissue, which also contained small sized RNAs (i.e. microRNAs), the Qiagen miRNeasy Kit protocol was modified by replacing RNeasy Mini columns with RNeasy MinElute columns. For RNA purification, the frozen tissues contained in a small amount of QIAzol lysis buffer were collected into different Eppendorf tubes, each tube representing different of cell populations. Extra QIAzol lysis reagent was then added to a total volume of 350 µl. The lysed cell suspensions were vortexed for 1

minute and then placed onto a 42°C heating block for 20 minutes. Thereafter, 70 µl of chloroform was added to the tubes and the tubes were shaken for 15 seconds. Then the tubes containing the homogenate were left at room temperature for 2–3 min, followed by centrifugation for 15 min by 12,000 g at 4°C. The upper aqueous phase was transferred to a new collection tube. 260 µl of 100% ethanol was then added and mixed, and the mixtures were transferred to RNeasy MinElute spin columns and centrifuged for 15 seconds at 1300 rpm. Column washing was performed by first adding 350 µl buffer RWT to the column, followed by centrifugation at 1300 rpm for 15 sec. Thereafter, an on-column DNase digest (27 units/column) was performed for 15 minutes at room temperature, followed by a second wash with 350µl Buffer RWT (full speed for 15 seconds) and two final washes with 500 µl buffer RPE (first by 13,000 rpm for 15 seconds, second for 2 min). The column was dried by centrifugation at 13,000 rpm for one minute without any liquid additions. The RNeasy MinElute spin columns were then placed in a new 1.5 ml collection tube, and the RNA eluted with 14 µl RNase-free water.

2.2.4 Total RNA and small RNA Quality Control

High RNA quality is a key factor for gene expression profiling experiments, so RNA quality was analyzed using an Agilent Bioanalyzer. The Agilent Bioanalyzer is a chip based capillary electrophoresis apparatus that allows the separation of small amounts of total RNA (200-5000 pg) and identification of the ribosomal RNA by fluorescence staining. The Agilent 2100 BioAnalyzer with RNA 6000 Pico LabChip Kit and small RNA Kit were used according to the manufacturers' protocol.

2.2.5 T7-based Amplification of cDNA and Klenow Labeling (TAcKLE)

Due to the low amount of total RNA from the LCM samples, the TAcKLE protocol was used to amplify sufficient amounts of RNA. TAcKLE utilizes mRNA amplification by in vitro transcription of cDNA, and fluorescent labeling by Klenow fragment. Initial mRNA is copied using a RNase H− Moloney murine leukaemia virus reverse transcriptase, using a modified oligo(dT)-primer which incorporates the promoter sequence of phage T7 RNA polymerase. RNase H treatment of the resulting heteroduplex creates RNA fragments that prime second-strand synthesis by *E.coli* DNA polymerase I. Repeated transcription from the T7 promoter on the cDNA template results in multiple copies of aRNA. Finally, aRNA is reverse transcribed into sense cDNA and used as template for Klenow fluorescence labelling, yielding mainly fluorescent antisense cDNA as a suitable target for oligonucleotide libraries oriented, in sense (Schlingemann et al., 2005).

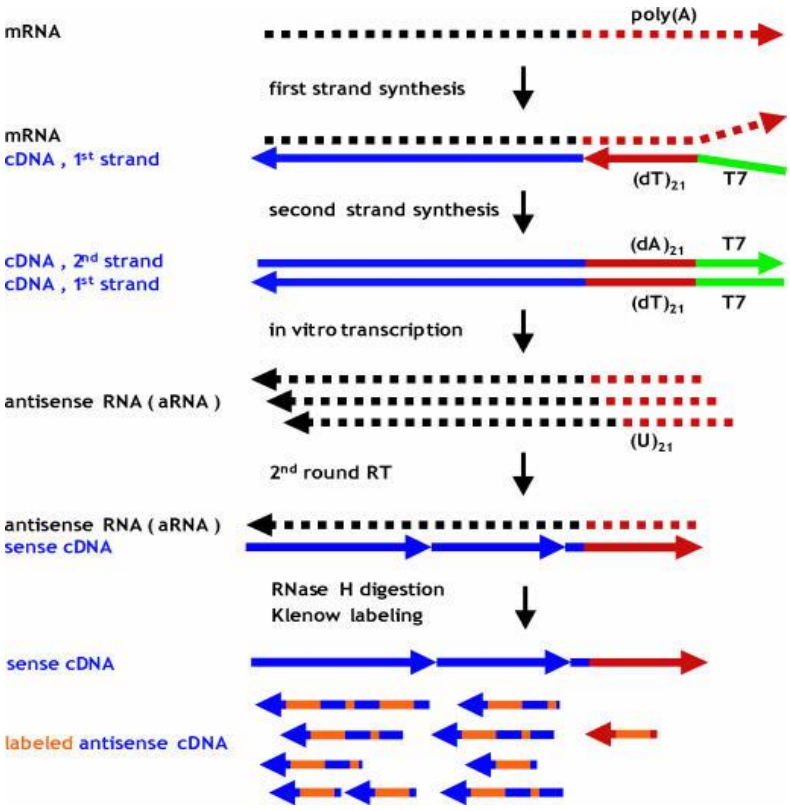

Figure 8. Schematic overview of the TAcKLE protocol. In the TAcKLE protocol, mRNA is linearly amplified by in vitro transcription ('T7 amplification'). The resulting aRNA is subsequently converted to cDNA and labelled by dye-dUTP incorporation using Klenow fragment.

2.2.5.1 First round amplification

For each first round amplification experiment, 25 ng of total RNA (both sample RNA and Universal Human Reference RNA) was loaded to initiate the first reverse transcription experiment.

2.2.5.1.1 Reverse transcription

5µl (25ng) total RNA (both samples and references RNA) and 1µl (dt)-T7 primer (100ng/µl) mix were denatured at 70°C on a heating block and then chilled on ice. Thereafter, the reverse transcription master mix containing 2 µl M-MuLV RT buffer, 0.5 µl 10mM dNTP, 0.5µl 5 mg/ml T4gp32, 0.5 µl RNAzin and 0.5 µl RevertAid reverse transcriptase were added. The total reaction mixture was

incubated at 50°C for 1 hour, followed by incubation at 65°C for 15 minutes and then at 4°C.

2.2.5.1.2 Second strand synthesis

The second strand synthesis master mix was pipetted and mixed on ice as follows: 15 µl 2nd strand buffer (5X), 10 mM dNTP for 1.5 µl, 2.22 µl DNA polymerase I (9 U/µl), 0.1 µl RNase H (10 U/µl), 0.5 µl DNA ligase (10 U/µl) and 45.68 µl RNase-free water. The total volume of this single master mix was 65 µl. The reverse transcription solution from the previous procedure was mixed with the second strand synthesis master mix, and then incubated at 15°C for 2 hours. Thereafter, 3.33 µl T4 DNA polymerase (3U/µl) was added to the solution and incubated for 15 minutes at 15°C, then heat inactivated at 70°C for 10 minutes. To wash salts and organic compounds out of the resulting double strand cDNA, the resulting mixture was extracted with 75 µl phenol-chloroform-isoamylalcohol (25:24:1), then centrifuged 5 minutes by 13,000 rpm at room temperature in a PLG heavy tube. In order to elute the purified cDNA, the upper phase in the PLG heavy tube was added to a prespun P-6 MicroSpin column and centrifuged for 4 minutes at 3500 rpm using a microfuge at room temperature.

2.2.5.1.3 In vitro transcription

Initially, the eluted cDNA solution was precipitated at -80°C for 1 hour in 220 µl ethanol with 3.5 µl NaCl (5M) and 1 µl Linear polyacrylamide (5µg/µl). The solution was then centrifuged at 13,000 rpm for half an hour at room temperature, the supernatant removed, the pellet washed with 500 µl of 70% ethanol, then centrifuged for 5 minutes at 13,000 rpm and the previous washing step repeated. Thereafter, the supernatant was completely removed, the pellet

was air-dried for 3 minutes at room temperature and then taken up in 10 µl RNase free water. The in vitro transcription experiment was performed using the RiboMAX Large Scale RNA Production System kit. The in vitro transcription master mix was prepared at room temperature as follows: 3 µl of each ATP, CTP, GTP, UTP; 8 µl of RNase free water; 8 µl of T7 transcription buffer (5X); and 4 µl of T7 Enzyme Mix. 10 µl of the second strand solution was added to the in vitro transcription master mix, and mixed well by gentle vortexing at room temperature. The mixed reaction solution was incubated for 10 hours at 37°C.

2.2.5.1.4 aRNA cleanup

The aRNA cleanup experiment was carried out using a Qiagen RNeasy Mini Kit. 40µl of the in vitro transcription product was added to 430 µl buffer composed of 350 µl RLT buffer, 76.5 µl RNase free water and 3.5 µl ß-mercapto-ethanol and mixed well. 250 µl of 100% ethanol was added to the previous solution and then applied to a RNeasy Mini column and micro-centrifuged at 9900 rpm for 15 seconds. The flow-through was discarded. The column was washed with 500 µl RPE buffer at 9900 rpm for 15 seconds, centrifuged at 13,000 rpm for two minutes at room temperature. This washing was repeated twice. The washed column was transferred to a new 2 ml collection tube and centrifuged at 13,000 rpm for 1 minute in order to remove residual buffer. The 2 ml collection tube was then discarded, the dried column was transfer to a new 1.5 ml collection tube and the total RNA was eluted with 30 µl RNase free water by centrifugation at 9900 rpm for 1 minute and repeated once. The eluted total RNA was precipitated at -80°C for 1 hour in 150 µl ice cold ethanol with 30 µl ammonium acetate solution (7.5 M) and 1 µl Linear polyacrylamide (5µg/µl). Thereafter, the tube was centrifuged at 13,000 rpm for half an hour at 4° C, the supernatant removed,

and the pellet washed with 500 µl ice cold 70% ethanol. The sample was centrifuged again for 5 minutes at 13,000 rpm/ 4°C and the previous washing step was repeated. Thereafter, the pellet was air-dried for 3 minutes at room temperature and then dissolved in 6 µl RNase free water. The concentration of total RNA was measured by a Nanodrop ND -1000 spectrometer.

2.2.5.2 Second round amplification

To initiate the second round of amplification, 300 ng aRNA (both sample and reference RNA) derived from the first in vitro transcription was applied for a second round of reverse transcription. The second round of amplification was carried out in a very similar way as the first round, except for small differences in reverse transcription and second strand synthesis. In the reverse transcription step, the 300 ng aRNA was denatured together with a N6 random primer instead of a T7-primer. The incubation procedure for the second round reverse transcription was performed sequentially using the following conditions: 37°C for 20 minutes, 42°C for 20 minutes, 50°C for 10 minutes, 55°C for 10 minutes, 65°C for 15 minutes, hold at 37°C for 5 minutes, add 1 unit RNase H, 37°C for 30 minutes, 95°C for 2 minutes, and finally cooled at 4° C. For the second round second strand synthesis, the 64 µl master mix which contains: 15 µl of 2nd strand buffer (5X), 1.5 µl of 10 mM dNTP, 2.22 µl of DNA Pol. I (9 U/µl), 0.1 µl of RNase H (10 U/µl) and 45.18 µl of RNase free water, was pipetted and mixed well. An important step in this second strand synthesis is that the cDNA products have to be denatured at 42 °C for 10 minutes and then chilled on ice with 100 ng oligo(dT)-T7 Primer, which was not present in the second strand synthesis step of the first round of amplification. The procedures for the second round amplification are the same as the first round.

2.2.5.3 cDNA Klenow labeling

After two rounds of amplification, 2µg of the amplified aRNA (both sample and reference RNA) were added for a third round of reverse transcription. The single strand cDNA product of the reverse transcription was then fragmented and labeled using the Klenow labeling system. The third round of the reverse transcription protocol was exactly the same as the second round reverse transcription. The 10µl cDNA from the third round reverse transcription was cleaned up and then added to the following mix: 40 µl of random primer solution (2.5X), 10 µl of dNTP (for Klenow labeling), 3 µl of Cy3/Cy5 labeled dUTP, 34 µl dd H_2O. The solution was mixed, 3 µl of Klenow fragment was added and the solution was mixed again. The total solution (100 ul) was incubated at 37°C for 16 hours.

2.2.6 Labeled sample clean up and labeling efficiency control

The 100µl of the sample was mixed with 350µl TE buffer and transfered to Microcon YM-30 Spin-columns. The Microcon columns were then centrifuged for 12 minutes by 13000 rpm at room temperature. The Microcon columns were washed with 450µl TE buffer, then centrifuged for 11 minutes at 13000 rpm at room temperature. 432µl TE buffer was added,, mixed well, and an aliquot was taken to measure the labeling efficiency using a Nanodrop spectrometer. 37.5 µl blocking mix was added into the Microcon columns and centrifuged for 15 minutes at13000 rpm in room temperature. The Microcon columns were placed upside down on a new collection tube, and centrifuged for 5 minutes in 6000 rpm at room temperature to harvest the labeled samples.

2.2.7 Preparation and post-processing of microarrays

Synthetic 70mer oligonucleotides ('Human Genome Oligo Set Version 2.1; consisting of 21,329 oligonucleotides representing human genes and transcripts plus 24 controls, as well as 'Human Genome Oligo Set Version 2.1 Upgrade', consisting of 5462 human 70mer probes) were dissolved in FBNC spotting buffer at 40 µM, using a MiniTrak robotic liquid handling system. DNA spotting was performed in duplicate on QMT epoxysilane coated slides using an OmniGrid Microarrayer equipped with Stealth SMP3 Micro spotting pins. Spot centers were 129 µm apart. DNA adhesion to the glass surface was accomplished by 1 h incubation at 60°C, followed by ultraviolet (UV) irradiation (2 x 120 mJ/cm2 at 254 nm) in a Stratalinker Model 2400 UV illuminator. Just prior to hybridization, the slides were washed for 2 min in 0.2% SDS (w/v), 2 min in ddH_2O at room temperature and 2 min in hot ddH_2O (95°C), followed by 3 min centrifugation at 2000 rpm.

2.2.8 Chip hybridization

2.2.8.1 Sample preparation

For the test experiments, the eluted samples were color switched with each other (cy3/cy5) and taken up in 520µl hybridization buffer (see Figure 9). For the actual experiments, the eluted samples were color switched with references in cy3/cy5 and combined together in 520µl hybridization buffer (see Figure 10). All the mixed solutions were incubated first for 30 minutes at 60°C and then for 10 minutes at 70°C in a thermo shaker at 750 rpm.

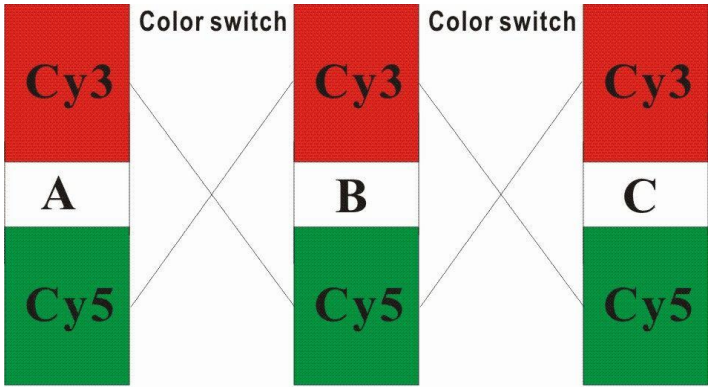

Figure 9. Color switch between samples with Cy-3/Cy-5 for test experiment.During the color switch the A labeled Cy3 was mixed with B labeled Cy5, and vise versa. A, B and C are laser microdissected samples from the same regions of consecutive sections (see Figure 6 in section 2.2.2.2).

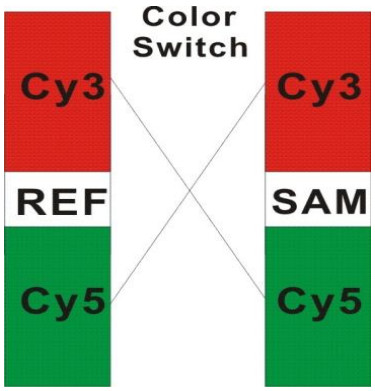

Figure 10 Color switch of sample against reference with Cy-3/Cy-5. During the color switch the sample labeled with Cy3 was mixed with reference labeled with Cy5, and vise versa. All the micro-dissected samples for actual experiments were color switched with references from the same Human Universal Reference RNA.

2.2.8.2 Chip denaturing

Slide blocking mix was prewarmed at 50°C in a water bath. Well printed chips were selected and incubated for 20 minutes in blocking mix at 50°C in a water bath. Thereafter, the chips were incubated for 2 minutes in double distilled water at room temperature with gentle agitation. Each chip was dipped for 10 seconds in hot water (~95°C) and pulled out slowly. The dry chips were stored in boxes.

2.2.8.3 Sample loading

The hybridization oven, SureHyb-chambers and gasket slides were prewarmed to 40°C, and then the sample/hybridization buffer mix was loaded within the gasket ring. The chips were placed onto the loaded gasket slide with the array surface touching the sample/buffer mix. The top of the SureHyb-chambers were put into place, the chambers locked and hybridized for 23 hours at 42°C.

2.2.8.4 Chip washing

Three washing buffers, medium stringency buffer, high stringency buffer and post wash buffer, were prewarmed in Hauser-cuvettes at 35°C and and mildly shaken (45 rpm) in a water bath. After 23 hours of hybridization, the gasket slide/chip-sandwiches were disassembled and put in medium stringency buffer at room temperature. The gasket slides were removed from the chip and put in medium stringency buffer in prewarmed Hauser-cuvettes. The released chips were washed for 4 minutes in medium stringency buffer, 4 minutes in high stringency buffer, 2 minutes in post wash buffer at 35°C and 45 rpm in a shaking water bath. Thereafter, the chips were incubated for 30 seconds in post wash plus Tween buffer at room temperature. The chips were then centrifuged 6 minutes at 2000 rpm with the barcode upside down in a Falcon tube. Finally, the dried chips were stored in a box protected from light until scanning.

2.2.9 Chip scanning and data processing

An Agilent Microarray Scanner (Agilent Technologies) was used to document the fluorescent signals of DNA samples hybridized to the gene-specific sequences printed on the array. Scanning resolution was 5µm; Red and Green PMT is 100%.
The scanned raw data consisted of pixel intensity values, which have to be correlated to the individual spots of oligonucleotide DNA found on the array.

Therefore, based on the list of the DNA sequences on the slide, a formatted data set was assembled as a grid file. The grid file was then loaded on the software GenePix Pro 5.0 to match each scanned spot on the array. In the GenePix Pro 5.0 software, the fluorescent intensity was calculated for each spot, and pixels from the surrounding area were measured as background values. Spots with fluorescent intensity closer to, or lower than, the background could not be taken into account, but were automatically marked by the software. The full dataset was then exported and saved as a "GPR" file, which was analyzed using the limma package (Smyth, 2004) of the statistical software package R (www.r-project.org). After the image analysis, low quality spots were filtered and the background intensity corrected by normexp (Ritchie et al., 2007). Quantized normalization was applied between arrays. Differential expression was assed by limma using a reference design and estimating effects for the different locations. Venn diagrams were used for identifying overlaps between the genes differently expressed between the different locations.

Pathway analyses were generated through the Ingenuity Pathways Analysis software (www.ingenuity.com). Data sets between four locations, inner tumor, tumor invasion front, adjacent lung tissue, and normal lung were uploaded on the Ingenuity Pathways webpage. In the uploaded gene list, only the genes with fold change higher than 2 with adjusted P value lower than 0.05 were set as differentially expressed genes. The "core analysis" was performed in the Ingenuity program, and the results were generated based on the Ingenuity Pathways Knowledge Base.

2.2.10 Immunohistochemistry

The glass slide cuvette was preheated with citrate buffer in a steamer for 20 minutes, at the same time, the 4 µm paraffin sections were immersed in following solutions step by step for deparaffinization: 2 times in Xylol for 5 minutes, 2 times in 100% ethanol for 2 minutes, 96% ethanol for 2 minutes, 70% ethanol for 2 minutes and 1 minute in distilled water. After deparaffinization, the slides were put in the heated citrate buffer for 40 minutes in a steamer, and then the slides with the cuvette were cooled down to room temperature for ca. 15 minutes. The slides were washed in distilled-water for 1 minute and 2 times in TBS buffer for 5 minutes. A circle was drawn surround each tissue section using a Dako pen. Three drops of hydrogen peroxide (3%) were then added to the surface of the tissue section and incubate for 10 minute at room temperature, and thereafter, the slides were washed two times in TBS solution for 5 minutes. The primary antibodies were diluted in antibody diluents as following: APLNR, 1: 500; GIMAP7, 1:400; CCL19, 1:150; PTGES1,1:200; PTGER1, 1:500; PTGER2, 1:800; PTGFS, 1:500; PTGFR, 1:700. The diluted antibodies were dropped onto the surface of the tissue sections and incubated overnight at 4°C. The primary antibody solutions were removed from the slides, and the slides were then washed in TBS solution twice for 5 minutes. The secondary antibody application and detection was performed using the Dako Real system. Briefly, the biotinylated secondary antibody was dropped onto the tissue section surface and incubated for 15 minutes at room temperature. Thereafter, the biotinylated secondary antibody solutions (Dako REAL Detection Systems) were removed from the slides, and the slides were washed in TBS solution twice for 5 minutes. Thereafter, the streptavidin peroxidase solution (Dako REAL Detection Systems) was dropped

onto the tissue section surface and incubated for 15 minutes at room temperature. Following this incubation, the streptavidin peroxidase solution was removed from slides and then slides were washed in TBS solution twice for 5 minutes. Thereafter, the detection solution was added onto the surface of the tissue section and incubated ~ 5 minutes at room temperature. The slides were then placed into a cuvette with distilled water, immersed thereafter in 1% hematoxylin for 5 minutes and rinsed with tap water for a further 10 minutes. The stained slides were then dehydrated and mounted by the following steps: 15 seconds in 70% ethanol, 15 seconds in 96% ethanol, 1 minute in 100% ethanol, 2 minute in 100% ethanol and twice for 5 minutes in xylol. The slides were then dried and covered using Eukitt mounting medium.

2.2.11 microRNA TaqMan Low Density Array

To study the microRNA expression in the four different areas of lung tumor tissue, the microRNA TaqMan Low Density Array (TLDA)-based on Applied Biosystems' 7900HT Micro Fluidic Cards were used to detect and quantify mature microRNAs according to the manufacturer's instructions.

The TLDA Human MicroRNA Panel v1.0 card contains assays for 365 different human microRNAs. In addition, two small nucleolar RNAs (snoRNAs), RNU44 (SNORD44) and RNU48 (SNORD48), function as endogenous controls for expression data normalization. TLDA experiments were run in two steps: In the first step, multiplex reverse transcription, consisting of eight pre-defined reverse transcription primer pools containing up to 48 RT primers each, was performed using the TaqMan MicroRNA Reverse Transcription Kit. The master mix for each reaction of this reverse transcription was: 0.2 µl of dNTPs (100mM), 2 µl MultiScript Reverse Transcriptase, 1 µl RT Buffer (10X), 0.1 µl RNaser Inhibitor,

3.7 µl RNase free water. 12.5 ng of total RNA in 2 µl was added into the master mix and vortexed. 1 µl of the Mutiplex Reverse Transcription Human microRNA pools, from pool 1 to pool 8, were finally added to 8 reverse transcription mix. The reverse transcription reaction was incubated as follows: 16°C for 30 minutes, 42°C for 30 minutes, 85°C for 5 minutes and then cooled to 4°C. In the second step, eight RT pools containing cDNA template were diluted 62.5 fold, mixed with the TaqMan Universal PCR Master Mix at a ratio of 1:1, and then injected into eight filling ports of the TLDA card. The card was centrifuged for 2 minute at 1200 rpm in a Multifuge 3S to load the cDNA and master mix into the hundreds of small wells on the microfluidic card. The cards were then sealed and analyzed using the ABI Prism 7900 HT Sequence Detection System. The thermal cycling conditions were 2 min at 50 °C and 10 min at 95 °C, followed by 45 cycles of 30 s at 97 °C and 1 min at 59.7 °C.

2.2.12 microRNA TaqMan Low Density Array Data Processing

The microRNA data was normalized according to Vandesompele's method (Vandesompele et al., 2002) after calculating the median expression from duplicates. The ct-values were converted to relative expression values. Differently expressed microRNAs were identified by SAM (Significance Analysis of Microarrays) (Tusher et al., 2001). All calculations were conducted in R using the libraries siggenes (Schwender et al., 2006) and SLqPCR. The differentially expressed microRNA list was uploaded to the website of miRWalk (www.ma.uni-heidelberg.de/apps/zmf/mirwalk) and then the data package, which contained differentially expressed microRNAs and their validated target genes was generated. The expressions of microRNAs and their predicted targets were compared over all paired measurements by calculating the Pearson correlation

coefficient using the statistical software R (www.r-project.org). All correlations with a correlation coefficient below -0.6 and above 0.6 were further inspected using the R program.

2.2.13 MicroRNA fluorescence in situ hybridization

The slides were deparaffinized by the following steps: Rotihistol twice for 40 minutes, 100% ethanol twice for 5 minutes, 75%, 50%, 25% ethanol, each for 5 minutes, double distilled water twice for 5 minutes, 0.2 N hydrochloride for 5 minutes, PBS solution twice for 5 minutes. Next, the slides were deproteinized using the following method: protein kinase K (10 µg/ml) for 2.5 minutes, 0.2% glycine twice for 1 minute, PBS twice for 1 minute. The slides were then processed through postfixation steps using: 10% formaldehyde for 10 minutes and PBS twice for 5 minutes, followed by acetic anhydride for 10 minutes and washing 5 times for 4 minutes in PBS. The slides were then dehydrated in 70% ethanol, 90% ethanol and 100% ethanol, each for 5 minutes and air-dried for 5 minutes. 750 µl of hybridization buffer (see Section 3.8.3) was added to the slide and pre-hybridized in a humidified, light protected chamber in a 53°C oven for 3 hours. During this time, 1.6 µl of the LNA probe were mixed with 160 µl hybridization buffer, denatured at 80°C for 5 minutes and then chilled on ice. After 3 hours of pre-hybridization, the pre-hybridization buffer was removed from the slide and the denatured probe was spread onto the slides. The slides were then covered with a paraffin membrane and hybridized in a humidified light protected chamber in a 53°C oven over night (>16 hours). On the next day, the hybridization buffer was removed from the slides, and the slides were washed in washing solution 1 for 5 minutes at room temperature, 3 times in SSC buffer for 5

minutes at 65°C and then rinsed in 3 times in PBS buffer. The washed slides were then blocked in buffer B1 for 10 minutes followed by blocking buffer B1 Plus for 1 hour under mild shaking at room temperature. The blocked slides were hybridized with mouse-anti DIG antibody (1:200 dilutions) for 4 hours at room temperature and then washed three times with blocking buffer B1 for 3 minutes. Thereafter, the blocking buffer was removed and the slides were hybridized with Alexa 594 goat anti-mouse IgG (1:600 dilution) for 4 hours at room temperature. Thereafter, the slides were washed three times with blocking buffer B1 for 5 minutes followed by PBS for 5 minutes. The slides were dipped twice in double distilled water and the excess water was removed. Finally, the slides were mounted using cover slides with soft mounting medium containing DAPI.

3 Results

3.1 Laser capture microdissection

3.1.1 High quality RNA is yielded from unstained cryosections after laser capture microdissection.

Staining protocols designed to protect RNA for LCM and microarray analysis have been previously established to investigate gene expression profiling (Espina et al., 2006). However, total RNA quality is still a bottleneck for transcriptional profile experiments, especially using laser microdissected frozen tissue samples from patients. It appears obvious that any extra step, such as staining, would facilitate RNA degradation. To compare different protocols of protecting the total RNA quality of laser capture microdissected tissues, we isolated small pieces of tissue from RNA preserved hematoxylin and eosin stained cryosections and 100% ethanol treated unstained cryosections by laser capture microdissection, and then tested the quality of total RNA resulting from these two different protocols by the Agilent Bioanalyzer. In the unstained group, the RNA integrity numbers (RIN) are around 8.5, whereas the RNA protected hematoxylin and eosin stained samples are ~1 lower than the unstained group. RNA integrity numbers are ranked from 0 to 10, with 0 being the lowest integrity and 10 the highest. Therefore, the integrity of RNA from unstained 100% ethanol treated cryosections is higher than RNA protected hematoxylin and eosin staining (Figure 11 and 12).

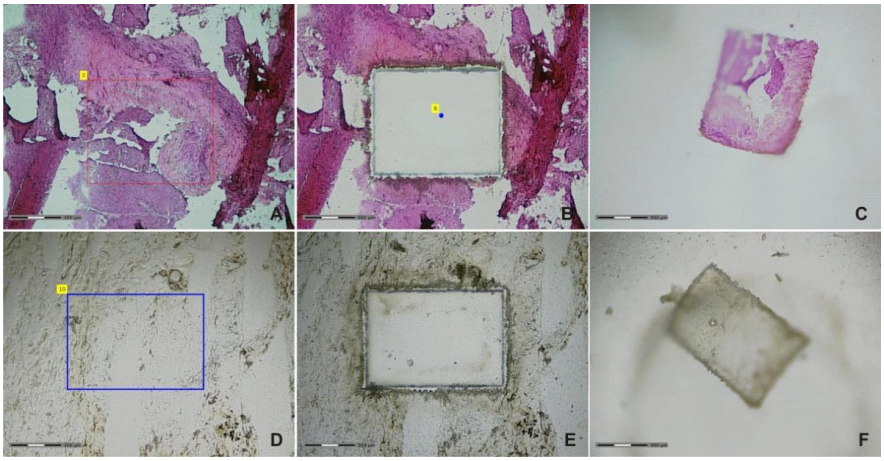

Figure 11. Laser capture microdissection from RNA protected hematoxylin and eosin stained- and unstained section. A, B, C, RNA protected hematoxylin and eosin stained cryosection; D, E, F, 100% ethanol treated unstained cryosection. A and D, cryosections before laser capture microdissection; B and E, cryosections after laser capture microdissection; C and F, microdissected tissues were captured on the cap of tube. Bar=300 µm

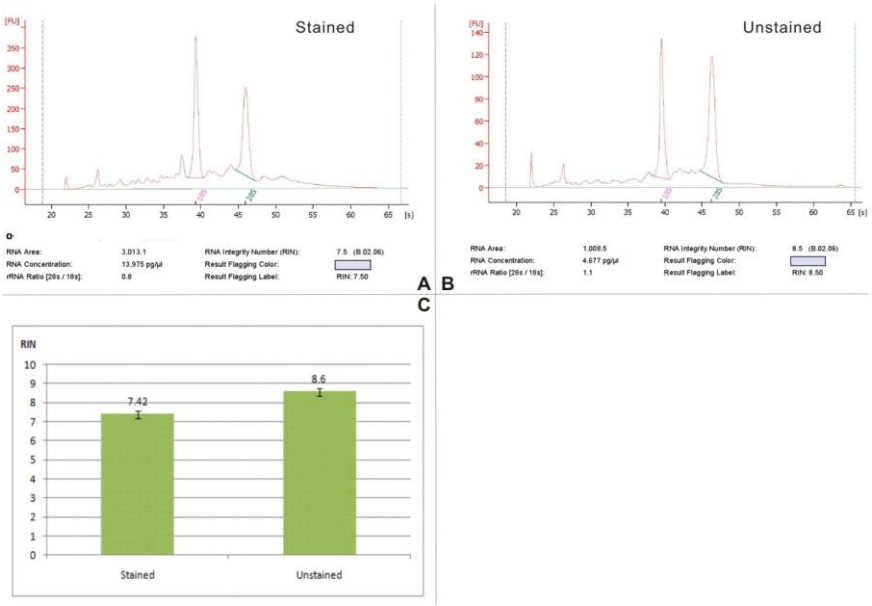

Figure 12. Total RNA from 100% ethanol treated unstained section have a higher integrity than hematoxylin and eosin stained sections. A. RNA integrity number (RIN) of one RNA sample from RNA protected hematoxylin and eosin stained sections (Agilent Bioanalyzer). RIN = 7.5; rRNA ratio[28S/18S] = 0.8; B. Agilent Bioanalyzer investigated RNA integrity number (RIN) of one RNA sample from 100% ethanol treated unstained sections. RIN = 8.5; rRNA ratio [28S/18S] = 1.1; C. Statistical comparison of the RNA integrity from 100% ethanol treated unstained cryosections showed higher values than RNA protected hematoxylin and eosin stained sections. Average value of RIN number for stained group is 7.42, whereas unstained group is 8.6, each group containing 5 cases of samples microdissected from the same 5 tumors.

3.1.2 Laser capture microdissection plus TAcKLE protocol and oligonucleotide microarray profiling are reproducible

The experiments in section 3.1.1., showed that total RNA with a high integrity was obtained from unstained sections. However, the laser capture microdissection only harvests a small portion of sample for RNA preparation. Therefore, RNA amplification using the TAcKLE protocol was established and proved to be a reliable method for RNA amplication and oligonucleotide microarray analysis. To test its reproducibility, we made a series of serial cryosections and then microdissected the same tissue regions (Figure 13). We then pooled the microdissected tissue as described in section 2.2.3 and extracted total RNA for amplification followed by oligonucleotide microarray analysis. The raw chip data were uploaded into the in-house developed ChipYard program for bioinformatic analysis. In ChipYard, the Pearson correlation coefficient of fluorescence intensities from individual spots was high for RNA from consecutive sections. As we could assume that the laser microdissected tissues from consecutive sections of the same region are homogeneous, the results of plotting showed that the Cy3 and Cy5 channel intensity was almost of equal value (Figure 14 A, B) which reflects a reliable laser capture microdissection, RNA amplification and consistent labeling with both Cy5- and Cy3-dUTPs. Data from Chip 1 Cy3 and Chip 2 Cy5 channels were plotted in one graphic. Since Chip 1 Cy3 and Chip 2 Cy5 channels are from the same original samples, all the data points are centrally localized in a small region (Figure 14 C). This scatter plot proves that the two chips are well correlated, and the integrated platform is reproducible.

In TAcKLE amplification, all dye labeling reactions using Klenow fragment were made from separately amplified RNA aliquots. One round of RNA amplification

resulted in approximately 10^3 fold amplification of starting mRNA and two rounds amplification yielded up to 10^5 fold of the starting amount, as determined by spectrophotometry based on an estimated initial mRNA content of 2%.

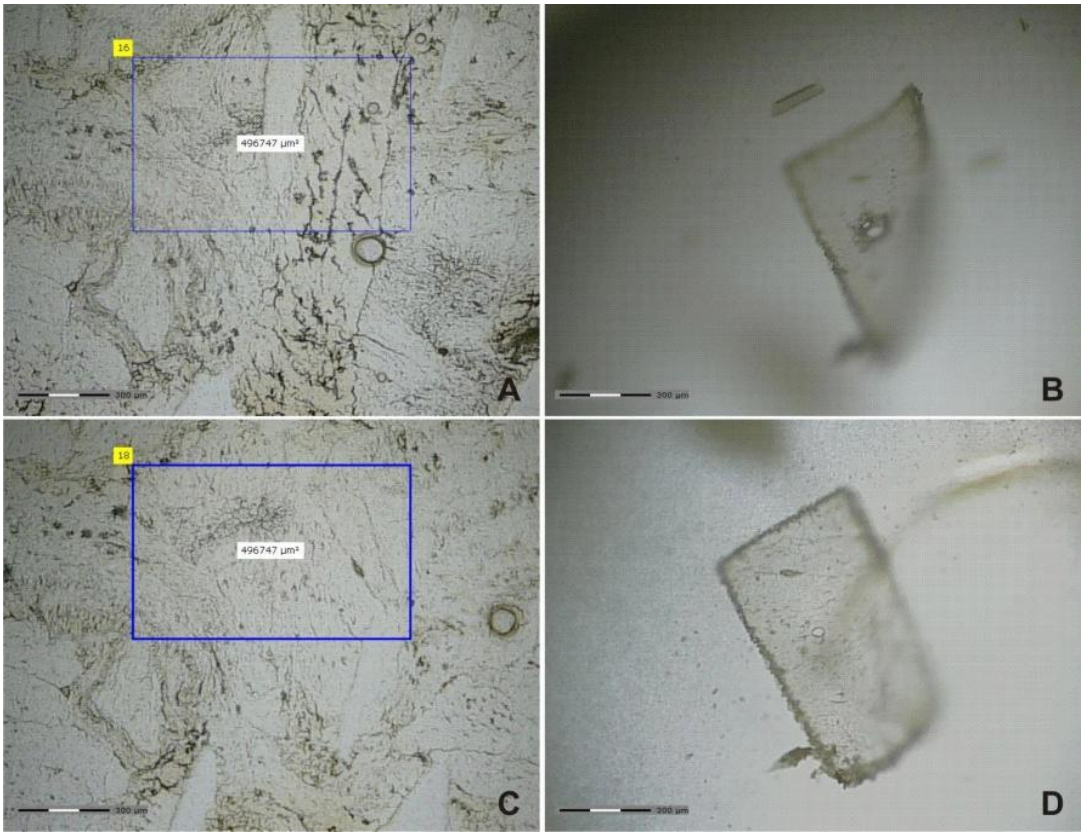

Figure 13. The consecutive unstained cryosections were microdissected, and captured from the same tissue region. A, C, unstained sections before microdissection, the blue area shows the same region of the two consecutive sections to be dissected. B, D, the dissected tissues captured on tube caps.

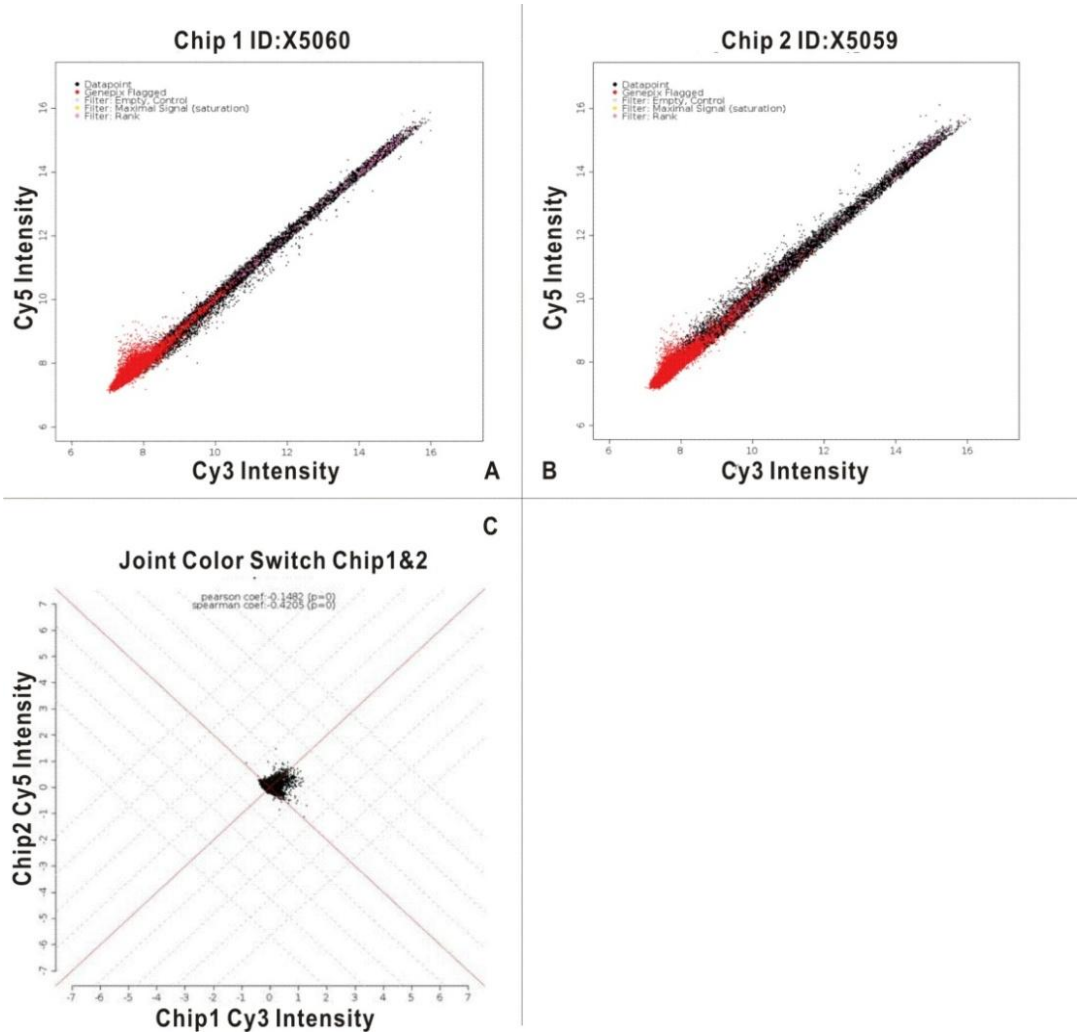

Figure 14. Scatter plots of fluorescence intensities after two rounds of amplification and labeling reactions. Co-hybridizations of independently amplified total RNA from consecutive sections were used to assess the reproducibility of amplification and laser capture microdissections. A. Color switch scatter plot of sample A with Cy3 and sample B with Cy5. The data plotting shows that the intensity of Cy5 and Cy3 are similar. B. Scatter plot of color switch of sample A with Cy5 and sample B with Cy3. The data plotting shows that the intensities of Cy3 and Cy5 are similar: C. Joint color switch showing the two color channels from sample A but from different chips, the scatter plot presents a good correlation of signals.

3.1.3 Punch aided laser capture microdissection samples yield total RNA with high quality

RNA is a very unstable molecule and offen degraded by remaining RNases under humid conditions. In laser capture microdissection experiments, we need to stain the target cells and capture them, but the staining protocols often accelerate RNA degradation. To yield high quality total RNA for transcriptional analysis of target cells, we developed punch aided laser capture microdissection to target and capture 4 zones in tissue sections: inner tumor cells, tumor invasion front cells, adjacent lung cells and normal lung cells. The procedure was described in section 2.2.2.3. and showed that by using the three punching holes for orientation it was possible to localize the target areas on the unstained slides by matching the cutting elements from the adjacent consecutive stained sections. The targeted cells were precisely dissected and captured on the caps of microfuge collection tubes (Figure 15). The total RNA extracted from the target cells showed high integrity upon analysis using the Agilent Bioanalyzer (Figure 16), illustrating that punch aided laser capture mcirodissection proved a novel methodical tool to collect specific cell populations for transcriptome analysis.

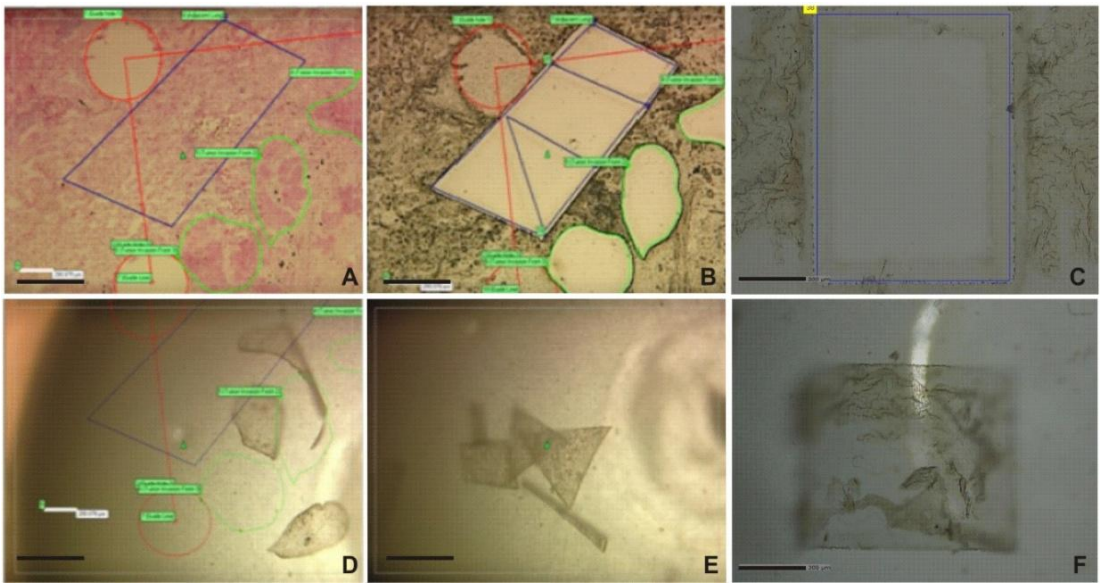

Figure 15. Punch aided laser capture microdissection harvest target cell populations. A. Reference sides with hematoxylin and eosin staining. The red circle shows the two reference points; the third reference point is outside of the microscopic field. The green circle marks the targeted tumor invasion front cell populations and the blue area marks the adjacent lung tissue. B. The cutting elements were matched to the target slides guided by the reference points. The target cell populations in the tumor invasion front and adjacent lung were removed from the cryosections. C. Normal lung cell were removed from the cryosection. D, E, F. The tumor invasion front cells populations, adjacent lung cells and normal lung tissue was captured in a cap of a tube. Bar = 300 µm.

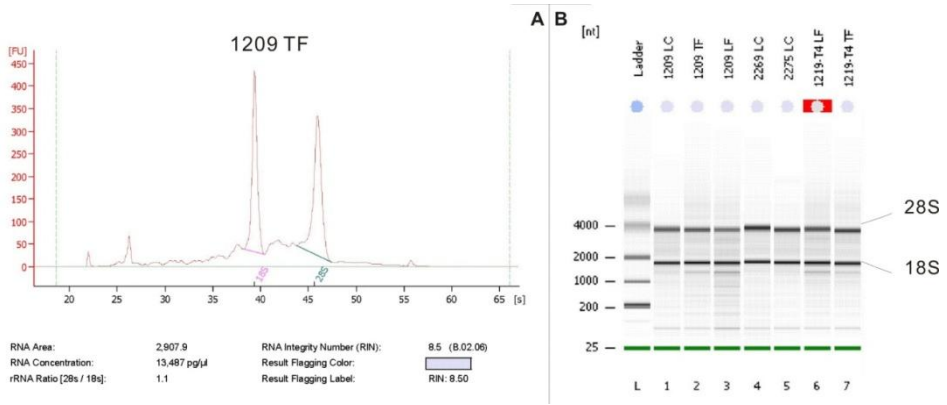

Figure 16. Punch aided laser capture microdissection yields high quality total RNA A. Quality control of total RNA from the tumor invasion front of patient 1209. RIN = 8.5, rRNA ratio [28S/18S]= 1.1 B. Quality control of total RNA from various microdissected samples. With the exception of lane 3, all other RNA samples have a high integrity with distinct 28S and 18S rRNA band.

3.2 Transcriptional profiles of tumor sub-zones

In order to analyze both mRNA and microRNA transcription, two techniques, oligonucleotide microarray and TaqMan Low Density Array were applied in parallel. Different from traditional expression profiling, microdissection aided profiling enriches specific cell populations but yields lower amounts of analytes for genomic, transcriptomic or proteomic analysis. To gain enough cDNA for oligonucleotide microarray experiments, we applied RNA amplification using the TAcKLE protocol. In addition, TaqMan Low Density Arrays were also used to investigate microRNA expression patterns (Figure 17). The TaqMan Low Density Array, a sensitive micro-fluidic based method, does not require RNA pre-amplification, which sometimes causes bias. The stem loop specific reverse transcription reaction was implemented to obtain mature microRNA cDNAs (Figure 17). In the present study of expression profile in tumor sub-zones, we did pairwise comparisons of four different cell populations in order to investigate deregulated genes and pathways involved in tumor invasion and to identify tumor-microenvironment interactions.

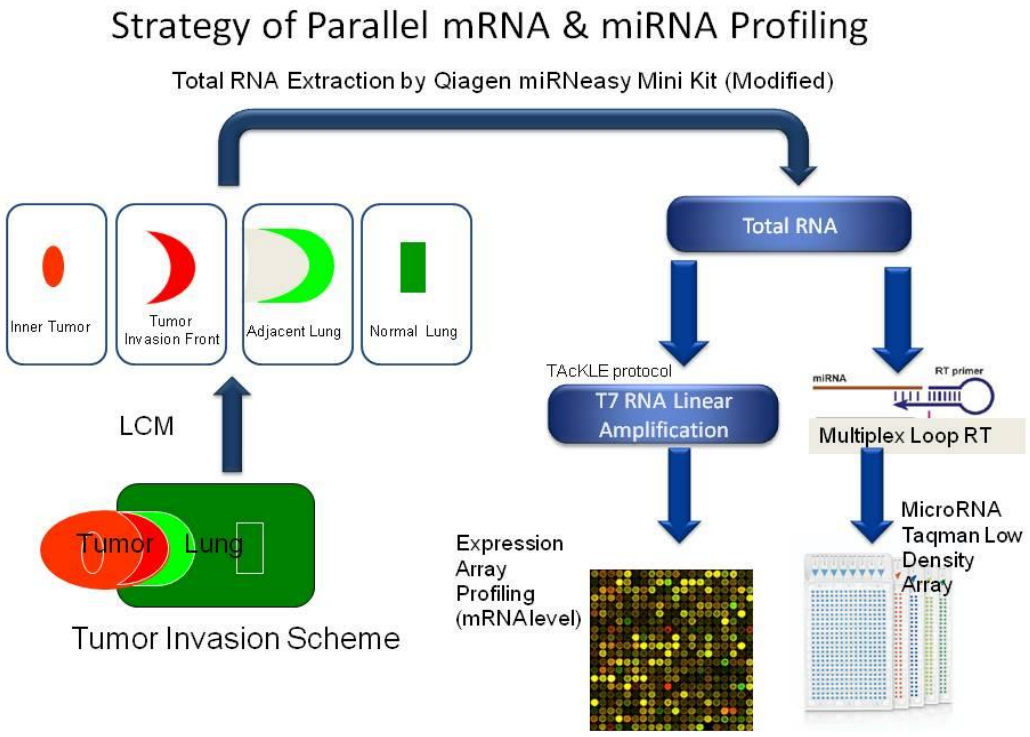

Figure 17. Strategy of parallel mRNA and microRNA transcription profiling. Four zonal tissues; inner tumor, tumor invasion front, adjacent lung and normal lung, were microdissected and captured. The total RNA from these four cell populations were extracted and used for oligonucleotide microarray and microRNA TaqMan Low Density Array via TAcKLE amplification and multiplex loop reverse transcription reactions.

In the oligonucleotide microarray experiments, we analyzed 18 tumors from 17 patients by hybridization of more than 160 microarray chips. We discarded chips which, upon hybridization, did not meet the quality control standards. Finally, we analyzed the data for 128 chips using the ChipYard data analysis platform. In the TaqMan Low Density Array experiments, we analyzed 9 tumors from the same sample pools of oligonucleotide microarray using 35 micro-fluidic cards (Table 7).

Table.7 Identification of patient samples used for microdissection

	Inner Tumor		Invasion Front		Adjacent Lung Tissue		Normal Lung	
Patient No.	Operon	TLDA	Operon	TLDA	Operon	TLDA	Operon	TLDA
1209	X	X	X	X	X	X	X	X
2269	X	X	X	X	X	X	X	X
2275	X	X	X	X	X	X	X	X
1219-T3	X	X	X	X	X	X	X	X
1219-T4	X	X	X	X	X	X		
1299	X	X	X	X	X	X	X	X
2502	X	X	X	X	X	X	X	X
1316	X	X	X	X	X	X	X	X
1317	X	X	X	X	X	X	X	X
2490	X		X		X		X	
2505	X		X		X		X	
1331	X		X		X		X	
1404	X		X		X		X	
1297	X		X		X		X	
1417	X		X		X		X	
2496	X		X		RNA not good		X	
1418	No Center		X		X		X	
2690	No Center		X		X		X	

"X" means the sample has been screened on either an oligonucleotide microarray chip or TaqMan Low Density Array card. "X" with highlighted blue background means the chip was analyzed without color switching. Samples highlighted in red were either not studied or no sample was available.

3.2.1 Messenger RNA gene expression profile in squamous cell lung carcinoma

3.2.1.1 Unsupervised clustering and statistical analysis reveals heterogeneity of tumor, adjacent and normal lung tissue

To study the gene expression profile in different locations of the tumor tissue, we randomly selected 100 genes from the microarray dataset and analyzed these data by unsupervised clustering. The clustering results demonstrated that tumor tissue and lung tissue samples are well separated in two different clusters. The

normal lung and adjacent lung clusters are also well separated, which indicates that the gene expression profile of normal lung is highly different from the tumor adjacent lung. In contrast, the clusters of the tumor invasion and the inner tumor are poorly separated, indicating only slight difference of gene expression between these two tissues (Figure 18).

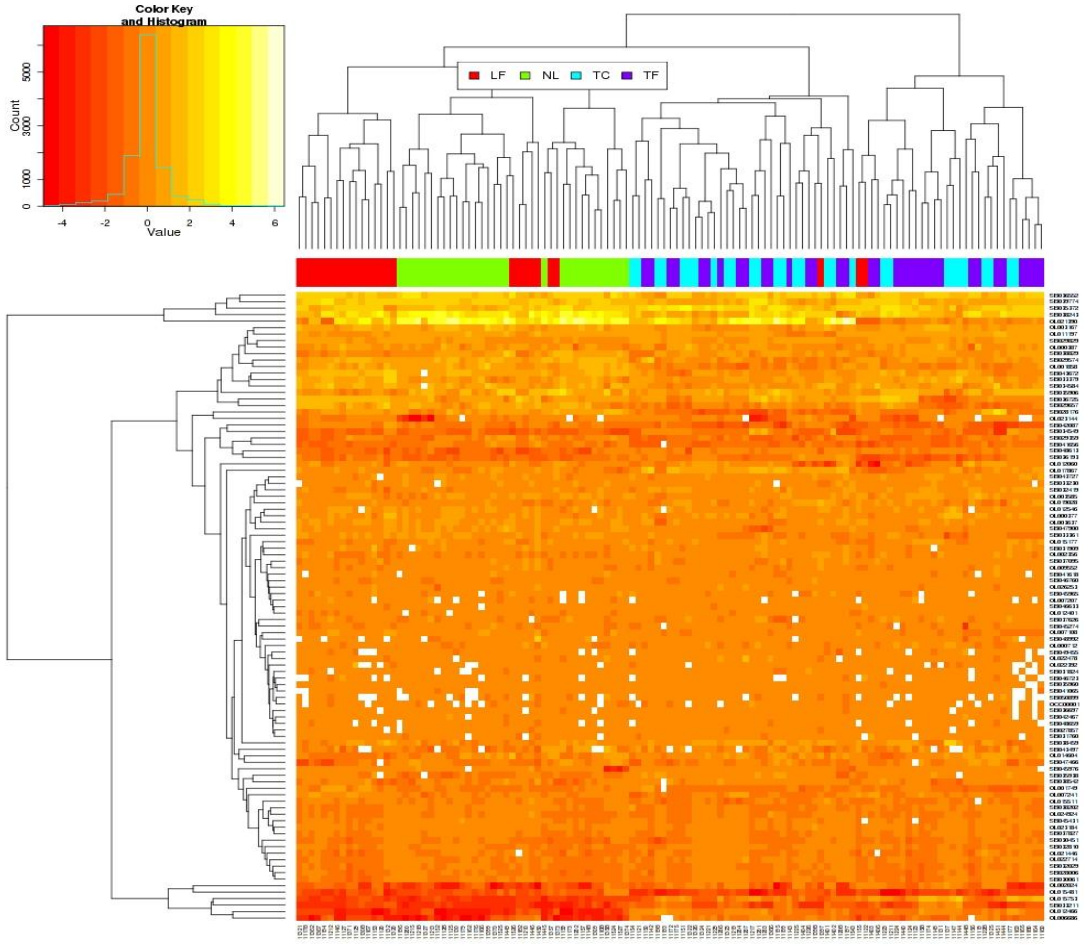

Figure 18. Unsupervised cluster analysis reveals heterogeneity of tumor, adjacent and normal lung tissue. 100 genes from the microarray dataset were selected for unsupervised clustering analysis. NL: normal lung (green); LF: adjacent lung tissue (red); TF: tumor invasion front (dark blue); TC: inner tumor (weak blue).

Limma and Venn diagram analyses were used to analyze the normalized gene expression microarray data. The Venn diagrams revealed relationships of the differentially expressed genes according to the location of tumor or lung cells. Compared to the inner tumor cells, the tumor invasion front has only 13 genes

differentially expressed, and 10 of them are unique for the tumor invasion front when compared to the other three sub-regions. Interestingly, the adjacent lung tissue has thousands of differentially expressed, compared to any of the other three tissues, which demonstrates that the gene expression pattern in adjacent lung tissue has been strongly altered due to the interaction with the tumor tissue (Figure 19).

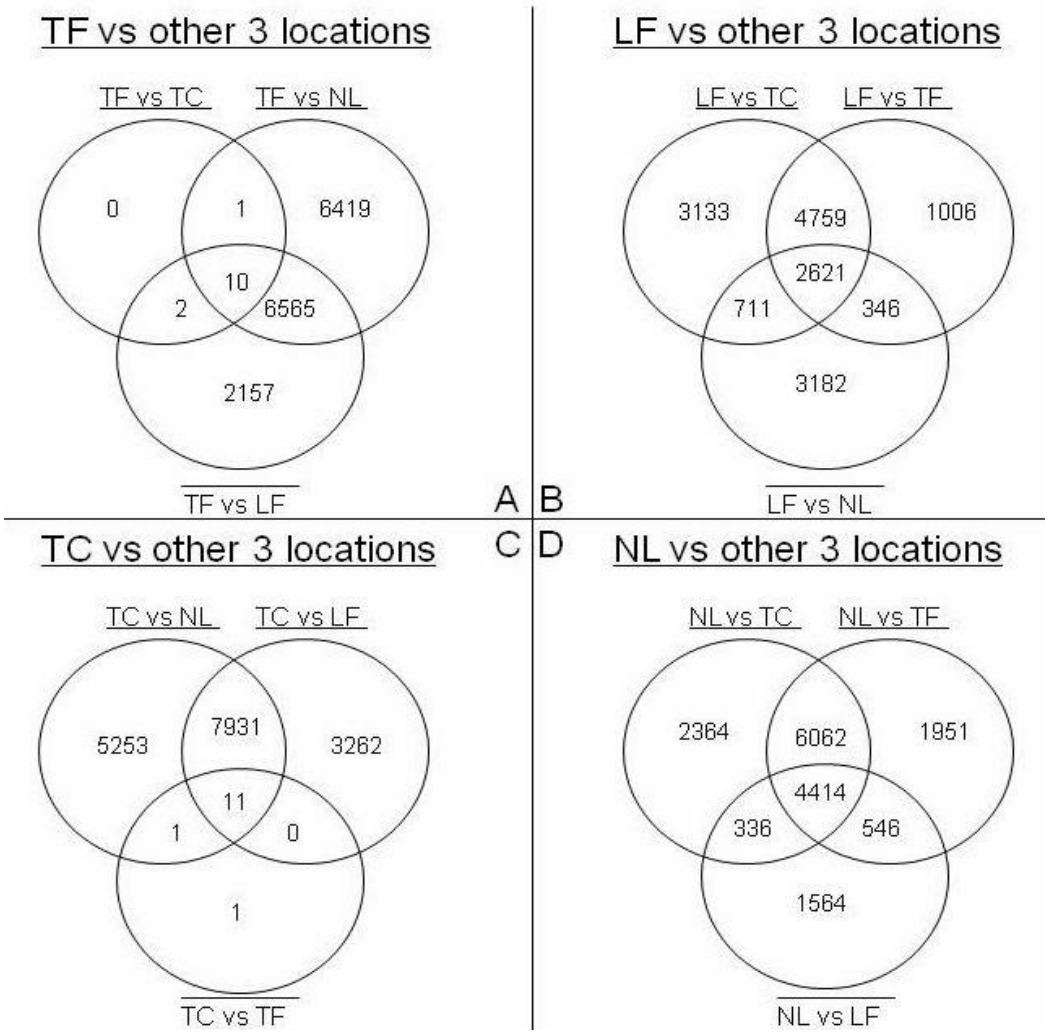

Figure 19. Limma Venn diagram analysis revealed relationships of the differentially expressed genes according their location as tumor or lung cells. A. Genes differentially expressed between tumor invasion front and the other three regions; B. Genes differentially expressed between adjacent lung tissue and the other three regions; C. Genes differentially expressed between inner tumor and the other three regions; D. Gene differentially expressed between normal lung and the other three regions. NL: normal lung; LF: adjacent lung Tissue; TF: tumor invasion front; TC: inner tumor.

3.2.1.2 Genes differentially expressed between tumor invasion front and the inner tumor.

One assumption has been made that the gene signature in the tumor invasion front should be highly related to tumor invasion and metastasis. Upon oligonucleotide microarray and statistical analysis, 13 candidate genes were identified as being differentially expressed between the tumor invasion front and the inner tumor (adjusted P value lower than 0.05, see Table 8). The 13 genes are *L3MBTL, AMT, LST, CD1A, AMICA1, CCL18, GIMAP7, APLNR, HLA-DRB7, SFTPC, LTB, LILRB4* and *CCL19*. *AMT* and *L3MBTL* were the only two genes downregulated in the tumor invasion front. Three upregulated genes, *CCL19*, *APLNR* and *GIMAP7* were selected for further validation by immunohistochemistry due to their high statistical significance.

Table 8. List of differentially expressed genes of the tumor invasion front versus inner tumor.

Symbol	Mapping	adj.P.Val	Lin FC
CCL19	9p13.3	0.015311	3.26
APLNR	11q11	0.015311	2.39
GIMAP7	7q36.1	0.01633	2.16
CD1A	1q23.1	0.01633	1.82
LTB	6p21.3	0.01633	1.92
CCL18	17q12	0.018568	2.84
LILRB4	19q13.42	0.018568	1.35
SFTPC	8p21.3	0.029915	3.50
LST1	6p21.33	0.033905	1.72
L3MBTL	20q13.12	0.033905	-1.50
HLA-DRB7	6p21.3	0.045007	2.55
AMICA1	11q23.3	0.045007	1.86
AMT	3p21.31	0.049053	-1.90

13 genes were identified as being significant based on adjusted P value lower than 0.05. adj.P.Val: adjusted P value; Lin FC: linear fold change; Mapping: Chromosomal gene location. Minus sign means down regulation.

3.2.1.3 Genes differentially expressed between adjacent lung tissue and normal lung.

Global gene expression profiling of human cancer is normally conducted to compare tumor tissue and its corresponding normal organ tissue, and very few studies have investigated the corresponding organ tissue immediately adjacent to the neoplasm. Through biostatistics and bioinformatics processing of oligonucleotide microarray data, we identified 1,008 genes deregulated in adjacent lung tissue compared to normal lung, with an adjusted P value lower than 0.05 and linear fold change higher than 2. *Keratin 5, 6, 16, 17* are among the top ten upregulated genes in the adjacent lung tissue. *LTF* (*lactotransferrin*) is 15.4 fold upregulated in adjacent lung tissue. *S100A2* (S100 calcium binding protein A2), *MYBPC2* (myosin binding protein C), *SAA2* (serum amyloid A2) and *CALML3* (calmodulin-like protein 3) are also highly deregulated in adjacent lung tissue. In the down-regulated gene list, the top candidate, *MYOC* (myocilin), is 5.4 fold lower than normal lung tissue. *HBB* (hemoglobin-β protein), *C2ORF40*, *LYZ* (lysozyme), *CXCR1* (chemokine (C-X-C motif) receptor 1), *CA4* (carbonic anhydrase), *ECM2* (extracellular matrix protein 2), *SYNPO2* (synaptopodin 2), *CLC* (Charcot-Leyden crystal protein) and *WIF1* (WNT inhibitory factor 1) are also top downregulated genes in adjacent lung tissue compared to normal lung (Table 9). The complete list of significantly deregulated genes are found in the Supplemental Table 1 and Table 2.

Table 9. Top 10 down and up regulated genes in adjacent lung tissue.

Symbol	Mapping	adj.P.Val	Lin Fc
KRT6A	12q13.13	5.34E-19	42.74
KRT6B	12q13.13	2.89E-18	28.75
KRT17P1	17p11.2	4.61E-12	23.65
KRT17	17q21.2	1.50E-12	23.34
KRT5	12q13.13	1.14E-14	18.98
AC022596.6	17p11.2	1.92E-07	15.66
LTF	3p21.31	8.17E-07	15.43
KRT14	17q21.2	1.84E-06	13.91
S100A2	1q21.3	3.85E-09	12.35
MYBPC2	19q13.33	1.08E-14	11.20
MYOC	1q24.3	7.01E-16	-5.41
HBB	11p15.4	5.20E-10	-4.98
C2orf40	2q12.2	3.24E-06	-4.86
LYZ	12q15	3.69E-14	-4.84
IGSF10	3q25.1	5.15E-12	-4.73
IL8RA	2q35	3.58E-12	-4.68
CA4	17q23.1	2.12E-09	-4.57
ECM2	9q22.31	1.70E-11	-4.49
SYNPO2	4q26	1.91E-08	-4.24
CLC	19q13.2	2.06E-14	-4.22

adj.P.Val: adjusted P value; Lin FC: linear fold change; Mapping: Chromosomal gene location. Minus sign means down regulation.

3.2.1.4 Genes differentially expressed between tumor and normal lung

As mentioned in Section 3.2.1.1, the tumor invasion front and inner tumor show very little differences in global gene expression, as such, with the exception of the 13 differentially regulated genes. Accordingly, they were considered as one compartment of tumor cells. Of the top ten upregulated genes, *Keratin 5, 6A/B, 15, 16, 17*, are significantly higher expressed in the tumor cells of the invasion front and inner tumor when compared to normal lung tissue. *DSG3* (desmoglein 3), *S100A2* (S100 calcium binding protein A2), *TRIM29* (tripartite motif-containing 29), *CALML3* (calmodulin-like protein 3) and *PTHLH* (parathyroid hormone-like hormone) are the top upregulated genes in tumor cells. *FOSB* (FBJ

murine osteosarcoma viral oncogene homolog B), *SFTPB* (surfactant protein B), *SFTBC* (surfactant protein B), *FAM100B* (family with sequence similarity 100, member B) et al., are the top downregulated in tumor cells when compared to normal lung (Table 10). The total signficant gene lists can be found in Supplemental Table 3, 4, 5, 6.

Table 10 A. Top 10 down and up regulated gene in inner tumor compared to normal lung.

Symbol	Mapping	adj.P.Val	Lin Fc
KRT6B	12q13.13	2.62E-32	137.35
KRT17P1	17p11.2	4.63E-23	101.90
KRT17	17q21.2	2.34E-23	97.59
KRT6A	12q13.13	5.75E-27	91.18
KRT15	17q21.2	2.17E-22	68.89
S100A2	1q21.3	2.17E-20	55.33
KRT5	12q13.13	1.75E-24	51.95
KRT16	17q21.2	9.37E-21	50.06
CALML3	10p15.1	8.59E-23	49.94
PTHLH	12p11.22	6.34E-21	44.79
AGER	6p21.32	9.71E-33	-79.29
SFTPC	8p21.3	1.81E-17	-58.70
INMT	7p14.3	2.64E-38	-39.91
C7	5p13.1	3.44E-34	-36.95
MFAP4	17p11.2	1.76E-39	-33.96
SFTPB	2p11.2	3.16E-16	-32.37
CLIC5	6p21.1	1.32E-34	-30.72
SFTA3	14q13.3	1.81E-25	-30.38
AC105046.10	8p21.3	4.15E-21	-29.94
C19orf59	19p13.2	3.44E-21	-29.08

adj.P.Val: adjusted P value; Lin FC: linear fold change; Mapping: Chromosomal gene location. Minus sign means down regulation.

Table 10. B. Top 10 up and down regulated gene in the tumor invasion front compared to normal lung.

Symbol	Mapping	adj.P.Val	Lin Fc
KRT6B	12q13.13	4.30E-34	154.56
KRT6A	12q13.13	5.39E-31	137.11
KRT17P1	17p11.2	3.97E-25	118.34
AC022596.6	17p11.2	3.97E-20	113.58
KRT17	17p11.2	1.79E-25	108.62
KRT17	17q21.2	1.95E-24	97.00
KRT16	17q21.2	1.91E-25	84.18
KRT15	17q21.2	1.14E-23	70.93
DSG3	18q12.1	1.85E-24	60.50
S100A2	1q21.3	3.46E-21	53.69
AGER	6p21.32	1.14E-29	-46.89
MFAP4	17p11.2	6.77E-43	-40.78
INMT	7p14.3	6.21E-37	-30.59
FOSB	19q13.32	6.9E-22	-23.70
A2M	12p13.31	6.2E-39	-22.66
C7	5p13.1	1.17E-30	-22.28
WISP2	20q13.12	8.79E-37	-21.36
CLIC5	6p21.1	7.64E-32	-21.11
FXYD1	19q13.12	5.37E-37	-18.93
ITLN2	1q23.3	3.66E-18	-18.74

adj.P.Val: adjusted P value; Lin FC: linear fold change; Mapping: Chromosomal gene location. Minus sign means down regulation.

Eicosanoid signaling, a cellular pathway producing prostaglandins and other bioactive lipid products (Funk, 2001), ranks first in both the tumor invasion front and in the inner tumor cell analyses using the Ingenuity software. As such, we made a separate clustering of all the genes in the eicosanoid pathway for each of the locations and tumor samples. We found prostaglandin synthase E and F are highly expressed in tumor cells irrespective of the location, but are expressed at very low levels in normal lung. The prostaglandin molecular function is mediated by the activation of specific receptors. Surprisingly, we found prostaglandin E and

F receptors are highly expressed in lung tissue, but expressed at very low levels in tumor cells (Figure 20, Table 11, Table 12).

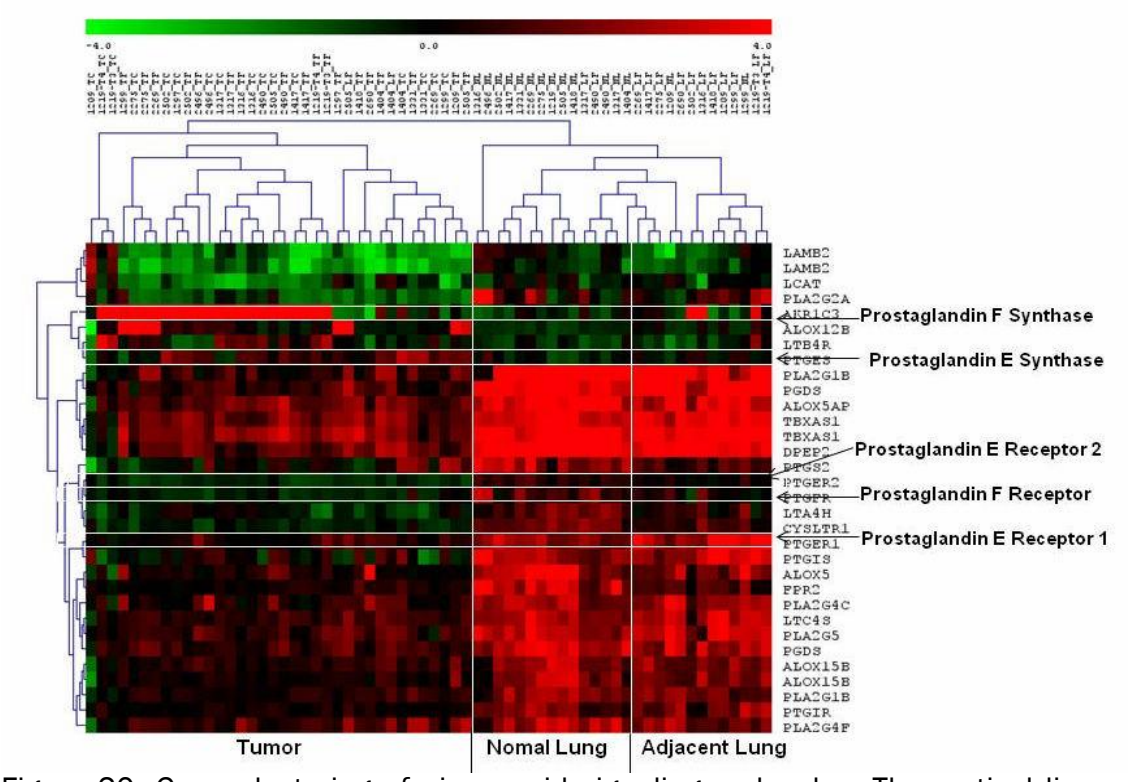

Figure 20. Gene clustering of eicosanoid signaling molecules. The vertical lines divide the graph into different locations tumor, adjacent lung and normal lung. The tumor invasion front and inner tumor are not separately clustered. The horizontal white lines show different prostaglandins and their receptors. The red color means that the gene is highly expressed and the green color means that the gene shows low expression. The intensity of the color indicates the expression value of the gene.

Tab 11. Prostaglandin E and F synthase expression in tumor cells versus adjacent lung tissue

Prostaglandin Synthase	Tumor Invasion Front vs Adjacent Lung		Inner Tumor vs Adjacent Lung	
Gene Symbol	Adj. P-Value	Lin. FC	Adj. P-Value	Lin. FC
PTGES	0.006074423	1.870465	1.8271E-06	2.234084
PGFS	0.000153797	5.66029	7.46722E-07	10.26025
PTGES2	0.0103	1.4	0.0013	1.48

Adj. P-Value: adjusted P-Value; Lin. FC: linear fold change.

Tab 12. Prostaglandin E and F receptor expression in tumor cells versus adjacent lung tissue

Prostaglandin Receptor	Adjacent Lung VS Tumor Invasion Front		Adjacent Lung VS Tumor Center	
Gene Symbol	Adj. P-Value	Lin. FC	Adj. P-Value	Lin. FC
PTGER1	1.35E-19	6.333121	8.14523E-21	7.146448
PTGER2	6.07E-10	1.654693	1.24031E-09	1.661729
PTGER3	0.774239965	1.05332	0.819730122	0.985361
PTGER4	0.190931189	1.193341	0.169856299	1.1957
PTGFRN	4.77E-05	0.518428	9.57512E-05	0.522704
PTGFR	0.000740221	1.801733	0.00015387	1.962605

Adj. P-Value: adjusted P-Value; Lin. FC: linear fold change.

3.2.2 MicroRNA expression profile in squamous cell lung carcinoma

In parallel with mRNA expression profiling, the transcription profile of 365 mature microRNAs was accessed by multiplex reverse transcription and TaqMan Low Density Array. Through data processing, we identified 66 microRNAs differentially expressed between tumor cells when compared to normal lung and 24 microRNAs differentially expressed in adjacent lung tissue when compared to normal lung.

3.2.2.1 Hsa-mir-196a is differentially expressed between the tumor invasion front and the inner tumor

The tumor invasion front is the leading tissue directly adjacent to the host organ; therefore the differentially expressed microRNAs between the tumor invasion front and the inner tumor might be crucial for tumor invasion, metastasis or tumor microenvironment interactions. Similar to what was seen by mRNA gene expression, the differential expression of microRNAs between the tumor invasion front and inner tumor is limited. Almost all of the microRNAs from the 365 probe pool could not pass the statistical threshold, with the exception of hsa-mir-196a.

The expression of hsa-mir-196a is 2.2 fold higher in inner tumors than in the tumor invasion front (Figure 21).

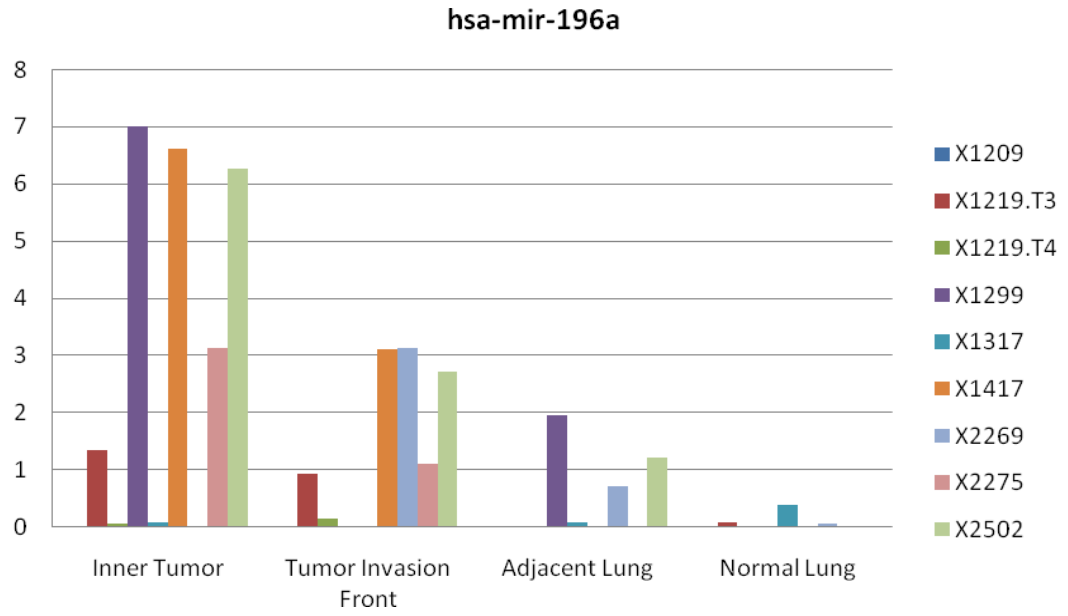

Figure 21. The hsa-mir-196a expression in each tumor and its four compartments. The hsa-mir-196a expression is distinctly higher in the inner tumor than in the other three compartments. Y axis is the normalized expression value; X axis shows individual patient values clustered into the four different regions; Different colors show tumors from individual patients.

The expression pattern of hsa-mir-196a suggests a role in tumor invasion and metastasis. In 2008, hsa-mir-196a was found to mediate Annexin A1 down-regulation in esophageal cancers (Luthra et al., 2008). Furthermore, Annexin A1 has been found to regulate TGF-β signaling to promotes metastasis formation in basal-like breast cancer cells. Annexin A1 is a candidate regulator of the EMT-like phenotypic switch, a pivotal event in breast cancer progression (de Graauw et al., 2010). Therefore, the role of hsa-mir-196a in tumor epithelia cells might be one of a negative regulator of metastasis induced by EMT. To correlate the expression of hsa-mir-196a and Annexin A1, we plotted the Annexin A1 gene expression data in the same manner as the microRNA TLDA. The result showed that the

expression of *Annexin A1* is negatively correlated to hsa-mir-196a in squamous cell lung carcinoma epithelial cells (Figure 22).

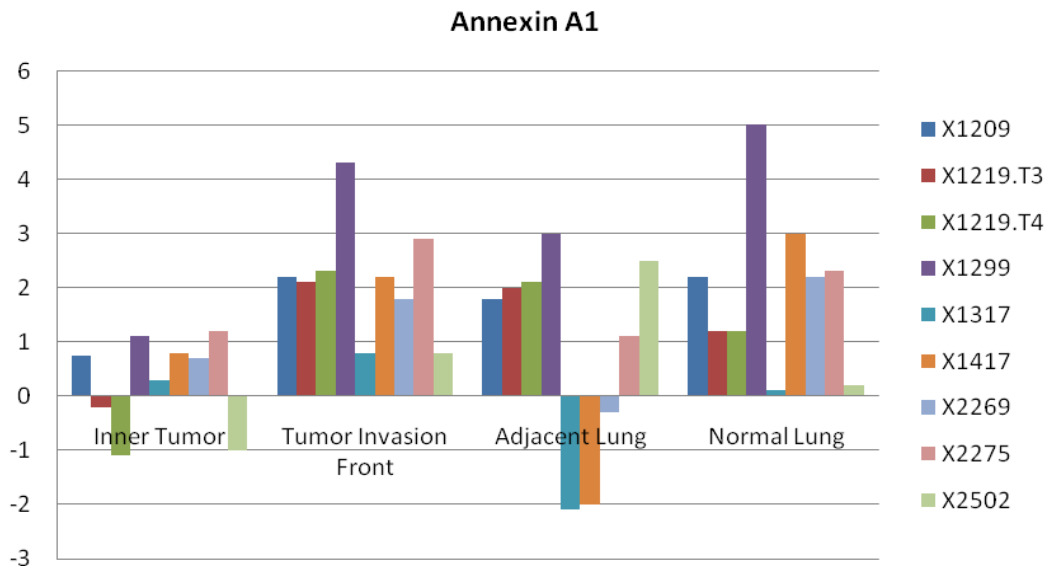

Figure 22. Annexin A1 expression in each tumor and its four compartments. The expression of Annexin A1 in inner tumor is lower than in the invasion front and is negative correlated to hsa-mir-196a expression. X axis is samples from the four compartments; Y axis is expression value (log ratio).

3.2.2.2 MicroRNA differentially expressed between adjacent lung tissue and normal lung

In a manner similar to mRNA gene expression (mentioned in 3.2.1.3), the alternation of microRNA expression may also be a key issue in tumor microenvironment interactions, including the induction of inflammation in adjacent lung tissue. Through TLDA and bioinformatic analysis, we identified 24 deregulated miroRNAs in adjacent lung tissue with Q-values lower than 0.05, and fold change higher than 2 (Table 13). Hsa-mir-433, hsa-mir-650, hsa-mir-137 and hsa-mir-210, are highly upregulated in adjacent lung tissue. 20 microRNAs, including hsa-mir-190 and has-let-7 et al., were downregulated in adjacent lung tissue.

Table 13. Differentially expressed microRNAs in adjacent lung tissue compared to normal lung

microRNA	Q-Value	Fold Change
hsa-miR-433	0.025316077	10.57598397
hsa-miR-650	3.86E-05	5.808063346
hsa-miR-137	0.021360267	5.703475901
hsa-miR-210	0.043911705	3.188950488
hsa-miR-95	0.023848067	-2.194771481
hsa-miR-335	0.039497801	-2.195165373
hsa-miR-422a	0.046082697	-2.221146149
hsa-let-7c	0.008132383	-2.27251243
hsa-miR-133a	0.016569005	-2.282230572
hsa-miR-101	0.01346168	-2.295140765
hsa-miR-145	0.004326968	-2.347864178
hsa-miR-125b	0.048659078	-2.351938022
hsa-miR-130a	0.009679214	-2.362390002
hsa-miR-195	0.011213984	-2.40643741
hsa-miR-497	0.004326968	-2.469582395
hsa-miR-486	0.004326968	-3.076607132
hsa-miR-30e-5p	0.009396757	-3.191827329
hsa-miR-23b	0.011213984	-3.209615817
hsa-miR-143	0.009679214	-3.905281922
hsa-miR-501	0.033524141	-4.636553761
hsa-miR-135a	0.01534985	-4.743729606
hsa-miR-451	0.005643732	-5.712331781
hsa-let-7e	0.021793669	-7.971231659
hsa-miR-190	0.023999975	-7.982318253

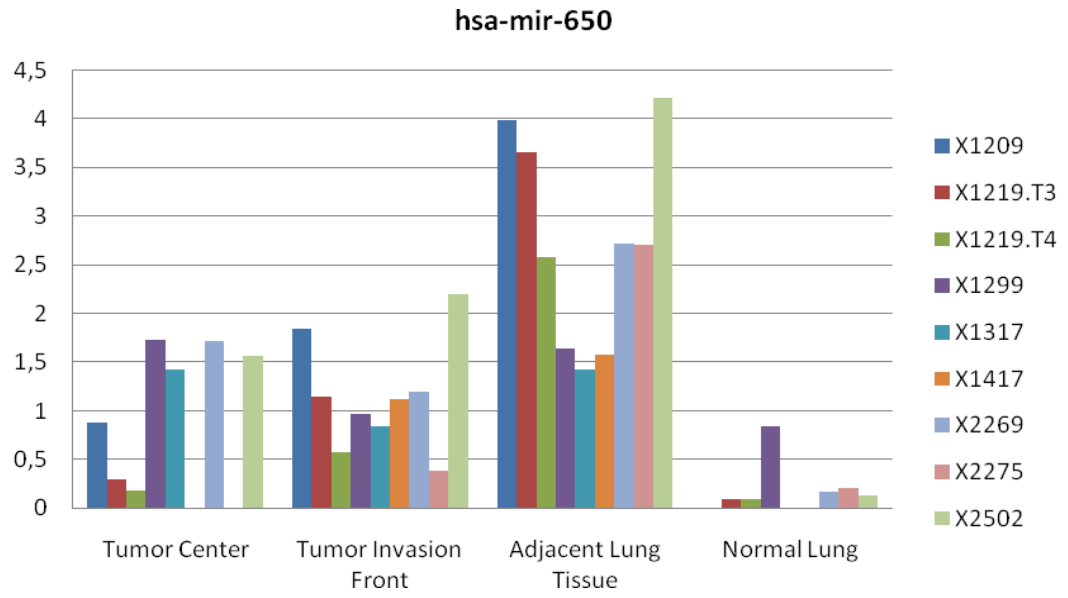

Figure 23. Hsa-mir-650 is highly expressed in adjacent lung tissue. Hsa-mir-650 expression in adjacent lung tissue is 2.7 fold higher than in the tumor invasion front (Q-value: 0.07), 3.7 fold higher than inner tumor (Q-value:0.033) and 5.8 fold higher than normal lung (Q-value:0.025). The Y axis shows the expression value; The X axis shows individual patient data for miR-650 clustered by tumor compartment; different colors indicate different patients.

3.2.2.3 MicroRNA differentially expressed between tumor and normal lung

Lung cancer has characteristic microRNA expression patterns that allow their distinction from normal lung epithelia and could facilitate clinical prognosis (Diederichs and Haber, 2006). The heterogeneity of expressed microRNAs within a primary lung tumor has not been studied, as yet, by large scale microarray analysis. We used laser capture microdissction to enrich epithelial tumor cells for microRNA TLDA analysis. The comparison of microRNA expression between tumor cells and normal lung cells was conducted by data normalization and statistical processing as described in the section of Materials and Methods. Using a threshold Q-value lower than 0.05 and a fold change higher than 2, we identified 66 microRNAs differentially expressed between the inner tumor and the normal

lung, and 52 microRNAs differentially expressed between the tumor invasion front and the normal lung. The major parts of the 52 microRNA pool overlap with the 66 microRNA pool. 32 microRNAs were identified as being upregulated in inner tumor cells and 14 microRNAs were identified as upregulated in tumor invasion front cells, when compared to normal lung tissue. The 14 upregulated microRNAs in the tumor invasion front were included in the 32 microRNA pool (Table 14). Hsa-mir-205 ranked as the top upregulated microRNA and hsa-mir-190 ranked as the most downregulated microRNA in our study. Hsa-mir-190 has never been reported in lung cancer as an important candidate. The downregulated microRNA candidates are shown in the Supplemental Tables 7 and 8.

Table 14. Upregulated microRNAs in tumor cells

A

microRNA	Q-Value	Fold Change
hsa-miR-205	0.000988	11.94508
hsa-miR-137	0.008302	11.74847
hsa-miR-9	0.003448	8.931858
hsa-miR-9	0.00394	8.526588
hsa-miR-196a	0.003231	6.30874
hsa-miR-7	0.033032	6.183923
hsa-miR-432	0.02561	4.957977
hsa-miR-424	0.035715	4.753276
hsa-miR-130b	0.003356	4.666076
hsa-miR-21	0.006074	4.575175
hsa-miR-182	0.001457	4.43515
hsa-miR-196b	0.002304	4.31914
hsa-miR-337	0.035785	4.26977
hsa-miR-31	0.017075	4.042417
hsa-miR-210	0.002304	4.03041
hsa-miR-301	0.031854	3.843081
hsa-miR-452	0.011149	3.799441
hsa-miR-622	0.038638	3.505388
hsa-miR-224	0.004675	3.503059
hsa-miR-183	0.00197	3.439698
hsa-miR-200a	0.008937	3.404669
hsa-miR-203	0.029232	3.07379
hsa-miR-93	0.010894	3.020925
hsa-miR-429	0.029082	2.92244
hsa-miR-187	0.035785	2.87298
hsa-miR-149	0.001457	2.676644
hsa-miR-629	0.018407	2.567627
hsa-miR-193b	0.019016	2.503741
hsa-miR-615	0.020806	2.222016
hsa-miR-485-3p	0.029307	2.082046
hsa-miR-17-5p	0.00958	2.005979

B

microRNA	Q-Value	Fold Change
hsa-miR-205	0.000652	9.4800581
hsa-miR-149	0.022288	6.7032696
hsa-miR-210	4.27E-05	6.580751
hsa-miR-183	0.002822	5.0147267
hsa-miR-93	0.035671	4.9028400
hsa-miR-31	0.020747	4.4424260
hsa-miR-182	0.001182	3.4961395
hsa-miR-196b	0.011146	2.9523322
hsa-miR-224	0.022191	2.8621574
hsa-miR-200a	0.01235	2.6338273
hsa-miR-200b	0.009567	2.5027317
hsa-miR-130b	0.011582	2.4660273
hsa-miR-196a	0.022512	2.2445466
hsa-miR-650	0.003402	2.0996220

A. Upregulated microRNAs in inner tumor cells. Thirty-one microRNAs are upregulated in the inner tumor compared to the normal lung; B. Up-regulated microRNAs in tumor invasion front. 14 microRNAs are upregulated in tumor invasion front compare to normal lung.

Hsa-mir-224 is around 3 fold up regulated in tumor cells when compared to normal lung (Table G and Figure 24). We chose hsa-mir-224 as a validation

candidate, as hsa-mir-224 is upregulated in HepG2 cells and is involved in cellular migration and invasion (Li et al., 2010).

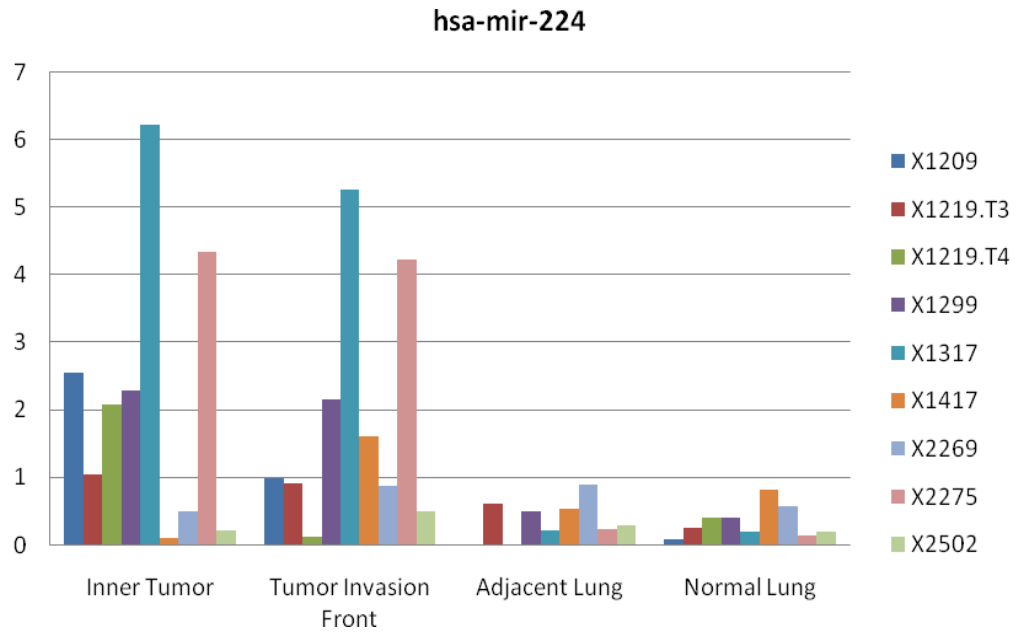

Figure 24. Hsa-mir-224 is highly expressed in tumor cells. Hsa-mir-224 expression in inner tumor cells is 3.5 fold higher than normal lung (Q-value: 0.005), in tumor invasion front cells it is 2.8 fold higher than in normal lung (Q-value:0.022). Y axis is normalized expression value, X axis is compartment of tumor as indicated; different colors indicate different tumors from patients.

3.2.3 Messenger RNA and microRNA crosstalk in squamous cell lung carcinoma

The transcriptional profile of mRNA and microRNA were done in parallel, so it is worthwhile and meaningful to explore the interaction of those two data sets and find microRNAs targeting molecular networks and pathways. As described in section 2.2.12, Pearson correlation analysis between the microRNA TLDA and the mRNA oligonucleotide microarray data was implemented. Twelve microRNAs were identified as being well correlated to their target mRNAs with p-values lower than 0.6 (Figure 25 A). Hsa-mir-205 expression is highly correlated to *BOC* mRNA gene

and has-let-7 is highly correlated to *MKI67* mRNA gene with a P-value lower than 0.5 (Figure 25 B and C).

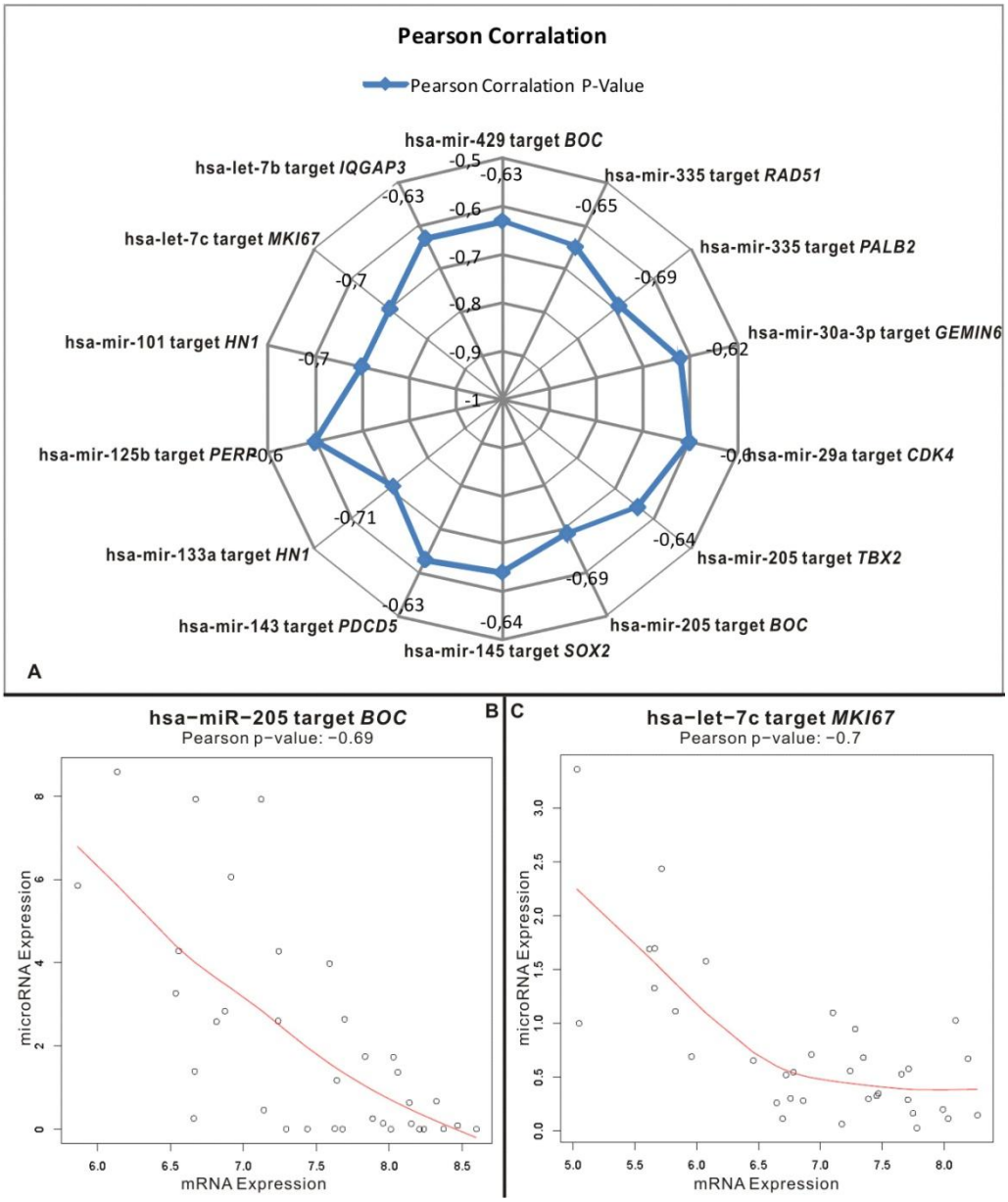

Figure 25. Pearson Correlations of microRNAs and their targets. A. 12 microRNAs are well correlated to mRNA genes at the transcription level. -1, perfect correlation, -1 to -0.5, close correlation. Each concentric circle indicates a different p-value of the Pearson correlation. B, C, Two plotting examples of the Pearson correlations for microRNA and mRNA gene expression. B. hsa-mir-205 correlated to BOC with p-Value = -0.69; C. hsa- let- 7c correlated to MKI67 with p-Value= -0.7. X axis is the mRNA expression value; Y axis is the microRNA expression value; Red line indicates the correlation trend.

3.3 Validation of zonal transcriptional profiling of squamous cell lung carcinoma

3.3.1 Verification of *CCL19*, *GIMAP7* and *APLNR* expression in the tumor invasion front by immunohistochemistry

Using three genes, which were shown by microarray analysis to be relatively highly expressed in the tumor invasion front (*CCL19*, *GIMAP7* and *APLNR*), protein immunohistochemistry experiments were carried out to biologically validate the oligonucleotide microarray mRNA expression analysis using tissue from the same patients in which the microarray analysis was performed.

As can be seen in Figure 26, CCL19 protein is strongly expressed in the tumor invasion front of tumor epithelial cells, tumor stroma cells and adjacent lung tissue, but weakly expressed in the inner tumor cells. Positive staining for CCL19 was typically localized at the subcellular level to the cytoplasm of tumor epithelial cells or the tumor stroma cells, close to the leading edge of the tumor invasion front.

GIMAP7 and APLNR expression were both highly enriched in epithelial tumor cells in the tumor invasion front. No GIMAP7 and APLNR expression in stroma cells were identified. GIMAP7 and APLNR proteins were both localized in the cytoplasm of the positive lung epithelial tumor cells (Figure 27).

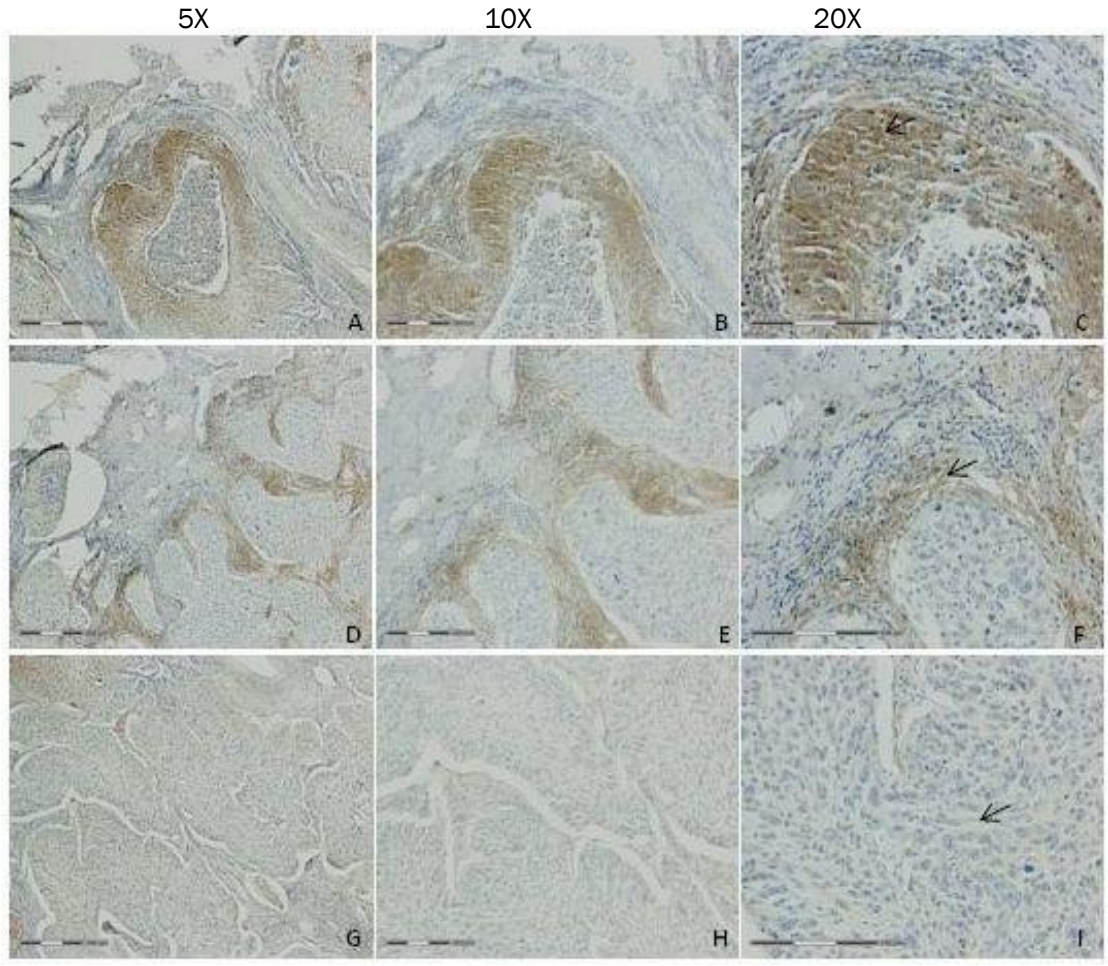

Figure 26. The CCL19 protein is highly expressed in the tumor invasion front. Vertical rows show different magnifications of the image. CCL19 is distinctly expressed in the leading edge of the tumor invasion front and adjacent lung tissue. A, B and C show the positive CCL19 staining in the tumor epithelial cells in the tumor invasion front. D, E and F show the positive CCL19 staining in tumor stroma cells of invasion front. G, H and I show the weak staining intensity of CCL19 protein in the inner tumor. Bar= 300 μm.

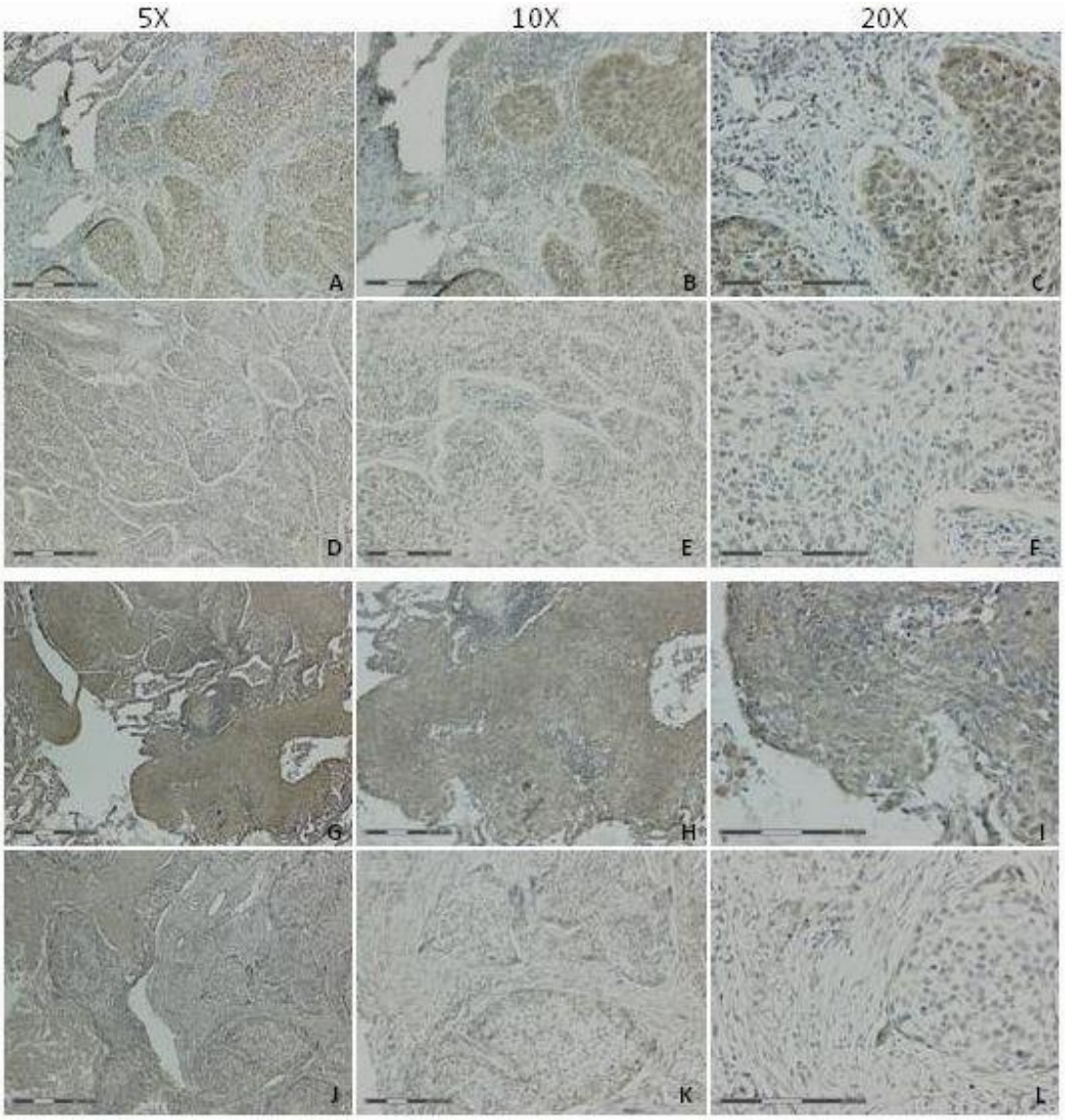

Figure 27. GIMAP7 and APLNR proteins are highly expressed in the tumor invasion front. A-F, GIMAP7 staining, G-L, APLNR staining. Vertical rows show different magnifications of the image. A-C shows the positive GIMAP7 staining in the tumor epithelial cells of the tumor invasion front. D-F shows the weak GIMAP7 staining in the inner tumor cells. G-I shows the positive APLNR staining in the tumor epithelial cells of the invasion front; and J-L shows the weak staining intensity of APLNR protein in the inner tumor. GIMAP7 stained in tumor tissue section from patient 2496, APLNR stained in tumor tissue section from patient 2505. Bar= 300 μm

3.3.2 Prostaglandin E and F's role in tumor-microenvironment interactions

Immunohistochemistry staining in patient tissue sections using antibodies directed against several members of the eicosanoid pathway also validate the microarray findings (Figure 28). Prostaglandin E synthase is highly expressed in tumor tissues and a low expression level is found in lung tissue; the positive staining is localized in the tumor epithelial cells and in lymphocytes (Figure 28 D). There is very weak expression of both the prostaglandin E receptor 1 and receptor 2 in tumor cells, either in epithelial tumor cells or lymphoid cells of tumor associated tissue, whereas in macrophage cells in the adjacent lung tissue, the prostaglandin E receptor 1 is highly expressed. Interestingly, the prostaglandin E receptor 2 expression occurs in a line of cells, which are at the interface of the tumor and lung tissue.

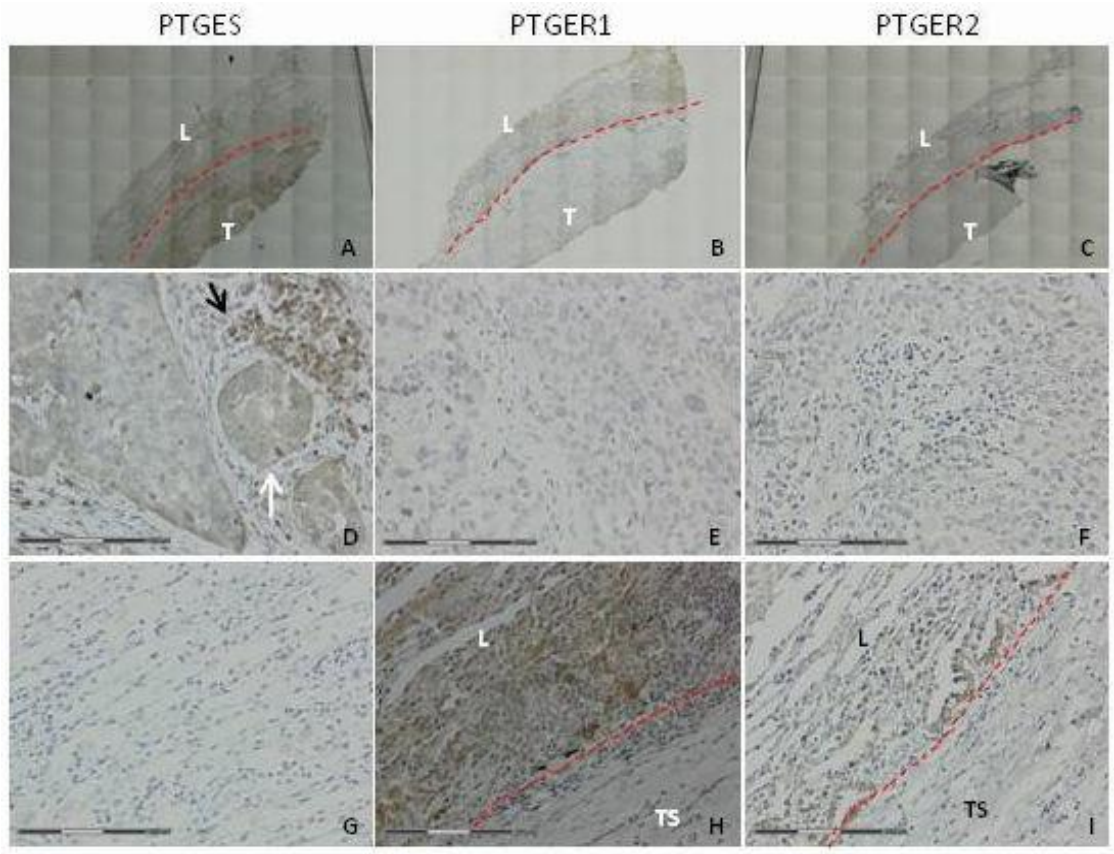

Figure 28. The expression pattern of prostaglandin E synthase and its receptors. A, B, C show an overview of the staining in whole tissue sections using antibodies to prostaglandin E synthase and its receptors. D,E, F show prostaglandin E synthase and receptors staining in the tumor area. D. Prostaglandin E synthase is expressed in the tumor area, the white arrow shows the tumor epithelial cells; the black arrow shows the lymphocytes. They both express prostaglandin synthase. G. Prostaglandin E synthase is not expressed in the cells of the tumor area, neither in tumor epithelial cells nor in tumor stroma cells. H. Prostaglandin E receptor 1 is expressed in macrophages close to the leading edge between tumor and lung. I. Prostaglandin E receptor 2 is expressed in the lung epithelia in the leading edge between the tumor and lung. T: Tumor, L: Lung, TS, Tumor side. Red line: leading edge between tumor and lung. Bar= 300 μm.

Prostaglandin F synthase is strongly expressed in the cytoplasma of tumor epithelial cells, but its receptor is not specifically expressed either in tumor- or lung tissue (Figure 29). The protein expression pattern of the prostaglandin E and F synthase reveal that those two prostaglandins are mainly synthesized in tumor tissues including the lymphoid cells of tumor associated tissue. The protein expression patterns of the prostaglandin E receptors suggest that prostaglandin E

executes its function in the macrophage cells or lung epithelial cells in adjacent lung tissue areas. The unspecific prostaglandin F receptor protein expression pattern might suggest that prostaglandin F implements its function in both tumor and lung tissues.

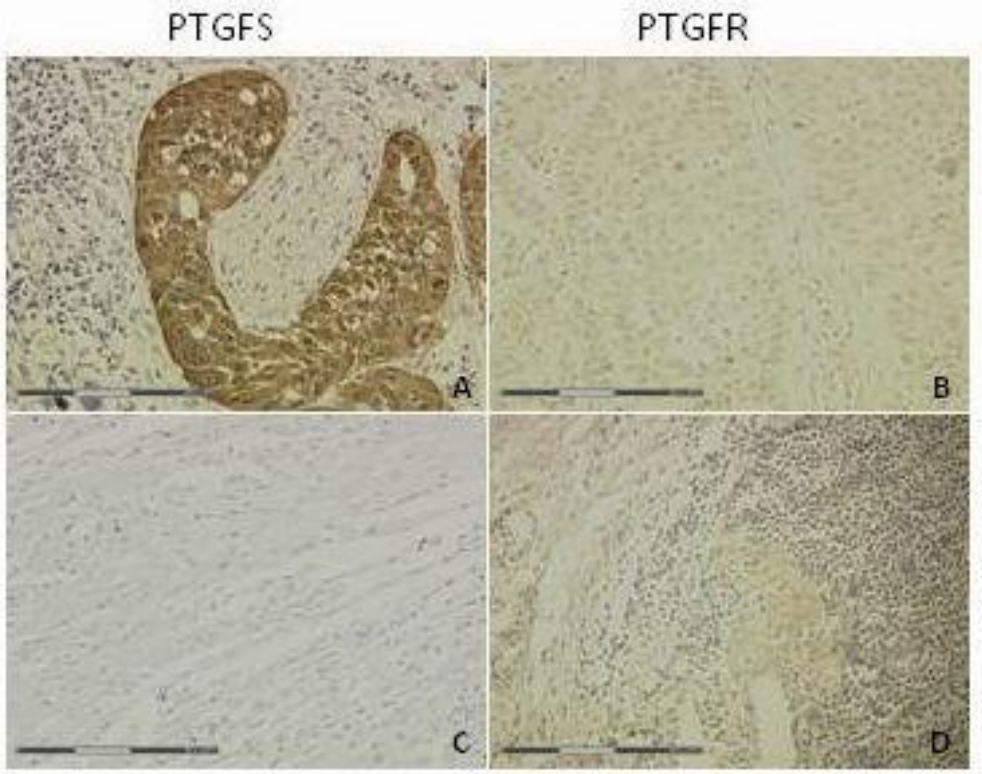

Figure 29. The expression pattern of prostaglandin F synthase and its receptor. A. Strong prostaglandin F synthase positive staining is found in tumor epithelial cells. B. Prostaglandin F receptor expression in the tumor area is weak and non specific. C. Prostaglandin F synthase is not expressed in lung tussue. D. Prostaglandin F receptor expression in adjacent lung tissue with lymphoid cells. Bar= 300 µm

3.3.3 Verification of hsa-mir-224, hsa-mir-196a and hsa-mir-650 expression by microRNA fluorescence in situ hybridization.

Since we found using the microRNA TLDA that hsa-mir-224 is about 3 fold upregulated in tumor cells, we used a locked nucleic acid (LNA) probe to detect the hsa-mir-224 expression by fluorescence in situ hybridization experiments. The fluorescent signal was only detected in tumor cells; no signal was identified in normal lung cells. The hsa-mir-224 was localized in the cytoplasm (Figure 30).

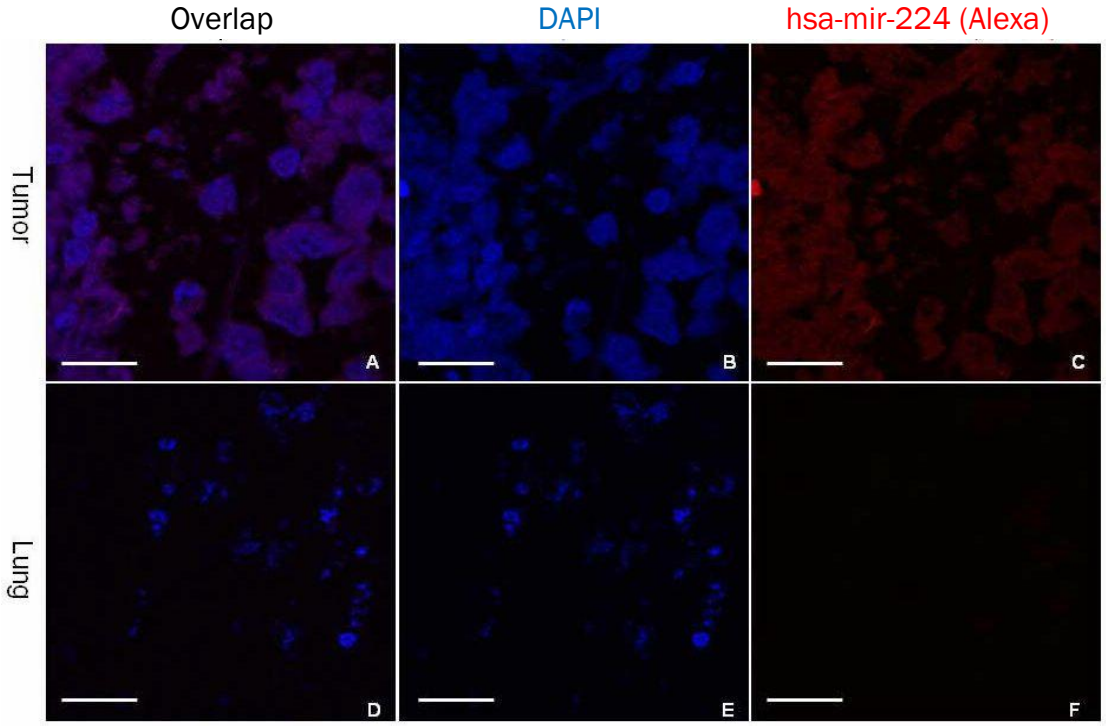

Figure 30. Has-mir-224 is expressed in tumor tissue but not in normal lung. A, B, C tumor area in different fluorescence channels. D, E, F lung area in different fluorescence channels. Bar=30µm Alexa 594 fluor channel fluorescence was only detected in the cytoplasm of tumor cells.

By microRNA TLDA screening, hsa-mir-196a is the only candidate differentially expressed between the tumor invasion front and the inner tumor. MicroRNA in situ hybridization confirmed our TLDA findings that hsa-mir-196a expression is much higher in the inner tumor region than in the tumor invasion front (Figure 31). Hsa-mir-196a is highly expressed in inner tumor cells but expressed at a lower level in tumor invasion front cells.

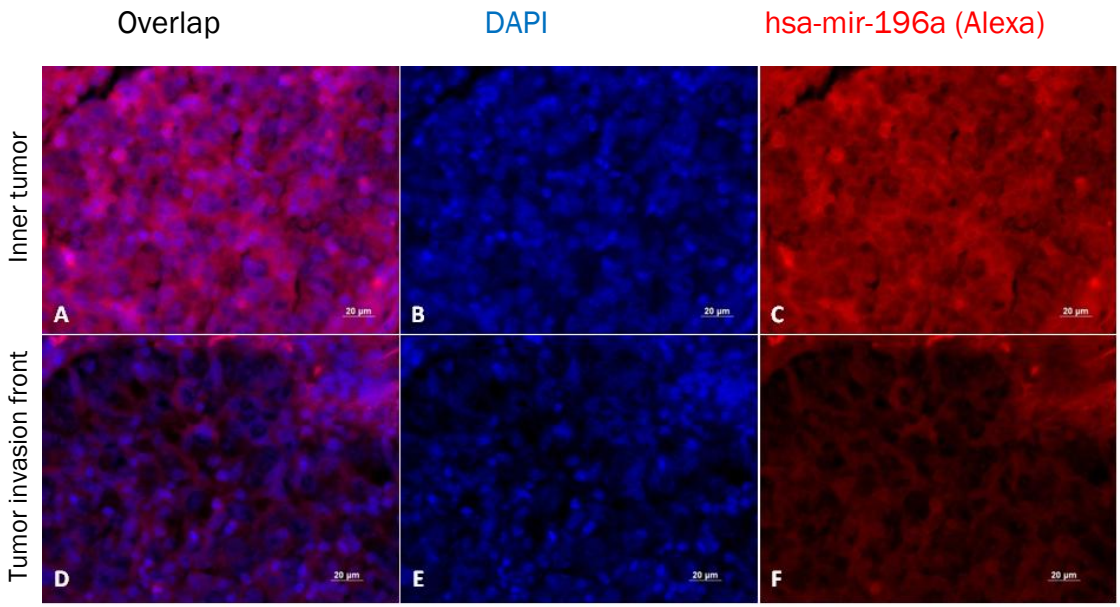

Figure 31. Has-mir-196a is highly expressed in inner tumor cells, but expressed at a lower level in tumor invasion front cells. A, B, C tumor invasion front in fluorescence channels. D, E, F inner tumor area in fluorescence channels. Bar=20µm.

Through TLDA screening, hsa-mir-650 has been found as the only microRNA highly expressed in adjacent lung tissue when compared to any other of the three cellular compartments. Using fluorescence in situ hybridization, the hsa-mir-650 is strongly expressed in adjacent lung tissue; the strongest expressed region being in the immediate leading edge between tumor and lung (Figure 32). In the tumor invasion front, the hsa-mir-650 expression is weak. Hsa-mir-650 expression in the inner tumor is also weak compared to the adjacent lung tissue. Hsa-mir-650 expression in normal lung tissue is slightly stronger than the inner tumor region, but still weaker than the adjacent lung tissue. The hsa-mir-650 expression is localized to the cytoplasm (Figure 32).

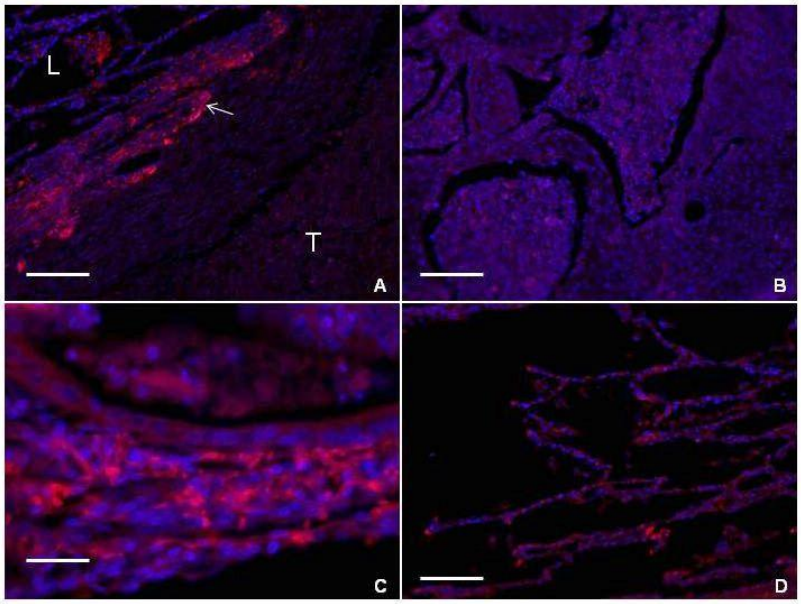

Figure 32. hsa-mir-650 is an unique microRNA highly expressed in adjacent lung area. A. Hsa-mir-650 is highly expressed in the adjacent lung at the leading edge between tumor and lung area. The arrow shows one of the strongest hsa-mir-650 expression cell populations. B. Hsa-mir-650 expression in the inner tumor is weak. C. Magnification of the region shown by the arrow in "A" Hsa-mir-650 is highly expressed in the adjacent lung area. D. Hsa-mir-650 expression in normal lung. red channel: Alexa 594 labeled hsa-mir-650; blue channel: DAPI labeled cell nuclei. A, B, D Bar=150 μm; C Bar=30 μm.

4 Discussion

4.1 Laser capture microdissection and transcriptome analysis

Laser capture microdissection, LCM, is a technique for isolating highly pure cell populations from a heterogeneous tissue section, a cytological preparation, or from live cell culture via direct visualization of the cells. LCM is applicable to molecular profiling of tissue, permitting correlation of cellular molecular signatures with specific cell populations, and comparison of cellular elements within the tissue microenvironment. Applications for laser microdissection have been found for every step associated with the dogma of molecular biology, from DNA to RNA to protein in specific cell populations. “Omic studies”, including genomic and proteomic molecular profiling in all three molecular compartments have been analyzed by the laser capture microdissection technique (Wulfkuhle et al., 2003; Sheehan et al., 2005; Bonner et al., 1997; Simone et al., 2000; Gulmann et al., 2005; Grubb et al., 2003; Elliott et al., 2003; Emmert-Buck et al., 2000; Chen et al., 2002). Laser capture microdissection has been combined with recent epigenetics studies of DNA methylation of spermatogenesis (Hartmann et al., 2006). Protein extracted from microdissected cells can be applied to reverse-phase protein microarrays (Iyengar et al., 2005; Wulfkuhle et al., 2003; Sheehan et al., 2005; Petricoin et al., 2005; Gulmann et al., 2005; Grubb et al., 2003; Paweletz et al., 2001; Liotta et al., 2003), 2D gel electrophoresis (Wulfkuhle et al., 2002; Ornstein et al., 2000; Jones et al., 2002), western blotting and mass spectrometry (Ornstein et al., 2000; Jones et al., 2002; Martinet et al., 2004).

Laser capture microdissection in combination with oligonucleotide microarray based expression profiling via linear RNA amplification allowed us to investigate

mRNA transcription in small amounts of specific cell populations. RNA preserved hematoxylin and eosin staining is widely used to identify the tissue morphology and cell populations in current LCM assist microarray studies, but even if it is a RNA preserved method, the staining step, based on our observations, may result in RNA degradation. It is hard to control the final RNA quality from LCM, especially for clinical samples. The quick and simple 100% ice cold ethanol treatment appears to keep good RNA quality for laser microdissection, but makes it hard to find target cell populations. A novel method, punch aided laser capture microdissection, overcomes the RNA quality problem, still allowing a staining step and the capture of target cell populations guided by reference slides.

To target the cells expressing specific proteins, immuno-LCM, which captures immunostained cells, has been developed to study gene expression in dopaminergic neurons by q-RT PCR (Uz et al., 2005), but the RNA quality may not be good enough to perform gene expression microarrays. To overcome this problem, punch aided laser microdissection method could potentially be applied to find and capture cell populations expressing specific proteins by reference immuno-stained slides, keeping a high integrity of RNA for genome wide expression microarray analysis.

There are also drawbacks to punch aided laser capture microdissection. If the cell clusters are two small, for example less than 100 cells in one section layer, or the target cells are scattering around the section, it might be quite difficult to localize the target cell populations by matching with the reference slides. The ideal target cell population contains more than ~300 cells in one layer of the section and is grouped together.

4.2 Zonal gene expression profile comparison of squamous cell lung carcinoma

4.2.1 Unsupervised cluster analysis of gene expression between the tumor invasion front and the inner tumor

Laser capture microdissection was first designed to investigate tumor cells (Emmert-Buck et al., 1996), and in recent decades, it has been widely used to study the heterogeneity of tumor tissue. Using laser capture microdissection combined wtih gene expression profiling on oligonucleotide microarrays, investigators compared the gene expression of ductal carcinoma in situ (DCIS) and invasive ductal carcinoma (IDC) cells of human breast cancer (Schuetz et al., 2006), the invasion front and inner tumor, as well as the dedifferentiated and non-dedifferentiated invasion fronts, of human colorectal cancer (Oku et al., 2008; Staub et al., 2007), as well as the peripheral zone and central zone tumor mass of human pancreatic cancer xenografts in mouse (Nakamura et al., 2007). Similar to our unsupervised cluster of the tumor invasion front and inner tumor, most of the previous comparison studies also could not well separate distinct clusters between two groups of tumor cells (Figure 33).

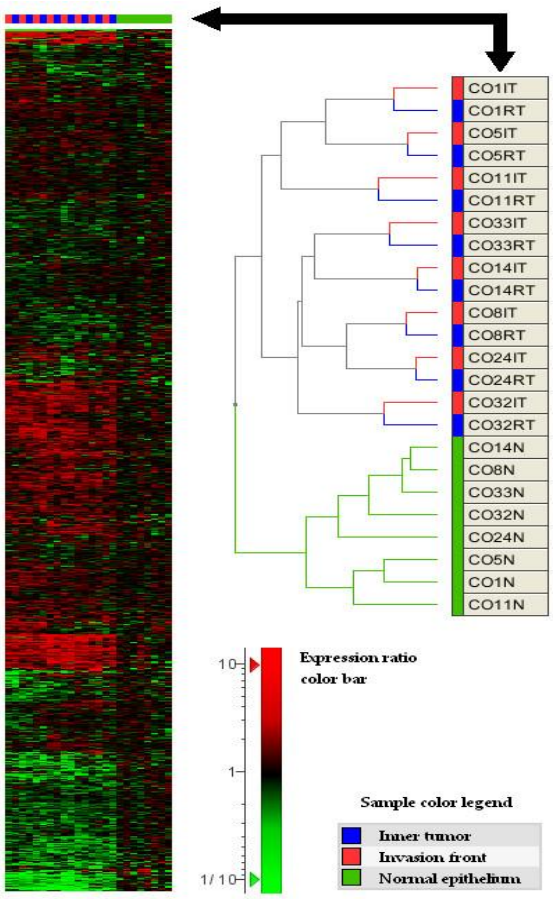

Figure 33. Two-way hierarchical clustering of tumor and normal epithelia samples based on expression profiles of 7433 genes. The heat map shows expression changes relative to the average signal in normal tissues. Red means up-regulation, green means down-regulation (see expression ratio color bar at the bottom). The dendrogram shows the hierarchical order of similarities between patient samples. Note that all normal samples are separated from tumors and both samples of a patient that stem from different tumor compartments clustered as neighbors (Staub et al., 2007).

One question that arises is what is the difference between the tumor invasion front and the inner tumor. The gene expression profiles have already shown us that, to a great extent, there is little difference between those two areas. In addition, we do not know with certainty, if we have captured the “right” tumor invasion front, and if tumor invasion front cell populations are homogeneous. There is no authoritative exactly defined area of the “tumor invasion front”. If we narrowed our target invasion front from 500 µm to very few layers of cells close to the leading edge between tumor and lung, more differences might have arisen

from our current study of the tumor center and tumor front. Using 83 differentially expressed genes, investigators have shown hierarchical clustering between dedifferentiated and non-dedifferentiated phenotype invasion fronts of human colorectal cancer (Oku et al., 2008); the result indicated small difference between these two tumor cell populations, and did not contain unsupervised clustering. As such, we could not evaluate and compare them with our current clustering results. The future transcription profiles of tumor invasion front in lung cancer might focus on more specific populations, which express special phenotypic markers. For example, one could focus on the cells with EMT phenotype in the tumor invasion front, and try to profile the cells which express EMT markers using immunostaining and the punch aided laser capture microdissections method.

4.2.2 Genes differentially expressed between tumor invasion front and inner tumor of squamous cell lung carcinoma

Through gene expression profiling with oligonucleotide microarrays, we identified 13 genes differentially expressed between the tumor invasion front and the inner tumor. The gene expression profile datasets were uploaded into the Ingenuity software package to analyze molecular networks and pathways. The large majority of the candidate genes, 9 in total, were identified as being involved in a molecular network comprising 42 genes, which function in cell-to-cell signaling and interaction, inflammatory response, cellular movement, gene expression and cell cycle arrest (Figure 34). These biological functions are crucial for tumor invasion and metastasis. The tumor necrosis factor (*TNF*) gene plays a central role in this molecular network by interacting with other genes, for example *NF-κB*, *IL10*, *RELA*, and *RELB*, although *TNF*, itself, is not differentially expressed between the

tumor invasion front and the inner tumor. Two interleukin genes, *IL4* and *IL10*, are also involved in the network. They both negatively regulate *TNFα* expression (Boussiotis et al., 1994; Körholz et al., 1997). Two C-C motif chemokine members, *CCL18* and *CCL19*, are also present in the network. *CCL18* is reported to possess a function in the regulation of pulmonary inflammation and fibrosis (Pochetuhen et al., 2007). The chemokine molecules may also play an important role in attracting immune cells to the tumor stroma microenvironment and in regulating tumor growth and invasion. *CCL19* has been reported to be involved in head and neck squamous cell carcinoma invasion (Wang et al., 2005).

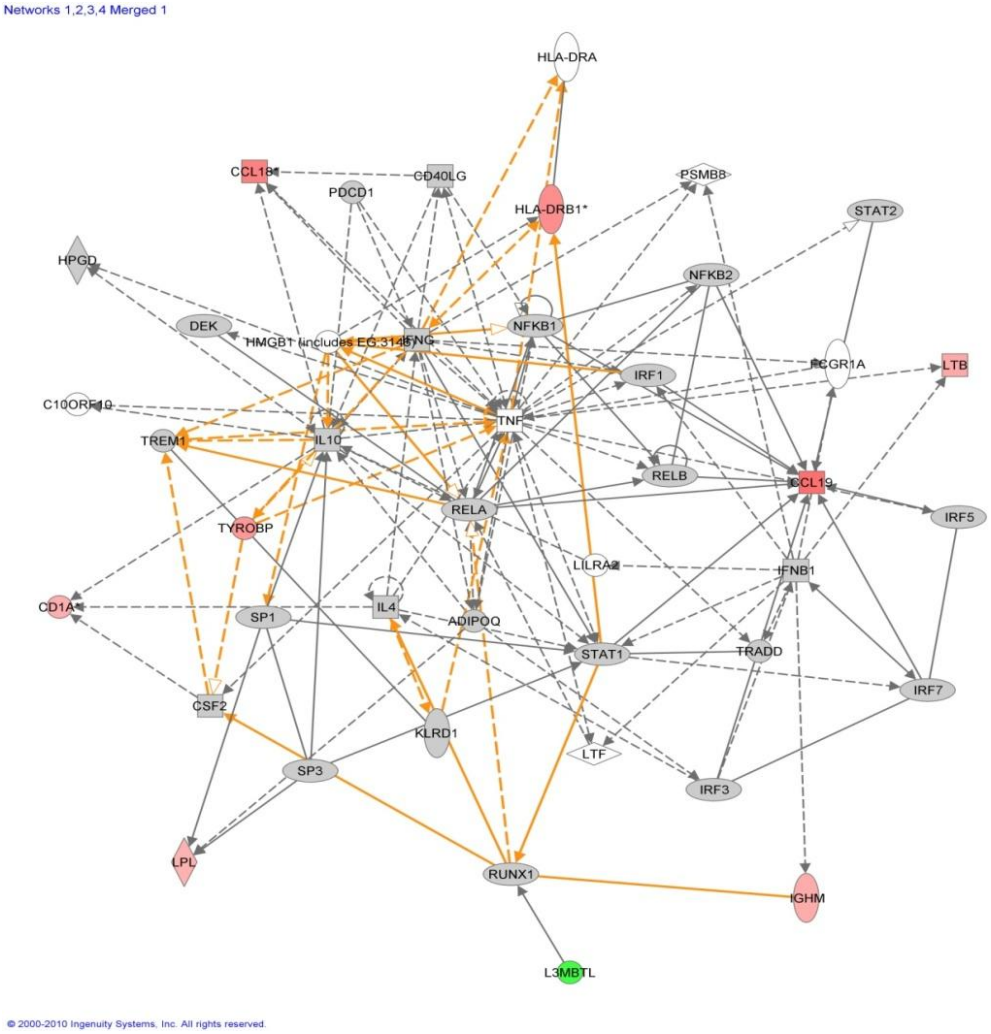

Figure 34. A visual representation of the gene expression network of tumor invasion front versus inner tumor. The red color shows upregulated genes in the tumor invasion front compared to the inner tumor; the green color shows a downregulated gene in the tumor invasion front compared to the inner tumor; gray or white colors show genes not significantly changed between tumor invasion front and the inner tumor.

4.2.3 Deregulated genes in squamous cell lung carcinoma cells

Through oligonucleotide microarray, we identified around 13,000 genes differentially expressed between tumor and lung. Among the deregulated genes, keratin 15 is a hair follicle stem cell and progenitor cell markers (Kanoh et al., 2008). *FOSB* and *CFOS* are down regulated in tumor cells compared to normal lung; indicating that the *AP-1* pathway plays an important role in squamous cell lung cancer progression. In contrast, *FOSB* and its role in lung cancer have not

been revealed. *P63* is a specific marker that distinguishes squamous cell lung carcinoma from lung adenocarcinoma (Rossi et al., 2009) and is 3 fold upregulated in tumor cells when compared to normal lung. *EGFR*, a key therapy target gene in non small cell lung cancer (Belani, 2010), is 2.2 fold upregulated in tumor cells. *DSG3*, 40~60 fold upregulated in lung cancer cells, was recently identified to be a squamous cell lung carcinoma diagnostic marker (Savci-Heijink, et al., 2009). Interestingly, cancer cells undergoing EMT can acquire invasive properties and enter the surrounding stroma, so EMT is involved in cancer progression and metastasis (Iwatsuki et al., 2010). Whereas EMT specific genes such as *TWIST*, *SNAIL*, *SIP1*, *CDH1*, *CTNNA1*, *JUP*, *VIM* and *CDH2* are not significantly deregulated in tumor cells compared to normal lung cells.

4.2.4 Canonical pathways in squamous cell lung carcinoma cells

In order to understand the biological implications of our data on lung oncogenesis, it was of biological interest to investigate the genes contained in the gene expression signature in further detail. Therefore, the Ingenuity software program was applied to study pathway deregulation in the specific tumor regions. The tumor invasion front and inner tumor cells shared many of the top scoring canonical pathways. Metabolic pathways ranked high and were frequent in the deregulated pathway list, for example, eicosanoid signaling, arachidonic acid metabolism, glutamate metabolism, linoleic acid metabolism, and fatty acid metabolism. Most of these pathways are related to fatty acid metabolism and bioactive lipid mediated signal transduction (Figure 35, 36).

As stated in the introduction, prostaglandins are very important in tumor progression. Previously, investigators have found that PGE2 helps to shift the tumor microenvironment from anti-tumor T helper 1 (*TH1*) responses to

immunosuppressive T helper 2 (*TH2*) responses by downregulation of TH1 cytokines (tumor necrosis factor-α (*TNFα*), interferon-γ (*IFNγ*) and *IL-2*) and upregulation of TH2 cytokines (*IL-4*, *IL-10* and *IL-6*) in immune cells (Snijdewint et al., 1993; Stolina et al., 2000; Hang et al., 1998). Moreover, PGE2 directly inhibits the activity of cytotoxic T cells through the upregulation of a CD94 and NKG2A complex and induces regulatory T cell function in vitro (Zeddou et al., 2005; Baratelli et al., 2005). PGE2 produced by tumor cells can also indirectly abolish the anti-tumor effects of cytotoxic T cells in vivo and in vitro through the downregulation of both direct antigen presentation by tumor cells and cross-presentation by dendritic cells (Ahmadi et al., 2008). In this study, prostaglandin E and F, their receptors' and their localized expression patterns (Figure 28, 29) seem to indicate that the prostaglandin E and F were synthesized in tumor cells and then drift into adjacent lung regions to conduct their biological functions. EP1 expression is observed in macrophages but not T cell lymphocytes, and EP2 is located in lung epithelial cells in the leading edge. This suggests that prostaglandin E may act as a messenger molecule that drifts from the tumor tissue to adjacent lung cells and possesses different functions in different cells of the adjacent lung, in macrophages it could play a role in tumor immune-tolerance, while in lung epithelial cell it could modulate fibrosis or hypoxia. The roles of prostaglandin E in these different cells need further validation throuh functional studies. Prostaglandin F is highly expressed in lung tumor epithelial cells but the FP receptor is not specifically expressed in any cell types. However, prostaglandin F is still produced in lung tumor and could act in tumor microenvironments interactions between the tumor and the adjacent lung tissue.

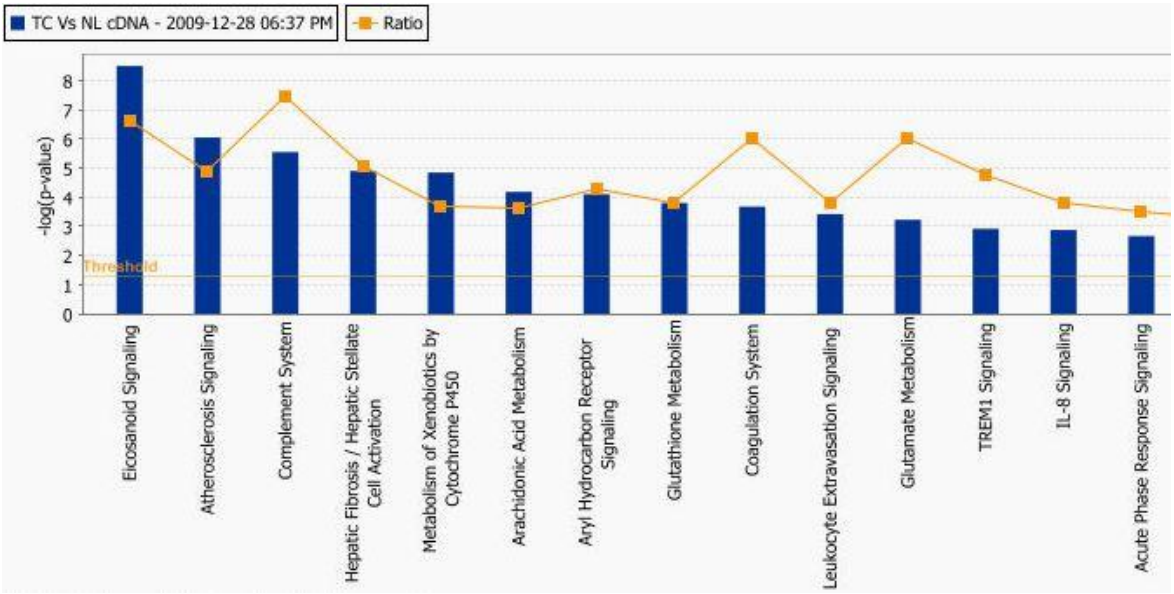

Figure 35. Top 16 canonical pathways present in inner tumor cells. The canonical pathways were ranked by p-value, threshold is a p-value < 0.05, ratio: number of deregulated factors in the pathway.

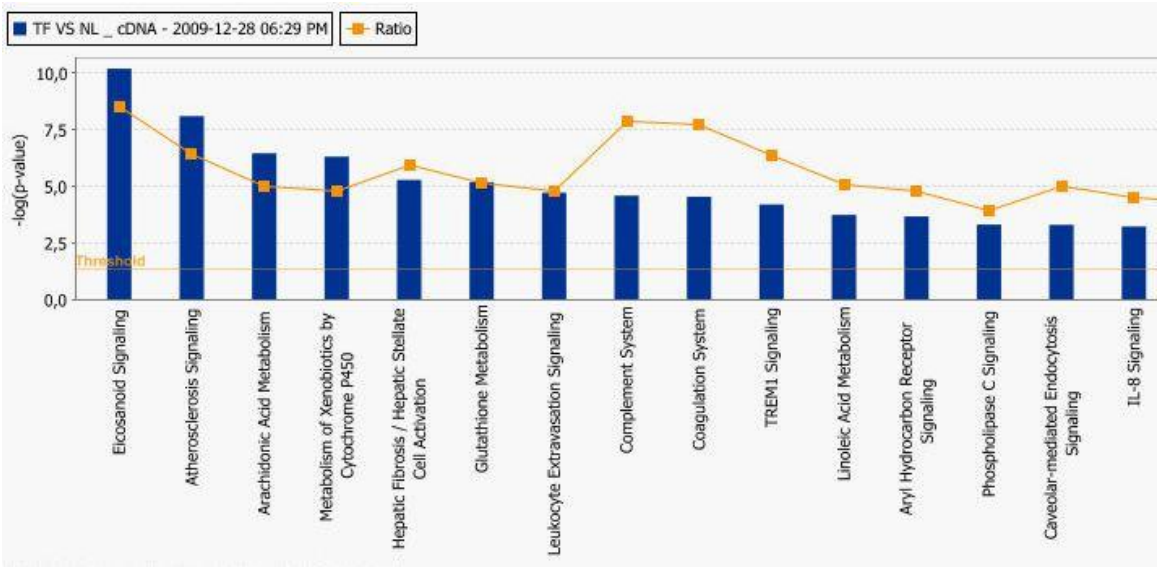

Figure 36. Top canonical pathways present in tumor invasion front cells. The canonical pathways were ranked by p-value, threshold is a p-value < 0.05, Ratio: number of deregulated factors in the pathway.

In addition to the metabolic pathways, hepatic fibrosis signaling and the sonic hedgehog signaling pathway are also activated in lung tumor cells (Figure 37).

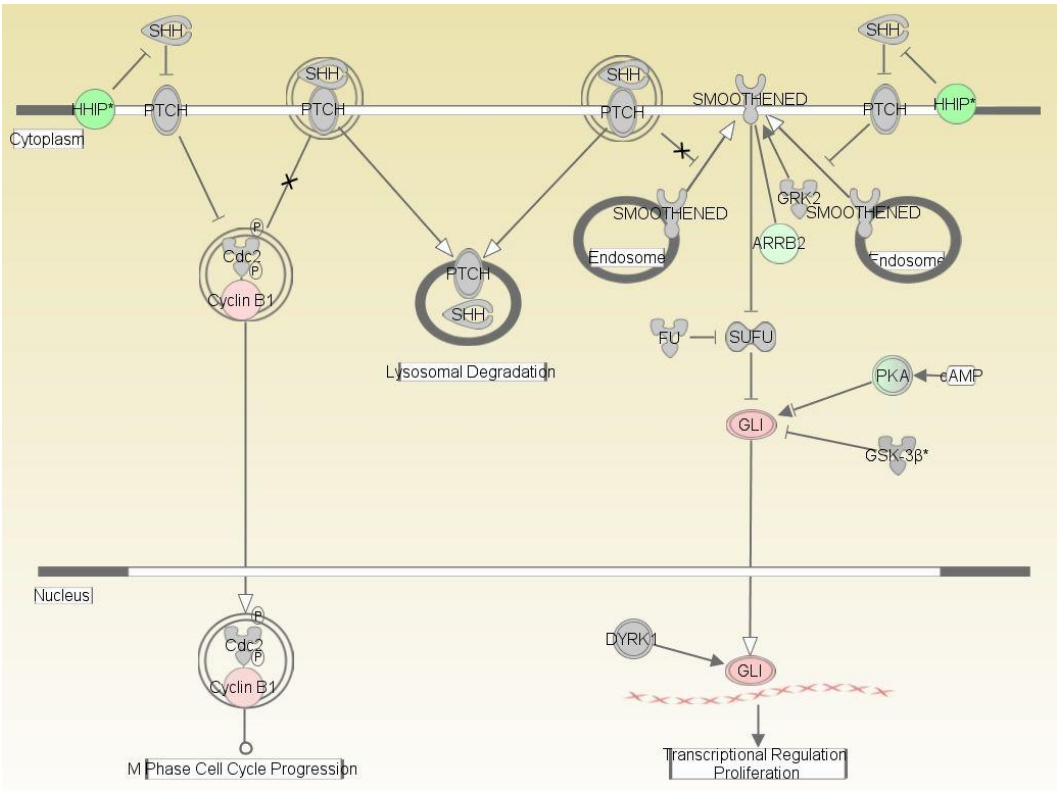

Figure 37. Sonic Hedgehog Signaling is activated in squamous cell lung carcinoma. The plasma membrane protein HHIP decreases inhibition of PTCH [Patched] protein(s) in plasma membrane, which is increased by Shh protein in the extracellular space. The down-regulation of HHIP may result in the inhibition of PTCH; due to PTCH induced inhibition of the protein CDC2, the down-regulation of HHIP may finally result in the activation of CDC2. CCND2 was 6.6 fold upregulated in this study and forms a protein complex with activated CDC2. The CCND2-CDC2 complex might then be transported into the cell nucleus and would promote M-phase cell cycle progression. As an important player in the Sonic Hedgehog signaling cascade, GLI was 3 fold upregulated in tumor cells. Down regulation of PKA might result in increased activation of GLI protein by reducing inhibition. The GLI proteins would then be transported into the cell nuclei to control transcription and promote proliferation. The green coloring means mRNA down-regulation; red coloring means mRNA up-regulation; gray and white colors mean no change in the mRNA level.

4.3 Chemokines in tumor microenvironment interactions

Based on the structure of their N-terminal cysteine motifs, chemotactic cytokines, which are low-molecular-weight cytokines, traditionally divided into four subgroups: C, CC, CX3C and CXC; the current nomenclature within these broad divisions assigns serial numbers to individual chemokines ligands (Zlotnik and Yoshie, 2000). Chemokines regulate the chemotaxis of leukocytes and play an essential

role in inflammation (Gerard and Rollins, 2001). The chemokine CCL19 is expressed especially in lymphoid tissues (Fevang et al., 2009), and also in medullary epithelial cells (Annunziato et al., 2000). The ability of CCL19 to chemoattract T cells (Kim et al, 1998a, 1998b, 1999; Ngo et al, 1998), B cells (Kim et al, 1998a, 1999), DC (Dieu et al, 1998), macrophage progenitor cells (Kim et al, 1998c) and NK cells (Kim et al, 1999) is mediated through the specific G protein-coupled seven transmembrane domain chemokine receptor CCR7. In recent studies, murine breast tumor cells transduced by a retroviral vector expressing CCL19 were rejected in vivo by a mechanism that involves both CD4+ and NK cells (Braun et al, 2000).

In the microarray data, CCL19 is highly expressed in the tumor invasion front and adjacent lung tissue. Further, our immunohistochemistry staining verified these findings. The high expression of CCL19 in adjacent tissues could easily explain the ability of CCL19 to attract lymphocytes to the leading edge of tumor and trigger imuno-defense against tumor invasion and progression. Although the high expression of CCL19 in lung tumor epithelial cells has not been reported, a report on CCL21, a chemokine sharing the same receptor as CCL19, reveals that invasive cancer cells secrete CCL21 in 3D conditions, and reports a surprising function of CCL21 in the promotion of tumor growth by suppression of the hosts' adaptive immune response (Shields et al., 2010). Aside from the altered trafficking of immune cells into and out of tumor tissue, authors show that the tumor tissue formed by CCL21-expressing cancer cells selectively accumulate more tumor suppressive immune cells, such as regulatory T cells and myeloid-derived suppressor cells, resulting in the formation of an immune tolerogenic stromal structure. The CCL19 expressed in the tumor invasion front of the

epithelial tumor cells might also function by the above mechanism of immune tolerogenic. Therefore, there might be two CCL19 functional patterns in the interface of lung and tumor, the first one is that CCL19 is highly expressed in adjacent lung tissue and attracts lymphoid cells close to the tumor and triggers immune defense against tumor invasion and progression; the second possibility might be, similar to CCL21 expression in epithelial tumor cells, to selectively accumulate more tumor suppressive immune cells, such as regulatory T cells to establish an immune tolerogenic stroma structure and promote tumor invasion and progression. These two mechanisms need to be followed upon by extra in vivo and/or in vitro experiments.

In our findings, prostaglandins E and F play crucial roles in tumor microenvironment interactions. As small molecule products of eicosaniod metabolism, prostaglandin E and F could raft between the tumor tissue and adjacent lung tissue and trigger signal response by activating prostaglandin receptors. Previous studies have shown that the addition of prostaglandin E2 was required for effective migration of monocyte-derived dendritic cells toward CCL19 and CCL21 (Scandella et al., 2004). Costimulation with PGE2 enhanced the expression of the CCL19/CCL21 receptor CCR7 on the cell surface of monocyte-derived dendritic cells, when they matured with soluble CD40 ligand or proinflammatory cytokines (Scandella et al., 2002). Therefore, prostaglandin E, CCL19 and their receptors appear to work together to mediate tumor microenvironment interactions and inflammation.

4.4 MicroRNA and lung cancer

4.4.1 MicroRNA expression between adjacent lung and normal lung tissue

Through TLDA, we found four microRNAs, hsa-mir-433, hsa-mir-650, hsa-mir-137 and hsa-mir-210, that are upregulated in adjacent lung tissue. Hsa-mir-433 is 10 fold upregulated in adjacent lung tissue and was shown previously to be regulated by the nuclear receptors ERRgamma/SHP (Song and Wang, 2008). Hsa-mir-433 was shown to be down regulated in gastric cancers and to target *GRB2*, *RAB34* and *RAB39* (Luo et al., 2009). Grb2 signaling is critical for cell cycle progression and actin-based cell motility, and, consequently, more complex processes such as epithelial morphogenesis, angiogenesis and vasculogenesis (Giubellino et al., 2008). RAB34 and RAB39 are RAS signalling molecules and *RAB39* may be a short variant of *RAB34* involved in cellular endocytosis (Chen et al., 2003). Hsa-miR-137 is 5.8 fold upregulated in adjacent lung tissue and has been shown to target *CDC42* expression, induce cell cycle G1 arrest, and inhibit invasion in colorectal cancer (Liu et al., 2010). Hsa-mir-210 is expressed in various human cancers, is related to the modulation of hypoxia pathways (Huang et al., 2010), and is 3 fold upregulated in adjacent lung tissue in this study. Hsa-mir-650 is the most novel microRNA found in this analysis. Hsa-mir-650 is highly upregulated in adjancent lung tissue when compared to any of the other 3 compartments (Figure 19). Hsa-mir-650 targets *ING4* and is involved in lymphatic and distant metastasis in human gastric cancer (Zhang et al., 2010). It has been found that microRNAs can be actively transported out of the cell via the exosome (Valadi et al., 2007; Taylor and Gercel-Taylor, 2008) and that chronic inflammation can lead to lung cancer (Engels, 2008). It is interesting to speculate as to whether an

inflammatory microenvironment leads to the interstitial transport of microRNAs from alveolar macrophages into lung epithelial cells, which could eventually lead to the initiation of tumor pathogenesis. This hypothesis remains to be tested.

4.4.2 MicroRNA expression between squamous cell lung carcinoma tumor cells and normal lung tissue

We have profiled the expression of 365 microRNAs in laser microdissected lung SCC samples by TaqMan Low Density Array and found 66 microRNAs were deregulated in lung SCC tumor cells. In contrast to our above findings, most of members of the miR-17-92 cluster were not highly expressed in lung SCC. The hsa-miR-17-92 cluster has been found to be overexpressed in many cancers, including lung cancer, and has been implicated as an oncogene (Hayashita et al., 2005; He et al., 2005; Mendell, 2008). Hsa-miR-106a, hsa-mir-20b, hsa-mir-93, and hsa-mir-106b, which are paralogues of the hsa-mir-17-92 cluster, have been previously found to be upregulated in lung SCC and leukemias and associated with oncogenesis (Garzon et al., 2006; Landais et al., 2007). Only one member of hsa-mir-17-92 cluster, hsa-mir-17-5p, was 2 fold upregulated in SCC tumor cells in our study. In addition, we found has-let-7e and has-let-7c (and its cluster member miR-125a) expressed at a low level in lung SCC, which is consistent with previous reports (Takamizawa et al., 2004; Johnson et al., 2005; Mayr et al., 2007).

Our results were compared with that of Yanaihara and colleagues, who profiled microRNA expression in NSCLC samples using an alternative array containing 190 human microRNAs (Yanaihara et al., 2006). They found 16 microRNAs differentially expressed between 39 SCC and 39 matched normal lung tissues. Six of the 16 microRNAs were in common between their data set and our (hsa-mir-

205, hsa-mir-210, hsa-mir-203, hsa-mir-21, hsa-mir-143 and has-mir-30a-5p) showing the same general direction of differential expression (Yanaihara et al., 2006). We also compared our result with that of Mitch Raponi and colleagues (Raponi et al., 2009). They found 15 microRNAs differentially expressed between SCC and normal lung. 9 of the 15 microRNAs showed the same type of expression pattern between their date set and ours (hsa-mir-210, hsa-mir-17-5p, hsa-mir-203, hsa-let-7e, hsa-mir-200a, hsa-mir-93, hsa-mir-182, hsa-mir-183, hsa-mir-224). Our identification of hsa-mir-224 up-regulation in lung tumor tissue compared to normal lung confirmed the findings of Raponi and colleagues (Raponi et al., 2009), but was contrary to the findings of Yanaihara and colleagues (Yanaihara et al., 2006), Furthermore, we verified the expression pattern of hsa-mir-224 by microRNA FISH. In addition, in other studies hsa-mir-224 showed elevated expression in Perineural invasion (PNI) tumors when compared to non-PNI tumors in prostate cancer (Prueitt et al., 2008).

4.4.3 Differentially expressed microRNAs and molecular networks

Through correlation analysis between microRNA and mRNA array data, we identified 14 microRNAs that putatively inhibit verified target genes. As such, we uploaded the 14 candidate microRNAs with their target genes to the Ingenuity Pathway Analysis online platform to study microRNA targeting of molecular networks. Through this analysis, we identified a network including 274 factors. The molecules in the network are mainly associated with the known pathways “molecular mechanism of cancer”, “pancreatic adenocarcinoma signaling” and “hereditary breast cancer signaling”. The Ingenuity analysis indicates that the 12 microRNAs could play a crucial role in lung cancer progression in the analyzed patients.

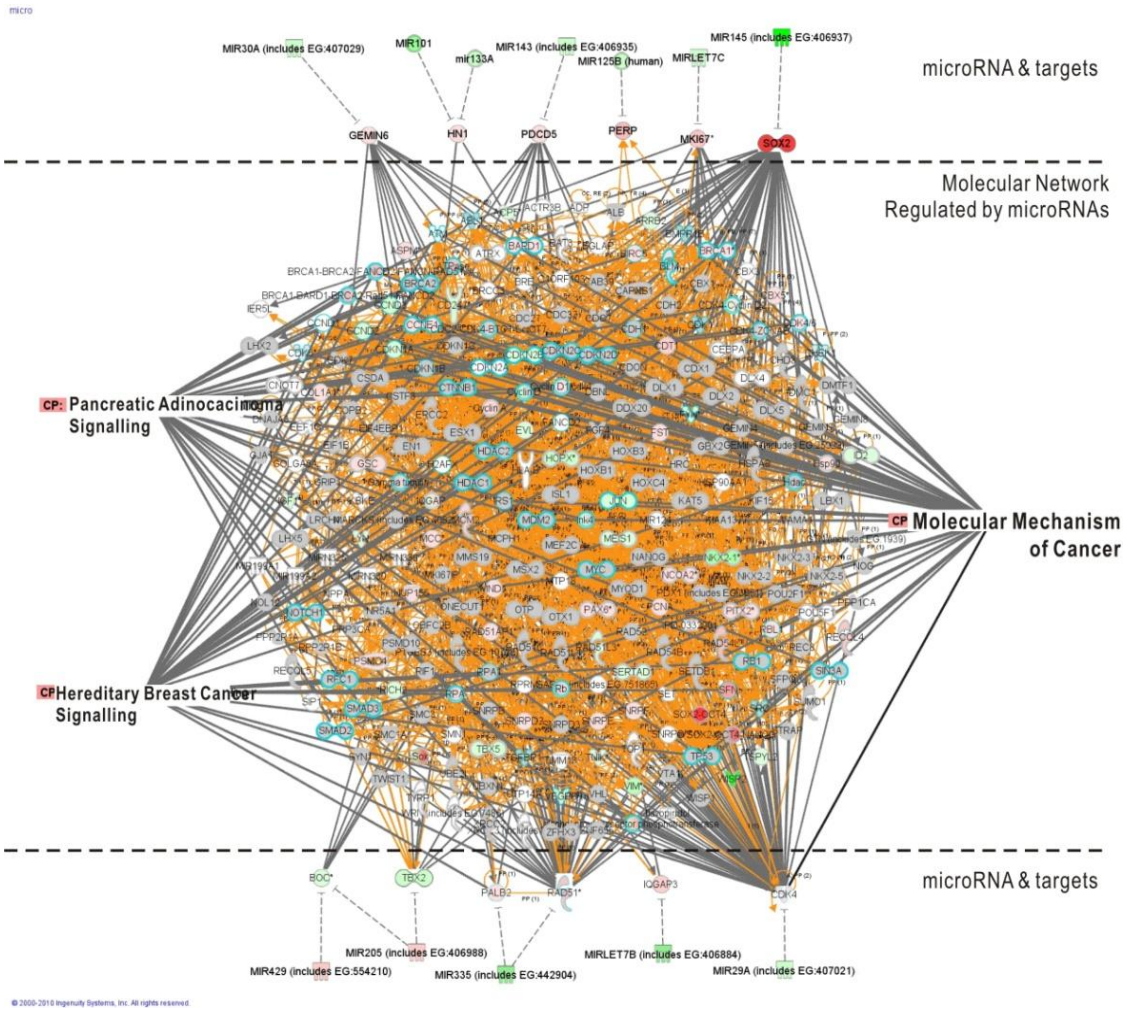

Figure 38. microRNA target molecule networks. The molecules between two dashed lines forming a network engaging in “molecular mechanism of cancer”, “pancreatic adenocarcinoma signaling” and “hereditary breast cancer signaling”. The molecules at the end of the two dashed line are microRNAs and their directly targeted mRNA genes. The green color indicates that the gene is downregulated in tumor cells; red color indicates that the gene is upregulated in tumor cells.

References

Ahmadi M, Emery DC, Morgan DJ. Prevention of both direct and cross-priming of antitumor CD8+ T-cell responses following overproduction of prostaglandin E2 by tumor cells in vivo. Cancer Res. 2008 Sep 15;68(18):7520-9.

Annunziato F, Romagnani P, Cosmi L, Beltrame C, Steiner BH, Lazzeri E, Raport CJ, Galli G, Manetti R, Mavilia C, Vanini V, Chantry D, Maggi E, Romagnani S. Macrophage-derived chemokine and EBI1-ligand chemokine attract human thymocytes in different stage of development and are produced by distinct subsets of medullary epithelial cells: possible implications for negative selection. J Immunol. 2000 Jul 1;165(1):238-46.

Alberts B, Johnson A, Lewis J, Raff M, Roberts K, Walter. Molecular Biology of the Cell, 4th edition. New York: Garland Science; 2002. pp-1333

Backlund MG, Mann JR, Holla VR, Buchanan FG, Tai HH, Musiek ES, Milne GL, Katkuri S, DuBois RN. 15-Hydroxyprostaglandin dehydrogenase is downregulated in colorectal cancer. J Biol Chem. 2005 Feb 4;280(5):3217-23.

Baker SJ, Fearon ER, Nigro JM, Hamilton SR, Preisinger AC, Jessup JM, vanTuinen P, Ledbetter DH, Barker DF, Nakamura Y, White R, Vogelstein B. Chromosome 17 deletions and p53 gene mutations in colorectal carcinomas. Science. 1989 Apr 14;244(4901):217-21.

Baratelli F, Lin Y, Zhu L, Yang SC, Heuzé-Vourc'h N, Zeng G, Reckamp K, Dohadwala M, Sharma S, Dubinett SM. Prostaglandin E2 induces FOXP3 gene expression and T regulatory cell function in human CD4+ T cells. J Immunol. 2005 Aug 1;175(3):1483-90.

Becker KF, Atkinson MJ, Reich U, Becker I, Nekarda H, Siewert JR, Höfler H. E-cadherin gene mutations provide clues to diffuse type gastric carcinomas. Cancer Res. 1994 Jul 15;54(14):3845-52.

Belani CP. The role of irreversible EGFR inhibitors in the treatment of non-small cell lung cancer: overcoming resistance to reversible EGFR inhibitors. Cancer Invest. 2010;28(4):413-23.

Berx G, Cleton-Jansen AM, Nollet F, de Leeuw WJ, van de Vijver M, Cornelisse C, van Roy F. E-cadherin is a tumor/invasion suppressor gene mutated in human lobular breast cancers. EMBO J. 1995 Dec 15;14(24):6107-15.

Barbone F, Bovenzi M, Cavallieri F, Stanta G. Cigarette smoking and histologic type of lung cance in men. Chest. 1997 Dec;112(6):1474-9.

Barnard WG. The nature of the oat-celled sarcoma of the mediastinum. J Pathol Bacteriol 1926;29:241

Bernstein E, Caudy AA, Hammond SM, Hannon GJ. Role for a bidentate ribonuclease in the initiation step of RNA interference. Nature. 2001 Jan 18;409(6818):363-6.

Bonner RF, Emmert-Buck M, Cole K, Pohida T, Chuaqui R, Goldstein S, Liotta LA. Laser capture microdissection: molecular analysis of tissue. Science. 1997;278(5342):1481,1483.

Borczuk AC, Gorenstein L, Walter KL, Assaad AA, Wang L, Powell CA. Non-small-cell lung cancer molecular signatures recapitulate lung developmental pathways. Am J Pathol. 2003 Nov;163(5):1949-60.

Boussiotis VA, Nadler LM, Strominger JL, Goldfeld AE. Tumor necrosis factor alpha is an autocrine growth factor for normal human B cells. Proc Natl Acad Sci U S A. 1994;91(15):7007-11.

Brambilla E, Negoescu A, Gazzeri S, Lantuejoul S, Moro D, Brambilla C, Coll JL. Apoptosis-related factors p53, Bcl2, and Bax in neuroendocrine lung tumors. Am J Pathol. 1996 Dec;149(6):1941-52

Braun SE, Chen K, Foster RG, Kim CH, Hromas R, Kaplan MH, Broxmeyer HE, Cornetta K. The CC chemokine CK beta-11/MIP-3 beta/ELC/Exodus 3 mediates tumor rejection of murine breast cancer cells through NK cells. J Immunol. 2000;164:4025–4031.

Blanco MJ, Moreno-Bueno G, Sarrio D, Locascio A, Cano A, Palacios J, Nieto MA. Correlation of Snail expression with histological grade and lymph node status in breast carcinomas. Oncogene. 2002 May 9;21(20):3241-6

Bryant A, Cerfolio RJ. Differences in epidemiology, histology, and survival between cigarette smokers and never-smokers who develop non-small cell lung cancer. Chest. 2007 Jul;132(1):185-92

Burbee DG, Forgacs E, Zöchbauer-Müller S, Shivakumar L, Fong K, Gao B, Randle D, Kondo M, Virmani A, Bader S, Sekido Y, Latif F, Milchgrub S, Toyooka S, Gazdar AF, Lerman MI, Zabarovsky E, White M, Minna JD. Epigenetic inactivation of RASSF1A in lung and breast cancers and malignant phenotype suppression. J Natl Cancer Inst. 2001 May 2;93(9):691-9.

Calin GA, Croce CM. MicroRNA signatures in human cancers. Nat Rev Cancer 2006;6:857-866

Calin GA, Sevignani C, Dumitru CD, et al. Human microRNA genes are frequently located at fragile sites and genomic regions involved in cancers. Proc Natl Acad Sci U S A 2004;101:2999-3004

Campese AF, Bellavia D, Gulino A, Screpanti I. Notch signalling at the crossroads of T cell development and leukemogenesis. Semin Cell Dev Biol. 2003 Apr;14(2):151-7.

Caputi M, De Luca L, Papaccio G, D'Aponte A, Cavallotti I, Scala P, Scarano F, Manna M, Gualdiero L, De Luca B. Prognostic role of cyclin D1 in non small cell lung cancer: an immunohistochemical analysis. Eur J Histochem. 1997;41(2):133-8.

Cavenee WK, Dryja TP, Phillips RA, Benedict WF, Godbout R, Gallie BL, Murphree AL, Strong LC, White RL. Expression of recessive alleles by chromosomal mechanisms in retinoblastoma. Nature. 1983 Oct 27-Nov 2;305(5937):779-84.

Chang SH, Ai Y, Breyer RM, Lane TF, Hla T. The prostaglandin E2 receptor EP2 is required for cyclooxygenase 2-mediated mammary hyperplasia. Cancer Res. 2005;65(11):4496-9.

Chen T, Han Y, Yang M, Zhang W, Li N, Wan T, Guo J, Cao X. Rab39, a novel Golgi-associated Rab GTPase from human dendritic cells involved in cellular endocytosis. Biochem Biophys Res Commun. 2003 Apr 18;303(4):1114-20

Chen X, Cheung ST, So S, Fan ST, Barry C, Higgins J, Lai KM, Ji J, Dudoit S, Ng IO, Van De Rijn M, Botstein D, Brown PO. Gene expression patterns in human liver cancers. Mol Biol Cell. 2002 Jun;13(6):1929-39.

Chuang JC, Jones PA. Epigenetics and microRNAs. Pediatr Res. 2007 May;61(5 Pt 2):24R-29R

Claudio PP, Howard CM, Pacilio C, Cinti C, Romano G, Minimo C, Maraldi NM, Minna JD, Gelbert L, Leoncini L, Tosi GM, Hicheli P, Caputi M, Giordano GG, Giordano A. Mutations in the retinoblastoma-related gene RB2/p130 in lung tumors and suppression of tumor growth in vivo by retrovirus-mediated gene transfer. Cancer Res. 2000 Jan 15;60(2):372-82.

Comijn J, Berx G, Vermassen P, Verschueren K, van Grunsven L, Bruyneel E, Mareel M, Huylebroeck D, van Roy F. The two-handed E box binding zinc finger protein SIP1 downregulates E-cadherin and induces invasion. Mol Cell. 2001 Jun;7(6):1267-78.

Croce CM. Oncogenes and cancer, N Engl J Med. 2008 Jan 31;358(5):502-11.

Curnen MG. Lung cancer in Connecticut women. Lancet. 1983 Oct 15;2(8355):906-7.

Dammann R, Li C, Yoon JH, Chin PL, Bates S, Pfeifer GP. Epigenetic inactivation of a RAS association domain family protein from the lung tumor suppressor locus 3p21.3. Nat Genet. 2000 Jul;25(3):315-9.

Dang TP, Eichenberger S, Gonzalez A, Olson S, Carbone DP. Constitutive activation of Notch3 inhibits terminal epithelial differentiation in lungs of transgenic mice. Oncogene. 2003 Apr 3;22(13):1988-97.

Dang TP, Gazdar AF, Virmani AK, Sepetavec T, Hande KR, Minna JD, Roberts JR, Carbone DP. Chromosome 19 translocation, overexpression of Notch3, and human lung cancer. J Natl Cancer Inst. 2000 Aug 16;92(16):1355-7

de Graauw M, van Miltenburg MH, Schmidt MK, Pont C, Lalai R, Kartopawiro J, Pardali E, Le Dévédec SE, Smit VT, van der Wal A, Van't Veer LJ, Cleton-Jansen AM, ten Dijke P, van de Water B. Annexin A1 regulates TGF-beta signaling and promotes metastasis formation of basal-like breast cancer cells. Proc Natl Acad Sci U S A. 2010 Apr 6;107(14):6340-5.

Denli AM, Tops BB, Plasterk RH, Ketting RF, Hannon GJ. Processing of primary microRNAs by the Microprocessor complex. Nature. 2004 Nov 11;432(7014):231-5

Diederichs S, Haber DA. Sequence variations of microRNAs in human cancer: alterations in predicted secondary structure do not affect processing. Cancer Res. 2006 Jun 15;66(12):6097-104.

Dieu MC, Vanbervliet B, Vicari A, Bridon JM, Oldham E, Ait-Yahia S, Briere F, Zlotnik A, Lebecque S, Caux C. Selective recruitment of immature and mature dendritic cells by distinct chemokines expressed in different anatomic sites. J Exp Med. 1998;188:373–386.

Driscoll B. Methods in Molecular Medicine: Lung Cancer. 2003. 61-73

Dosaka-Akita H, Hu SX, Fujino M, Harada M, Kinoshita I, Xu HJ, Kuzumaki N, Kawakami Y, Benedict WF. Altered retinoblastoma protein expression in nonsmall cell lung cancer: its synergistic effects with altered ras and p53 protein status on prognosis. Cancer. 1997 Apr 1;79(7):1329-37.

Edelman GM, Gallin WJ, Delouvée A, Cunningham BA, Thiery JP. Early epochal maps of two different cell adhesion molecules. Proc Natl Acad Sci U S A. 1983 Jul;80(14):4384-8.

Elliott JA, Osterlind K, Hirsch FR, Hansen HH. Metastatic patterns in small-cell lung cancer: correlation of autopsy findings with clinical parameters in 537 patients. J Clin Oncol. 1987 Feb;5(2):246-54.

Elliott K, Hill DS, Lambert C, Burroughes TR, Gill P. Use of laser microdissection greatly improves the recovery of DNA from sperm on microscope slides. Forensic Sci Int. 2003 Oct 14;137(1):28-36.

Emmert-Buck MR, Bonner RF, Smith PD, Chuaqui RF, Zhuang Z, Goldstein SR, Weiss RA, Liotta LA. Laser capture microdissection. Science. 1996 Nov 8;274(5289):998-1001.

Engels EA. Inflammation in the development of lung cancer: epidemiological evidence. Expert Rev Anticancer Ther. 2008 Apr;8(4):605-15.

Espina V, Wulfkuhle JD, Calvert VS, VanMeter A, Zhou W, Coukos G, Geho DH, Petricoin EF 3rd, Liotta LA. Laser-capture microdissection. Nat Protoc. 2006;1(2):586-603.

Esquela-Kerscher A, Slack FJ. Oncomirs - microRNAs with a role in cancer. Nat Rev Cancer. 2006 Apr;6(4):259-69

Fearon ER, Feinberg AP, Hamilton SH, Vogelstein B. Loss of genes on the short arm of chromosome 11 in bladder cancer. Nature. 1985 Nov 28-Dec 4;318(6044):377-80.

Ferlay J, Bray F, Pisani P, Parkin DM. Cancer Incidence, Mortality and Prevalence Worldwide, Globocan, 2000 (International Agency for Research on Cancer (IARC) Press, World Health Organization, Lyon, France, 2001)

Fevang B, Yndestad A, Damås JK, Halvorsen B, Holm AM, Beiske K, Aukrust P, Frøland SS. Chemokines and common variable immunodeficiency; possible contribution of CCL19, CCL21 and CCR7 to immune dysregulation. Clin Exp Immunol. 2009 Nov;158(2):237-45.

Fidler IJ. The pathogenesis of cancer metastasis: the 'seed and soil' hypothesis revisited. Nat Rev Cancer. 2003 Jun;3(6):453-8.

Finger LR, Harvey RC, Moore RCA, Showe LC, Croce CM. A common mechanism of chromosomal translocation in T- and B-cell neoplasia. Science 1986;234:982-985.

Fong KM, Sekido Y, Gazdar AF, Minna JD. Lung cancer. 9: Molecular biology of lung cancer: clinical implications. Thorax. 2003 Oct;58(10):892-900.

Funk CD. Prostaglandins and leukotrienes: advances in eicosanoid biology. Science. 2001;294(5548):1871-5.

Garzon R, Fabbri M, Cimmino A, Calin GA, Croce CM. MicroRNA expression and function in cancer. Trends Mol Med. 2006 Dec;12(12):580-7

Gazzeri S, Della Valle V, Chaussade L, Brambilla C, Larsen CJ, Brambilla E. The human p19ARF protein encoded by the beta transcript of the p16INK4a gene is frequently lost in small cell lung cancer. Cancer Res. 1998 Sep 1;58(17):3926-31.

Gerard C, Rollins BJ. Chemokines and disease. Nat Immunol 2001;2:108–115.

Giubellino A, Burke TR Jr, Bottaro DP. Grb2 signaling in cell motility and cancer. Expert Opin Ther Targets. 2008 Aug;12(8):1021-33.

Graziano SL, Gamble GP, Newman NB, Abbott LZ, Rooney M, Mookherjee S, Lamb ML, Kohman LJ, Poiesz BJ. Prognostic significance of K-ras codon 12 mutations in patients with resected stage I and II non-small-cell lung cancer. J Clin Oncol. 1999 Feb;17(2):668-75.

Greenburg G, Hay ED. Epithelia suspended in collagen gels can lose polarity and express characteristics of migrating mesenchymal cells. J Cell Biol. 1982 Oct;95(1):333-9

Greene FL, Page DL, Fleming ID, Fritz A, Balch CM, Haller DG, Morrow M. AJCC Cancer Staging Manual. 6th ed. New York: Springer; 2002.

Grubb RL, Calvert VS, Wulkuhle JD, Paweletz CP, Linehan WM, Phillips JL, Chuaqui R, Valasco A, Gillespie J, Emmert-Buck M, Liotta LA, Petricoin EF. Signal pathway profiling of prostate cancer using reverse phase protein arrays. Proteomics. 2003 Nov;3(11):2142-6.

Guilford P, Hopkins J, Harraway J, McLeod M, McLeod N, Harawira P, Taite H, Scoular R, Miller A, Reeve AE. E-cadherin germline mutations in familial gastric cancer. Nature. 1998 Mar 26;392(6674):402-5.

Gulmann C, Espina V, Petricoin E 3rd, Longo DL, Santi M, Knutsen T, Raffeld M, Jaffe ES, Liotta LA, Feldman AL. Proteomic analysis of apoptotic pathways reveals prognostic factors in follicular lymphoma. Clin Cancer Res. 2005 Aug 15;11(16):5847-55

Hambek M, Baghi M, Wagenblast J, Schmitt J, Baumann H, Knecht R. Inverse correlation between serum PGE2 and T classification in head and neck cancer. Head Neck. 2007;29(3):244-8.

Hanahan D, Weinberg RA. The hallmarks of cancer. Cell. 2000 Jan 7;100(1):57-70

Hanawalt PC, Ford JM, Lloyd DR. Functional characterization of global genomic DNA repair and its implications for cancer. Mutat Res. 2003 Nov;544(2-3):107-14.

Haqqani AS, Nesic M, Preston E, Baumann E, Kelly J, Stanimirovic D. Characterization of vascular protein expression patterns in cerebral ischemia/reperfusion using laser capture microdissection and ICAT-nanoLC-MS/MS. FASEB J. 2005 Nov;19(13):1809-21.

Hartmann S, Bergmann M, Bohle RM, Weidner W, Steger K. Genetic imprinting during impaired spermatogenesis. Mol Hum Reprod. 2006 Jun;12(6):407-11.

Hayashita Y, Osada H, Tatematsu Y, Yamada H, Yanagisawa K, Tomida S, Yatabe Y, Kawahara K, Sekido Y, Takahashi T. A polycistronic microRNA cluster, miR-17-92, is overexpressed in human lung cancers and enhances cell proliferation. Cancer Res. 2005 Nov 1;65(21):9628-32.

He L, Thomson JM, Hemann MT, Hernando-Monge E, Mu D, Goodson S, Powers S, Cordon-Cardo C, Lowe SW, Hannon GJ, Hammond SM. A microRNA polycistron as a potential human oncogene. Nature. 2005 Jun 9;435(7043):828-33.

Helin K, Holm K, Niebuhr A, Eiberg H, Tommerup N, Hougaard S, Poulsen HS, Spang-Thomsen M, Norgaard P. Loss of the retinoblastoma protein-related p130 protein in small cell lung carcinoma. Proc Natl Acad Sci U S A. 1997 Jun 24;94(13):6933-8.

Hess FG Jr, McDowell EM, Trump BF. Pulmonary cytology: current status of cytologic typing of respiratory tract tumors. Am J Pathol. 1981 May;103(2):323-33

Huang M, Stolina M, Sharma S, Mao JT, Zhu L, Miller PW, Wollman J, Herschman H, Dubinett SM. Non-small cell lung cancer cyclooxygenase-2-dependent regulation of cytokine balance in lymphocytes and macrophages: up-regulation of interleukin 10 and down-regulation of interleukin 12 production. Cancer Res. 1998 Mar 15;58(6):1208-16.

Huang X, Le QT, Giaccia AJ. MiR-210--micromanager of the hypoxia pathway. Trends Mol Med. 2010 May;16(5):230-7.

Huber MA, Azoitei N, Baumann B, Grünert S, Sommer A, Pehamberger H, Kraut N, Beug H, Wirth T. NF-kappaB is essential for epithelial-mesenchymal transition and metastasis in a model of breast cancer progression. J Clin Invest. 2004 Aug;114(4):569-81.

Hughes D, Otani T, Yang P, Newman RA, Yantiss RK, Altorki NK, Port JL, Yan M, Markowitz SD, Mazumdar M, Tai HH, Subbaramaiah K, Dannenberg AJ. NAD+-dependent 15-hydroxyprostaglandin dehydrogenase regulates levels of bioactive lipids in non-small cell lung cancer. Cancer Prev Res (Phila Pa). 2008 Sep;1(4):241-9.

Higashiyama M, Doi O, Kodama K, Yokouchi H, Kasugai T, Ishiguro S, Takami K, Nakayama T, Nishisho I. MDM2 gene amplification and expression in non-small-cell lung cancer: immunohistochemical expression of its protein is a favourable prognostic marker in patients without p53 protein accumulation. Br J Cancer. 1997;75(9):1302-8

Ihrie RA, Reczek E, Horner JS, Khachatrian L, Sage J, Jacks T, Attardi LD. Perp is a mediator of p53-dependent apoptosis in diverse cell types. Curr Biol. 2003 Nov 11;13(22):1985-90.

Iwatsuki M, Mimori K, Yokobori T, Ishi H, Beppu T, Nakamori S, Baba H, Mori M. Epithelial-mesenchymal transition in cancer development and its clinical significance. Cancer Sci. 2010 Feb;101(2):293-9.

Iyengar P, Espina V, Williams TW, Lin Y, Berry D, Jelicks LA, Lee H, Temple K, Graves R, Pollard J, Chopra N, Russell RG, Sasisekharan R, Trock BJ, Lippman M, Calvert VS, Petricoin EF 3rd, Liotta L, Dadachova E, Pestell RG, Lisanti MP, Bonaldo P, Scherer PE. Adipocyte-derived collagen VI affects early mammary tumor progression in vivo, demonstrating a critical interaction in the tumor/stroma microenvironment. J Clin Invest. 2005;115(5):1163-76

Jiang SX, Sato Y, Kuwao S, Kameya T. Expression of bcl-2 oncogene protein is prevalent in small cell lung carcinomas. J Pathol. 1995 Oct;177(2):135-8.

Jemal A, Thomas A, Murray T, Thun M. Cancer statistics.CA Cancer J Clin 2002;52:23—47

Jemal A, Siegel R, Ward E, Murray T, Xu J, Smigal C, Thun MJ. Cancer statistics, 2006. CA Cancer J Clin. 2006 Mar-Apr;56(2):106-30.

Johnson SM, Grosshans H, Shingara J, Byrom M, Jarvis R, Cheng A, Labourier E, Reinert KL, Brown D, Slack FJ. RAS is regulated by the let-7 microRNA family. Cell. 2005;120(5):635-47.

Johnson SM, Lin SY, Slack FJ. The time of appearance of the C. elegans let-7 microRNA is transcriptionally controlled utilizing a temporal regulatory element in its promoter. Dev Biol. 2003 Jul 15;259(2):364-79.

Johnston RJ, Hobert O. A microRNA controlling left/right neuronal asymmetry in Caenorhabditis elegans. Nature. 2003 Dec 18;426(6968):845-9

Jones MB, Krutzsch H, Shu H, Zhao Y, Liotta LA, Kohn EC, Petricoin EF 3rd. Proteomic analysis and identification of new biomarkers and therapeutic targets for invasive ovarian cancer. Proteomics. 2002 Jan;2(1):76-84.

Kaiser U, Schilli M, Haag U, Neumann K, Kreipe H, Kogan E, Havemann K. Expression of bcl-2—protein in small cell lung cancer. Lung Cancer. 1996 Aug;15(1):31-40.
Khanna KK, Jackson SP. DNA double-strand breaks: signaling, repair and the cancer connection. Nat Genet. 2001 Mar;27(3):247-54.

Kang Y, Massagué J. Epithelial-mesenchymal transitions: twist in development and metastasis. Cell. 2004 Aug 6;118(3):277-9.

Kanoh M, Amoh Y, Sato Y, Katsuoka K. Expression of the hair stem cell-specific marker nestin in epidermal and follicular tumors. Eur J Dermatol. 2008 Sep-Oct;18(5):518-23.

Kawamori T, Uchiya N, Nakatsugi S, Watanabe K, Ohuchida S, Yamamoto H, Maruyama T, Kondo K, Sugimura T, Wakabayashi K. Chemopreventive effects of ONO-8711, a selective prostaglandin E receptor EP(1) antagonist, on breast cancer development. Carcinogenesis. 2001 Dec;22(12):2001-4.

Kawamori T, Uchiya N, Sugimura T, Wakabayashi K. Enhancement of colon carcinogenesis by prostaglandin E2 administration. Carcinogenesis. 2003 May;24(5):985-90.

Keith RL, Geraci MW, Nana-Sinkam SP, Breyer RM, Hudish TM, Meyer AM, Malkinson AM, Dwyer-Nield LD. Prostaglandin E2 receptor subtype 2 (EP2) null mice are protected against murine lung tumorigenesis. Anticancer Res. 2006 Jul-Aug;26(4B):2857-61.

Kim CH, Pelus LM, Appelbaum E, Johanson K, Anzai N, Broxmeyer HE. CCR7 ligands, SLC/6Ckine/Exodus2/TCA4 and CKbeta-11/MIP-3beta/ELC, are chemoattractants for CD56(+)CD16(−) NK cells and late stage lymphoid progenitors. Cell Immunol. 1999;193:226–235.

Kim CH, Pelus LM, White JR, Applebaum E, Johanson K, Broxmeyer HE. CK beta-11/macrophage inflammatory protein-3 beta/EBI1-ligand chemokine is an efficacious chemoattractant for T and B cells. J Immunol. 1998a;160:2418–2424.

Kim CH, Pelus LM, White JR, Broxmeyer HE. Differential chemotactic behavior of developing T cells in response to thymic chemokines. Blood. 1998b;91:4434–4443.

Kim CH, Pelus LM, White JR, Broxmeyer HE. Macrophage-inflammatory protein-3 beta/EBI1-ligand chemokine/CK beta-11, a CC chemokine, is a chemoattractant with a specificity for macrophage progenitors among myeloid progenitor cells. J Immunol. 1998c;161:2580–2585.

Kinsey DL. An experimental study of preferential metastasis. Cancer. 1960 Jul-Aug;13:674-6

Kondo M, Ji L, Kamibayashi C, Tomizawa Y, Randle D, Sekido Y, Yokota J, Kashuba V, Zabarovsky E, Kuzmin I, Lerman M, Roth J, Minna JD. Overexpression of candidate tumor suppressor gene FUS1 isolated from the 3p21.3 homozygous deletion region leads to G1 arrest and growth inhibition of lung cancer cells. Oncogene. 2001 Sep 27;20(43):6258-62.

Konopka JB, Watanabe SM, Singer JW, Collins SJ, Witte ON. Cell lines and clinical isolates derived from Ph1-positive chronic myelogenous leukemia patients express c-abl proteins with a common structural alteration. Proc Natl Acad Sci U S A 1985;82:1810-1814

Körholz D, Banning U, Bönig H, Grewe M, Schneider M, Mauz-Körholz C, Klein-Vehne A, Krutmann J, Burdach S. The role of interleukin-10 (IL-10) in IL-15-mediated T-cell responses. Blood. 1997 Dec 1;90(11):4513-21.

Kuroki T, Trapasso F, Yendamuri S, Matsuyama A, Alder H, Williams NN, Kaiser LR, Croce CM. Allelic loss on chromosome 3p21.3 and promoter hypermethylation of semaphorin 3B in non-small cell lung cancer. Cancer Res. 2003 Jun 15;63(12):3352-5.

Laconi E. The evolving concept of tumor microenvironments. Bioessays. 2007 Aug;29(8):738-44.

Lewis PD, Parry JM. In silico p53 mutation hotspots in lung cancer. Carcinogenesis. 2004 Jul;25(7):1099-107

Landais S, Landry S, Legault P, Rassart E. Oncogenic potential of the miR-106-363 cluster and its implication in human T-cell leukemia. Cancer Res. 2007 Jun 15;67(12):5699-707.

Landgraf P, Rusu M, Sheridan R, Sewer A, Iovino N, Aravin A, Pfeffer S, Rice A, Kamphorst AO, Landthaler M, Lin C, Socci ND, Hermida L, Fulci V, Chiaretti S, Foà R, Schliwka J, Fuchs U, Novosel A, Müller RU, Schermer B, Bissels U, Inman J, Phan Q, Chien M, Weir DB, Choksi R, De Vita G, Frezzetti D, Trompeter HI, Hornung V, Teng G, Hartmann G, Palkovits M, Di Lauro R, Wernet P, Macino G, Rogler CE, Nagle JW, Ju J, Papavasiliou FN, Benzing T, Lichter P, Tam W, Brownstein MJ, Bosio A, Borkhardt A, Russo JJ, Sander C, Zavolan M, Tuschl T. A mammalian microRNA expression atlas based on small RNA library sequencing. Cell. 2007 Jun 29;129(7):1401-14.

Li Q, Wang G, Shan JL, Yang ZX, Wang HZ, Feng J, Zhen JJ, Chen C, Zhang ZM, Xu W, Luo XZ, Wang D. MicroRNA-224 is upregulated in HepG2 cells and involved in cellular migration and invasion. J Gastroenterol Hepatol. 2010 Jan;25(1):164-71.

Liotta LA, Espina V, Mehta AI, Calvert V, Rosenblatt K, Geho D, Munson PJ, Young L, Wulfkuhle J, Petricoin EF 3rd. Protein microarrays: meeting analytical challenges for clinical applications. Cancer Cell. 2003 Apr;3(4):317-25.

Liu M, Lang N, Qiu M, Xu F, Li Q, Tang Q, Chen J, Chen X, Zhang S, Liu Z, Zhou J, Zhu Y, Deng Y, Zheng Y, Bi F. miR-137 targets Cdc42 expression, induces cell cycle G1 arrest and inhibits invasion in colorectal cancer cells. Int J Cancer. 2010 May 12. [Epub ahead of print]

Lu J, Getz G, Miska EA, Alvarez-Saavedra E, Lamb J, Peck D, Sweet-Cordero A, Ebert BL, Mak RH, Ferrando AA, Downing JR, Jacks T, Horvitz HR, Golub TR. MicroRNA expression profiles classify human cancers.Nature. 2005 Jun 9;435(7043):834-8.

Luo H, Zhang H, Zhang Z, Zhang X, Ning B, Guo J, Nie N, Liu B, Wu X. Downregulated miR-9 and miR-433 in human gastric carcinoma. J Exp Clin Cancer Res. 2009 Jun 16;28:82.

Luthra R, Singh RR, Luthra MG, Li YX, Hannah C, Romans AM, Barkoh BA, Chen SS, Ensor J, Maru DM, Broaddus RR, Rashid A, Albarracin CT. MicroRNA-196a targets annexin A1: a microRNA-mediated mechanism of annexin A1 downregulation in cancers. Oncogene. 2008 Nov 6;27(52):6667-78.

Maitra A, Amirkhan RH, Saboorian MH, Frawley WH, Ashfaq R. Survival in small cell lung carcinoma is independent of Bcl-2 expression. Hum Pathol. 1999 Jun;30(6):712-7

Malumbres M, Hunt SL, Sotillo R, Martín J, Odajima J, Martín A, Dubus P, Ortega S, Barbacid M. Driving the cell cycle to cancer. Adv Exp Med Biol. 2003;532:1-11.

Martin B, Paesmans M, Berghmans T, Branle F, Ghisdal L, Mascaux C, Meert AP, Steels E, Vallot F, Verdebout JM, Lafitte JJ, Sculier JP. Role of Bcl-2 as a prognostic factor for survival in lung cancer: a systematic review of the literature with meta-analysis. Br J Cancer. 2003 Jul 7;89(1):55-64.

Martinet W, Abbeloos V, Van Acker N, De Meyer GR, Herman AG, Kockx MM. Western blot analysis of a limited number of cells: a valuable adjunct to proteome analysis of paraffin wax-embedded, alcohol-fixed tissue after laser capture microdissection. J Pathol. 2004;202(3):382-8.

Matthews MJ. Morphologic classification of bronchogenic carcinoma. Cancer Chemother Rep 3. 1973 Mar;4(2):299–301.

Mayr C, Hemann MT, Bartel DP. Disrupting the pairing between let-7 and Hmga2 enhances oncogenic transformation. Science. 2007 Mar 16;315(5818):1576-9.

McLemore TL, Hubbard WC, Litterst CL, Liu MC, Miller S, McMahon NA, Eggleston JC, Boyd MR. Profiles of prostaglandin biosynthesis in normal lung and tumor tissue from lung cancer patients. Cancer Res. 1988 Jun 1;48(11):3140-7.

Melle C, Bogumil R, Ernst G, Schimmel B, Bleul A, von Eggeling F. Detection and identification of heat shock protein 10 as a biomarker in colorectal cancer by protein profiling. Proteomics. 2006 Apr;6(8):2600-8.

Mendell JT. miRiad roles for the miR-17-92 cluster in development and disease. Cell. 2008 Apr 18;133(2):217-22.

Meyer JA, Parker FB, Small cell carcinoma of the lung. Ann Thorac Surg, 1980, 30:602

Miettinen M, Sarlomo-Rikala M Expression of calretinin, thrombomodulin, keratin 5, and mesothelin in lung carcinomas of different types: an immunohistochemical analysis of 596 tumors in comparison with epithelioid mesotheliomas of the pleura. Am J Surg Pathol. 2003 Feb;27(2):150-8.

Miska EA, Alvarez-Saavedra E, Townsend M, Yoshii A, Sestan N, Rakic P, Constantine-Paton M, Horvitz HR. Microarray analysis of microRNA expression in the developing mammalian brain. Genome Biol. 2004;5(9):R68

Mori S, Ito G, Usami N, Yoshioka H, Ueda Y, Kodama Y, Takahashi M, Fong KM, Shimokata K, Sekido Y. p53 apoptotic pathway molecules are frequently and simultaneously altered in nonsmall cell lung carcinoma. Cancer. 2004 Apr 15;100(8):1673-82.

Mutoh M, Watanabe K, Kitamura T, Shoji Y, Takahashi M, Kawamori T, Tani K, Kobayashi M, Maruyama T, Kobayashi K, Ohuchida S, Sugimoto Y, Narumiya S, Sugimura T, Wakabayashi K. Involvement of prostaglandin E receptor subtype EP(4) in colon carcinogenesis. Cancer Res. 2002 Jan 1;62(1):28-32.

Nakamura T, Kuwai T, Kitadai Y, Sasaki T, Fan D, Coombes KR, Kim SJ, Fidler IJ. Zonal heterogeneity for gene expression in human pancreatic carcinoma. Cancer Res. 2007 Aug 15;67(16):7597-604.

Ngo VN, Tang HL, Cyster JG. Epstein–Barr virus-induced molecule 1 ligand chemokine is expressed by dendritic cells in lymphoid tissues and strongly attracts naive T cells and activated B cells. J Exp Med. 1998;188:181–191.

Nicholson SA, Okby NT, Khan MA, Welsh JA, McMenamin MG, Travis WD, Jett JR, Tazelaar HD, Trastek V, Pairolero PC, Corn PG, Herman JG, Liotta LA, Caporaso NE, Harris CC. Alterations of p14ARF, p53, and p73 genes involved in the E2F-1-mediated apoptotic pathways in non-small cell lung carcinoma. Cancer Res. 2001 Jul 15;61(14):5636-43.

Nowell PC. Clonal evolution of tumor cell sub-populations. Science 1976;194:23.

Oku Y, Shimoji T, Takifuji K, Hotta T, Yokoyama S, Matsuda K, Higashiguchi T, Tominaga T, Nasu T, Tamura K, Matsuura M, Miyata S, Kato Y, Yamaue H, Miki Y. Identification of the molecular mechanisms for dedifferentiation at the invasion front of colorectal cancer by a gene expression analysis. Clin Cancer Res. 2008 Nov 15;14(22):7215-22.

Ornstein DK, Englert C, Gillespie JW, Paweletz CP, Linehan WM, Emmert-Buck MR, Petricoin EF 3rd. Characterization of intracellular prostate-specific antigen from laser capture microdissected benign and malignant prostatic epithelium. Clin Cancer Res. 2000 Feb;6(2):353-6.

Oshima H, Matsunaga A, Fujimura T, Tsukamoto T, Taketo MM, Oshima M. Carcinogenesis in mouse stomach by simultaneous activation of the Wnt signaling and prostaglandin E2 pathway. Gastroenterology. 2006 Oct;131(4):1086-95.

Oster SK, Ho CS, Soucie EL, Penn LZ. The myc oncogene: MarvelouslY Complex. Adv Cancer Res. 2002;84:81-154.

Paget S. The distribution of secondary growths in cancer of the breast. 1889. Cancer Metastasis Rev. 1989 Aug;8(2):98-101

Pakunlu RI, Wang Y, Tsao W, Pozharov V, Cook TJ, Minko T. Enhancement of the efficacy of chemotherapy for lung cancer by simultaneous suppression of multidrug resistance and antiapoptotic cellular defense: novel multicomponent delivery system. Cancer Res. 2004 Sep 1;64(17):6214-24.

Pasquinelli AE, Reinhart BJ, Slack F, Martindale MQ, Kuroda MI, Maller B, Hayward DC, Ball EE, Degnan B, Müller P, Spring J, Srinivasan A, Fishman M, Finnerty J, Corbo J, Levine M, Leahy P, Davidson E, Ruvkun G. Conservation of the sequence and temporal expression of let-7 heterochronic regulatory RNA. Nature. 2000 Nov 2;408(6808):86-9..

Parada LF, Tabin CJ, Shih C, Weinberg RA. Human EJ bladder carcinoma oncogene is homologue of Harvey sarcoma virus ras gene. Nature. 1982 Jun 10;297(5866):474-8.

Parkin DM, Whelan SL, Ferlay J, Teppo L, Thomas BD. Cancer Incidence in the Five Continents VIII. IARC Scientific Publication No. 155 (International Agency for Research on Cancer (IARC) Press, Lyon, France, 2002).

Paweletz CP, Charboneau L, Bichsel VE, Simone NL, Chen T, Gillespie JW, Emmert-Buck MR, Roth MJ, Petricoin III EF, Liotta LA. Reverse phase protein microarrays which capture disease progression show activation of pro-survival pathways at the cancer invasion front. Oncogene. 2001 Apr 12;20(16):1981-9.

Paweletz CP, Liotta LA, Petricoin EF 3rd. New technologies for biomarker analysis of prostate cancer progression: Laser capture microdissection and tissue proteomics. Urology. 2001 Apr;57(4 Suppl 1):160-3.

Petricoin EF 3rd, Bichsel VE, Calvert VS, Espina V, Winters M, Young L, Belluco C, Trock BJ, Lippman M, Fishman DA, Sgroi DC, Munson PJ, Esserman LJ, Liotta LA. Mapping molecular networks using proteomics: a vision for patient-tailored combination therapy. J Clin Oncol. 2005 May 20;23(15):3614-21.

Pezzella F, Turley H, Kuzu I, Tungekar MF, Dunnill MS, Pierce CB, Harris A, Gatter KC, Mason DY. bcl-2 protein in non-small-cell lung carcinoma. N Engl J Med. 1993 Sep 2;329(10):690-4.

Pochetuhen K, Luzina IG, Lockatell V, Choi J, Todd NW, Atamas SP. Complex regulation of pulmonary inflammation and fibrosis by CCL18. Am J Pathol. 2007 Aug;171(2):428-37.

Prueitt RL, Yi M, Hudson RS, Wallace TA, Howe TM, Yfantis HG, Lee DH, Stephens RM, Liu CG, Calin GA, Croce CM, Ambs S. Expression of microRNAs and protein-coding genes associated with perineural invasion in prostate cancer. Prostate. 2008 Aug 1;68(11):1152-64.

Pulciani S, Santos E, Lauver AV, Long LK, Robbins KC, Barbacid M. Oncogenes in human tumor cell lines: molecular cloning of a transforming gene from human bladder carcinoma cells. Proc Natl Acad Sci U S A. 1982 May;79(9):2845-9.

Raponi M, Dossey L, Jatkoe T, Wu X, Chen G, Fan H, Beer DG. MicroRNA classifiers for predicting prognosis of squamous cell lung cancer. Cancer Res. 2009 Jul 15;69(14):5776-83.

Ratschiller D, Heighway J, Gugger M, Kappeler A, Pirnia F, Schmid RA, Borner MM, Betticher DC. Cyclin D1 overexpression in bronchial epithelia of patients with lung cancer is associated with smoking and predicts survival. J Clin Oncol. 2003 Jun 1;21(11):2085-93.

Reissmann PT, Koga H, Takahashi R, Figlin RA, Holmes EC, Piantadosi S, Cordon-Cardo C, Slamon DJ. Inactivation of the retinoblastoma susceptibility gene in non-small-cell lung cancer. The Lung Cancer Study Group. Oncogene. 1993 Jul;8(7):1913-9.

Richardson GE, Johnson BE. The biology of lung cancer. Semin. Oncol. 1993. 20: 105-127

Ritchie, ME, Silver, J, Oshlack, A, Holmes, M, Diyagama, D, Holloway, A, and Smyth, GK
A comparison of background correction methods for two-colour microarrays. Bioinformatics. 2007 Oct 15;23(20):2700-7

Rigas B, Goldman IS, Levine L. Altered eicosanoid levels in human colon cancer. J Lab Clin Med. 1993 Nov;122(5):518-23.

Rodenhuis S. Oncogenes and human lung cancer. Cancer Treat Res. 1989;45:89-106

Rodenhuis S, Slebos RJ. Clinical significance of ras oncogene activation in human lung cancer. Cancer Res. 1992 May 1;52(9 Suppl):2665s-2669s

Rossi G, Pelosi G, Graziano P, Barbareschi M, Papotti M. A reevaluation of the clinical significance of histological subtyping of non--small-cell lung carcinoma: diagnostic algorithms in the era of personalized treatments. Int J Surg Pathol. 2009 Jun;17(3):206-18.

Savci-Heijink CD, Kosari F, Aubry MC, Caron BL, Sun Z, Yang P, Vasmatzis G. The role of desmoglein-3 in the diagnosis of squamous cell carcinoma of the lung. Am J Pathol. 2009 May;174(5):1629-37.

Scandella E, Men Y, Gillessen S, Förster R, Groettrup M. Prostaglandin E2 is a key factor for CCR7 surface expression and migration of monocyte-derived dendritic cells. Blood. 2002 Aug 15;100(4):1354-61.

Scandella E, Men Y, Legler DF, Gillessen S, Prikler L, Ludewig B, Groettrup M. CCL19/CCL21-triggered signal transduction and migration of dendritic cells requires prostaglandin E2. Blood. 2004 Mar 1;103(5):1595-601.

Schlingemann J, Thuerigen O, Ittrich C, Toedt G, Kramer H, Hahn M, Lichter P. Effective transcriptome amplification for expression profiling on sense-oriented oligonucleotide microarrays. Nucleic Acids Res. 2005 Feb 17;33(3):e29.

Schuetz CS, Bonin M, Clare SE, Nieselt K, Sotlar K, Walter M, Fehm T, Solomayer E, Riess O, Wallwiener D, Kurek R, Neubauer HJ. Progression-specific genes identified by expression profiling of matched ductal carcinomas in situ and invasive breast tumors, combining laser capture microdissection and oligonucleotide microarray analysis. Cancer Res. 2006 May;66(10):5278-86.

Schwender H, Krause A, Ickstadt K. Identifying Interesting Genes with siggenes. RNews, 2006;6(5), 45–50

Sekido Y, Bader S, Latif F, Chen JY, Duh FM, Wei MH, Albanesi JP, Lee CC, Lerman MI, Minna JD. Human semaphorins A(V) and IV reside in the 3p21.3 small cell lung cancer deletion region and demonstrate distinct expression patterns. Proc Natl Acad Sci U S A. 1996 Apr 30;93(9):4120-5.

Sheehan KM, Calvert VS, Kay EW, Lu Y, Fishman D, Espina V, Aquino J, Speer R, Araujo R, Mills GB, Liotta LA, Petricoin EF 3rd, Wulfkuhle JD. Use of reverse phase protein microarrays and reference standard development for molecular network analysis of metastatic ovarian carcinoma. Mol Cell Proteomics. 2005 Apr;4(4):346-55.

Shields JD, Kourtis IC, Tomei AA, Roberts JM, Swartz MA. Induction of lymphoidlike stroma and immune escape by tumors that express the chemokine CCL21. Science. 2010;328(5979):749-52.

Shields TW, Higgins GA Jr, Lawton R, Heilbrunn A, Keehn RJ. Preoperative x-ray therapy as an adjuvant in the treatment of bronchogenic carcinoma. J Thorac Cardiovasc Surg. 1970 Jan;59(1):49-61

Shih C, Weinberg RA. Isolation of a transforming sequence from a human bladder carcinoma cell line. Cell. 1982 May;29(1):161-9.

Simone NL, Remaley AT, Charboneau L, Petricoin EF 3rd, Glickman JW, Emmert-Buck MR, Fleisher TA, Liotta LA. Sensitive immunoassay of tissue cell proteins procured by laser capture microdissection. Am J Pathol. 2000 Feb;156(2):445-52

Slebos RJ, Rodenhuis S. The molecular genetics of human lung cancer. Eur Respir J. 1989 May;2(5):461-9.

Smyth GK. Linear models and empirical bayes methods for assessing differential expression in microarray experiments. Stat Appl Genet Mol Biol. 2004;3:Article3.

Snijdewint FG, Kaliński P, Wierenga EA, Bos JD, Kapsenberg ML. Prostaglandin E2 differentially modulates cytokine secretion profiles of human T helper lymphocytes. J Immunol. 1993 Jun 15;150(12):5321-9.

Song G, Wang L. Transcriptional mechanism for the paired miR-433 and miR-127 genes by nuclear receptors SHP and ERRgamma. Nucleic Acids Res. 2008 Oct;36(18):5727-35.

Sonoshita M, Takaku K, Sasaki N, Sugimoto Y, Ushikubi F, Narumiya S, Oshima M, Taketo MM. Acceleration of intestinal polyposis through prostaglandin receptor EP2 in Apc(Delta 716) knockout mice. Nat Med. 2001 Sep;7(9):1048-51.

Sozzi G, Veronese ML, Negrini M, Baffa R, Cotticelli MG, Inoue H, Tornielli S, Pilotti S, De Gregorio L, Pastorino U, Pierotti MA, Ohta M, Huebner K, Croce CM. The FHIT gene 3p14.2 is abnormal in lung cancer. Cell. 1996 Apr 5;85(1):17-26.

Sporn MB. The war on cancer. Lancet. 1996 May 18;347(9012):1377-81.

Stark A, Bushati N, Jan CH, Kheradpour P, Hodges E, Brennecke J, Bartel DP, Cohen SM, Kellis M. A single Hox locus in Drosophila produces functional microRNAs from opposite DNA strands. Genes Dev. 2008 Jan 1;22(1):8-13.

Staub E, Groene J, Heinze M, Mennerich D, Roepcke S, Klaman I, Hinzmann B, Castanos-Velez E, Pilarsky C, Mann B, Brümmendorf T, Weber B, Buhr HJ, Rosenthal A. Genome-wide expression patterns of invasion front, inner tumor mass and surrounding normal epithelium of colorectal tumors. Mol Cancer. 2007 Dec 14;6:79.

Stephen S. Sternberg, Antonioli DA, Carter D, Mills SE, Oberman HA. Diagnostic Surgical Pathology Lippincott Williams & Wilkins 1994; 1051-1054

Stolina M, Sharma S, Lin Y, Dohadwala M, Gardner B, Luo J, Zhu L, Kronenberg M, Miller PW, Portanova J, Lee JC, Dubinett SM. Specific inhibition of cyclooxygenase 2 restores antitumor reactivity by altering the balance of IL-10 and IL-12 synthesis. J Immunol. 2000 Jan 1;164(1):361-70.

Subramanian J, Govindan R. Lung cancer in never smokers: a review. J Clin Oncol. 2007 Feb 10;25(5):561-70.

Sugarbaker ED. The organ selectivity of experimentally induced metastases in rats. Cancer. 1952 May;5(3):606-12.

Takamizawa J, Konishi H, Yanagisawa K, Tomida S, Osada H, Endoh H, Harano T, Yatabe Y, Nagino M, Nimura Y, Mitsudomi T, Takahashi T. Reduced expression of the let-7 microRNAs in human lung cancers in association with shortened postoperative survival. Cancer Res. 2004 Jun 1;64(11):3753-6.

Taylor DD, Gercel-Taylor C. MicroRNA signatures of tumor-derived exosomes as diagnostic biomarkers of ovarian cancer. Gynecol Oncol. 2008 Jul;110(1):13-21. Erratum in: Gynecol Oncol. 2010 Jan;116(1):153.

Tepass U, Gruszynski-DeFeo E, Haag TA, Omatyar L, Török T, Hartenstein V. shotgun encodes Drosophila E-cadherin and is preferentially required during cell rearrangement in the neurectoderm and other morphogenetically active epithelia. Genes Dev. 1996 Mar 15;10(6):672-85.

Terasaki H, Niki T, Matsuno Y, Yamada T, Maeshima A, Asamura H, Hayabuchi N, Hirohashi S. Lung adenocarcinoma with mixed bronchioloalveolar and invasive components: clinicopathological features, subclassification by extent of invasive foci, and immunohistochemical characterization. Am J Surg Pathol. 2003 Jul;27(7):937-51

Thiel A, Ganesan A, Mrena J, Junnila S, Nykänen A, Hemmes A, Tai HH, Monni O, Kokkola A, Haglund C, Petrova TV, Ristimäki A. 15-hydroxyprostaglandin dehydrogenase is downregulated in gastric cancer. Clin Cancer Res. 2009 Jul 15;15(14):4572-80.

Thomson JM, Parker J, Perou CM, Hammond SM. A custom microarray platform for analysis of microRNA gene expression. Nat Methods. 2004 Oct;1(1):47-53.

Toyooka S, Tsuda T, Gazdar AF. The TP53 gene, tobacco exposure, and lung cancer. Hum Mutat. 2003 Mar;21(3):229-39

Travis WD. Pathology of lung cancer. Clin Chest Med 2002;23:65-81

Travis WD, Travis LB, Devesa SS. Lung cancer. 1995, Jan, Cancer 75 (Suppl. 1): 191–202

Tsujimoto Y, Gorham J, Cossman J, Jaffe E, Croce CM. The t(14;18) chromosome translocations involved in B-cell neoplasms result from mistakes in VDJ joining. Science 1985;229:1390-1393.

Tusher VG, Tibshirani R, Chu G. Significance analysis of microarrays applied to the ionizing radiation response. Proc Natl Acad Sci U S A. 2001 Apr 24;98(9):5116-21

Uz T, Arslan AD, Kurtuncu M, Imbesi M, Akhisaroglu M, Dwivedi Y, Pandey GN, Manev H. The regional and cellular expression profile of the melatonin receptor MT1 in the central dopaminergic system. Brain Res Mol Brain Res. 2005 May 20;136(1-2):45-53.

Valadi H, Ekström K, Bossios A, Sjöstrand M, Lee JJ, Lötvall JO. Exosome-mediated transfer of mRNAs and microRNAs is a novel mechanism of genetic exchange between cells. Nat Cell Biol. 2007 Jun;9(6):654-9.

van Zandwijk N, Mooi WJ, Rodenhuis S. Prognostic factors in NSCLC. Recent experiences. Lung Cancer. 1995 Apr;12 Suppl 1:S27-33

Vandesompele J, De Preter K, Pattyn F, Poppe B, Van Roy N, De Paepe A, Speleman F. Accurate normalization of real-time quantitative RT-PCR data by geometric averaging of multiple internal control genes. Genome Biol. 2002 Jun 18;3(7)

Vaporciyan AA; Nesbitt JC, Lee JS. Cancer Medicine. BC Decker. 2000; 1227–92.

Virmani AK, Rathi A, Zöchbauer-Müller S, Sacchi N, Fukuyama Y, Bryant D, Maitra A, Heda S, Fong KM, Thunnissen F, Minna JD, Gazdar AF. Promoter methylation and silencing of the retinoic acid receptor-beta gene in lung carcinomas. J Natl Cancer Inst. 2000 Aug 16;92(16):1303-7.

Vogelstein B, Kinzler KW. The genetic basis of human cancer. New York: McGraw-Hill, Medical Pub. Division. 2002; 5.

Volinia S, Calin GA, Liu CG, Ambs S, Cimmino A, Petrocca F, Visone R, Iorio M, Roldo C, Ferracin M, Prueitt RL, Yanaihara N, Lanza G, Scarpa A, Vecchione A, Negrini M, Harris CC, Croce CM. A microRNA expression signature of human solid tumors defines cancer gene targets. Proc Natl Acad Sci U S A. 2006 Feb 14;103(7):2257-61.

Waldman SA, Terzic A Translating MicroRNA Discovery Into Clinical Biomarkers in Cancer, JAMA. 2007 May 2;297(17):1923-5.

Wang D, Dubois RN. Cyclooxygenase-2: a potential target in breast cancer. Semin Oncol. 2004 Feb;31(1 Suppl 3):64-73.

Wang D, Dubois RN. Eicosanoids and cancer. Nat Rev Cancer. 2010 Mar;10(3):181-93.

Wang D, Wang H, Shi Q, Katkuri S, Walhi W, Desvergne B, Das SK, Dey SK, DuBois RN. Prostaglandin E(2) promotes colorectal adenoma growth via transactivation of the nuclear peroxisome proliferator-activated receptor delta. Cancer Cell. 2004;6(3):285-95.

Wang D, Wang H, Guo Y, Ning W, Katkuri S, Wahli W, Desvergne B, Dey SK, DuBois RN. Crosstalk between peroxisome proliferator-activated receptor delta and VEGF stimulates cancer progression. Proc Natl Acad Sci U S A. 2006 Dec 12;103(50):19069-74.

Wang J, Zhang X, Thomas SM, Grandis JR, Wells A, Chen ZG, Ferris RL. Chemokine receptor 7 activates phosphoinositide-3 kinase-mediated invasive and prosurvival pathways in head and neck cancer cells independent of EGFR. Oncogene. 2005 Sep 1;24(38):5897-904.

Watanabe K, Kawamori T, Nakatsugi S, Ohta T, Ohuchida S, Yamamoto H, Maruyama T, Kondo K, Ushikubi F, Narumiya S, Sugimura T, Wakabayashi K. Role of the prostaglandin E receptor subtype EP1 in colon carcinogenesis. Cancer Res. 1999 Oct 15;59(20):5093-6.

Weinberg RA, The biology of cancer. Garland Science. 2006

Weinhold B. Epigenetics: the science of change.Environ Health Perspect.2006 Mar;114(3):A160-7.

Weitberg AB, Cancer of the Lung: from molecular biology to treatment guidelines. Humana Press, 2002;262

Wistuba II, Gazdar AF, Minna JD. Molecular genetics of small cell lung carcinoma. Semin Oncol. 2001 Apr;28(2 Suppl 4):3-13.

Witz IP. Tumor-microenvironment interactions: dangerous liaisons. Adv Cancer Res. 2008; 100:203-29.

Witz IP. Yin-yang activities and vicious cycles in the tumor microenvironment. Cancer Res. 2008 Jan 1;68(1):9-13.

Witz IP, Levy-Nissenbaum O. The tumor microenvironment in the post-PAGET era. Cancer Lett. 2006 Oct 8;242(1):1-10.

Wolf I, O'Kelly J, Rubinek T, Tong M, Nguyen A, Lin BT, Tai HH, Karlan BY, Koeffler HP. 15-hydroxyprostaglandin dehydrogenase is a tumor suppressor of human breast cancer. Cancer Res. 2006 Aug 1;66(15):7818-23.

Wolfle D. Enhancement of carcinogen-induced malignant cell transformation by prostaglandin F(2 alpha). Toxicology. 2003 Jun 30;188(2-3):139-47.

World Health Organization. The World Health Organization histological typing of lung tumors. 2nd ed. Am J Clin Pathol 1982;77:123-136

Woutersen RA, Appel MJ, van Garderen-Hoetmer A, Wijnands MV. Dietary fat and carcinogenesis. Mutat Res. 1999 Jul 15;443(1-2):111-27.

Wulfkuhle JD, Aquino JA, Calvert VS, Fishman DA, Coukos G, Liotta LA, Petricoin EF 3rd. Signal pathway profiling of ovarian cancer from human tissue specimens using reverse-phase protein microarrays. Proteomics. 2003 Nov;3(11):2085-90

Wulfkuhle JD, Sgroi DC, Krutzsch H, McLean K, McGarvey K, Knowlton M, Chen S, Shu H, Sahin A, Kurek R, Wallwiener D, Merino MJ, Petricoin EF 3rd, Zhao Y, Steeg PS. Proteomics of human breast ductal carcinoma in situ. Cancer Res. 2002 Nov 15;62(22):6740-9.

Yokoyama K, Kamata N, Hayashi E, Hoteiya T, Ueda N, Fujimoto R, Nagayama M. Reverse correlation of E-cadherin and snail expression in oral squamous cell carcinoma cells in vitro. Oral Oncol. 2001 Jan;37(1):65-71.

Yanaihara N, Caplen N, Bowman E, Seike M, Kumamoto K, Yi M, Stephens RM, Okamoto A, Yokota J, Tanaka T, Calin GA, Liu CG, Croce CM, Harris CC. Unique microRNA molecular profiles in lung cancer diagnosis and prognosis. Cancer Cell. 2006 Mar;9(3):189-98.

Zahm SH, Brownson RC, Chang JC, Davis JR. Study of lung cancer histologic types, occupation, and smoking in Missouri. Am J Ind Med. 1989;15(5):565-78

Zalatnai A. Molecular aspects of stromal-parenchymal interactions in malignant neoplasms. Curr Mol Med. 2006 Sep;6(6):685-93.

Zeddou M, Greimers R, de Valensart N, Nayjib B, Tasken K, Boniver J, Moutschen M, Rahmouni S. Prostaglandin E2 induces the expression of functional inhibitory CD94/NKG2A receptors in human CD8+ T lymphocytes by a cAMP-dependent protein kinase A type I pathway. Biochem Pharmacol. 2005 Sep 1;70(5):714-24.

Zhang B, Pan X, Cobb GP, Anderson TA. microRNAs as oncgenes and tumor suppressors. Dev Biol. 2007 Feb 1;302(1):1-12

Zhang X, Zhu W, Zhang J, Huo S, Zhou L, Gu Z, Zhang M. MicroRNA-650 targets ING4 to promote gastric cancer tumorigenicity. Biochem Biophys Res Commun. 2010;395(2):275-80.

Zlotnik A, Yoshie O. Chemokines: a new classification system and their role in immunity. Immunity. 2000 Feb;12(2):121-7.

Zochbauer-Müller S, Fong KM, Maitra A, Lam S, Geradts J, Ashfaq R, Virmani AK, Milchgrub S, Gazdar AF, Minna JD. 5' CpG island methylation of the FHIT gene is correlated with loss of gene expression in lung and breast cancer. Cancer Res. 2001 May 1;61(9):3581-5.

Zochbauer-Müller S, Gazdar AF, Minna JD. Molecular pathogenesis of lung cancer. Annu Rev Physiol. 2002;64:681-708

Supplementary Data

Table 1. Top upregulated genes in adjacent lung tissue compare to normal lung.

Symbol	Mapping	EnsEMBL.ID	adj.P.Val	Lin Fc
KRT6A	12q13.13	ENSG00000205420	5.34E-19	42.74305
KRT6B	12q13.13	ENSG00000185479	2.89E-18	28.75892
KRT17P1	17p11.2	ENSG00000131885	4.61E-12	23.65115
KRT17	17q21.2	ENSG00000128422	1.50E-12	23.34656
KRT5	12q13.13	ENSG00000186081	1.14E-14	18.98757
AC022596.6	17p11.2	ENSG00000226145	1.92E-07	15.66267
LTF	3p21.31	ENSG00000012223	8.17E-07	15.43855
KRT14	17q21.2	ENSG00000186847	1.84E-06	13.91658
S100A2	1q21.3	ENSG00000196754	3.85E-09	12.35406
MYBPC2	19q13.33	ENSG00000086967	1.08E-14	11.20308
SAA2	11p15.1	ENSG00000134339	8.81E-07	9.961397
CALML3	10p15.1	ENSG00000178363	1.71E-09	9.951596
SAA1	11p15.1	ENSG00000173432	3.56E-07	8.2685
DSG3	18q12.1	ENSG00000134757	2.05E-07	7.539553
CCL19	9p13.3	ENSG00000172724	3.85E-11	7.107972
PRSS2	7q34	ENSG00000235481	6.71E-07	6.95266
LGALS7B	19q13.2	ENSG00000178934	5.49E-05	6.871594
FAM83A	8q24.13	ENSG00000147689	7.54E-07	6.733668
TPX2	20q11.21	ENSG00000088325	2.31E-18	6.646319
CKMT1B	15q15.3	ENSG00000237289	1.50E-12	6.567734
KRT16	17q21.2	ENSG00000186832	0.000175	6.109429
KRT15	17q21.2	ENSG00000171346	1.93E-05	5.852895
TRIM29	11q23.3	ENSG00000137699	2.06E-08	5.688379
KRT6C	12q13.13	ENSG00000170465	0.000223	5.479243
KIF20A	5q31.2	ENSG00000112984	6.82E-17	5.401128
HIST1H2BG	6p22.2	ENSG00000187990	4.13E-10	5.331867
CXCR5	11q23.3	ENSG00000160683	2.45E-11	5.065173
CDH3	16q22.1	ENSG00000062038	3.89E-10	4.984587
GPR39	2q21.2	ENSG00000183840	2.26E-07	4.916462
KRT13	17q21.2	ENSG00000171401	0.000428	4.897326
VPREB3	22q11.23	ENSG00000128218	9.73E-09	4.864431
TCL1A	14q32.13	ENSG00000100721	2.07E-09	4.844407
SDS	12q24.13	ENSG00000135094	1.32E-07	4.822916
COL3A1	2q32.2	ENSG00000168542	1.98E-06	4.799831
SPRR2D	1q21.3	ENSG00000163216	0.00134	4.631536
SPRR1A	1q21.3	ENSG00000169474	0.001415	4.604374

adj.P.Val: adjusted P value; Lin FC: linear fold change; Mapping: Chromosomal gene location.

Table 2. Top downregulated genes in adjacent lung tissue compare to normal lung.

Symbol	Mapping	EnsEMBL.ID	adj.P.Val	Lin Fc
MYOC	1q24.3	ENSG00000034971	7.01E-16	-5.41607
HBB	11p15.4	ENSG00000223609	5.20E-10	-4.98704
C2orf40	2q12.2	ENSG00000119147	3.24E-06	-4.85811
LYZ	12q15	ENSG00000090382	3.69E-14	-4.8424
IGSF10	3q25.1	ENSG00000152580	5.15E-12	-4.7345
IL8RA	2q35	ENSG00000163464	3.58E-12	-4.68195
CA4	17q23.1	ENSG00000167434	2.12E-09	-4.56869
ECM2	9q22.31	ENSG00000106823	1.70E-11	-4.49015
SYNPO2	4q26	ENSG00000172403	1.91E-08	-4.24155
CLC	19q13.2	ENSG00000105205	2.06E-14	-4.22914
WIF1	12q14.3	ENSG00000156076	1.05E-08	-4.21616
ANGPTL1	1q25.2	ENSG00000116194	9.19E-22	-4.15988
CTGF	6q23.2	ENSG00000118523	1.20E-08	-4.07801
HBA1	16p13.3	ENSG00000206172	7.15E-13	-4.07704
ECM2	9q22.31	ENSG00000106823	4.86E-12	-4.06217
CLIC5	6p21.1	ENSG00000112782	2.03E-09	-4.01804
SDR	2q32.3	ENSG00000168497	1.50E-06	-4.01162
FPR2	19q13.41	ENSG00000171049	1.25E-19	-3.98478
HBEGF	5q31.3	ENSG00000113070	5.97E-08	-3.95495
ABCA8	17q24.2	ENSG00000141338	2.31E-18	-3.9473
CAV1	7q31.2	ENSG00000105974	4.97E-12	-3.94648
LMBRD1	6q13	ENSG00000168216	2.04E-12	-3.93343
SELE	1q24.2	ENSG00000007908	8.42E-08	-3.89084
TCF21	6q23.2	ENSG00000118526	1.21E-13	-3.88908
AHNAK	11q12.3	ENSG00000124942	2.63E-09	-3.84338
GPD1	12q13.12	ENSG00000167588	1.71E-11	-3.82156
OTUD1	10p12.2	ENSG00000165312	2.03E-21	-3.79825
IL1B	2q13	ENSG00000125538	2.31E-06	-3.79113
OLFML1	11p15.4	ENSG00000183801	8.60E-12	-3.77525
CCBE1	18q21.32	ENSG00000183287	2.28E-11	-3.77272
MRC1	10p12.33	ENSG00000120586	5.67E-11	-3.77094
AOC3	17q21.31	ENSG00000131471	4.14E-19	-3.73527
MSRB3	12q14.3	ENSG00000174099	8.43E-15	-3.73301
GDF10	10q11.22	ENSG00000107623	1.81E-12	-3.70436
CPE	4q32.3	ENSG00000109472	2.46E-08	-3.70354
MSR1	8p22	ENSG00000038945	2.44E-11	-3.69612
SPTBN1	2p16.2	ENSG00000115306	2.26E-14	-3.69206
PROK2	3p13	ENSG00000163421	7.99E-12	-3.67471

adj.P.Val: adjusted P value; Lin FC: linear fold change; Mapping: Chromosomal gene location. Minus sign means down regulation

Table 3. Top upregulated genes in inner tumor compare to normal lung.

Symbol	Mapping	EnsEMBL.ID	adj.P.Val	Lin Fc
KRT6B	12q13.13	ENSG00000185479	2.62E-32	137.3482997
KRT17P1	17p11.2	ENSG00000131885	4.63E-23	101.9028922
KRT17	17q21.2	ENSG00000128422	2.34E-23	97.59842807
KRT6A	12q13.13	ENSG00000205420	5.75E-27	91.18385546
KRT15	17q21.2	ENSG00000171346	2.17E-22	68.89307283
S100A2	1q21.3	ENSG00000196754	2.17E-20	55.33089972
KRT5	12q13.13	ENSG00000186081	1.75E-24	51.95136838
KRT16	17q21.2	ENSG00000186832	9.37E-21	50.06200426
CALML3	10p15.1	ENSG00000178363	8.59E-23	49.94995011
PTHLH	12p11.22	ENSG00000087494	6.34E-21	44.79530598
DSG3	18q12.1	ENSG00000134757	8.83E-21	42.18108798
KRT14	17p11.2	ENSG00000186847	1.92E-12	41.22537103
TRIM29	11q23.3	ENSG00000137699	2.45E-27	41.22151786
CKMT1B	15q15.3	ENSG00000237289	1.65E-33	40.67340403
GPR87	3q25.1	ENSG00000138271	1.29E-26	40.6721547
AKR1B10	7q33	ENSG00000198074	7.90E-19	35.80362158
FNTB	14q23.3	ENSG00000125954	3.39E-25	27.46894584
FAM83A	8q24.13	ENSG00000147689	2.94E-17	26.38889981
DST	6p12.1	ENSG00000151914	1.09E-26	26.28945395
SERPINB5	18q21.33	ENSG00000206075	2.07E-25	26.27429612
VTCN1	1p13.1	ENSG00000134258	7.76E-19	25.47528147
SOX2	3q26.33	ENSG00000181449	1.78E-18	25.29739878
LGALS7B	19q13.2	ENSG00000178934	1.67E-12	24.42788895
SLC6A8	Xq28	ENSG00000130821	2.70E-36	22.36216573
TPX2	20q11.21	ENSG00000088325	2.70E-36	21.72252417
AC022596.6	17p11.2	ENSG00000226145	3.09E-10	21.12563995
ALDH3A1	17p11.2	ENSG00000108602	7.37E-12	19.88970413
SERPINB4	18q21.33	ENSG00000206073	5.35E-12	19.4837423
KRT6C	12q13.13	ENSG00000170465	6.99E-12	19.38524893
ADH7	4q23	ENSG00000196344	9.44E-15	19.07081661
CLCA2	1p22.3	ENSG00000137975	2.14E-19	18.99121394
AKR1C1	10p15.1	ENSG00000187134	1.34E-10	18.51638597
LY6K	8q24.3	ENSG00000160886	1.20E-19	18.325241
IGFBP7	4q12	ENSG00000163453	1.11E-36	18.32179243
GJB5	1p34.3	ENSG00000189280	3.66E-26	17.51599679
KRT13	17q21.2	ENSG00000171401	1.15E-11	17.41587712
KLK6	19q13.41	ENSG00000167755	9.01E-11	16.08513954
CENPF	1q41	ENSG00000117724	1.59E-42	16.04178315

adj.P.Val: adjusted P value; Lin FC: linear fold change; Mapping: Chromosomal gene location.

Table 4. Top downregulated genes in inner tumor compare to normal lung.

Symbol	Mapping	EnsEMBL.ID	adj.P.Val	Lin Fc
AGER	6p21.32	ENSG00000204305	9.71E-33	-79.2911
SFTPC	8p21.3	ENSG00000168484	1.81E-17	-58.7035
INMT	7p14.3	ENSG00000106125	2.64E-38	-39.9104
C7	5p13.1	ENSG00000112936	3.44E-34	-36.9524
MFAP4	17p11.2	ENSG00000166482	1.76E-39	-33.9663
SFTPB	2p11.2	ENSG00000168878	3.16E-16	-32.3742
CLIC5	6p21.1	ENSG00000112782	1.32E-34	-30.7284
SFTA3	14q13.3	ENSG00000229415	1.81E-25	-30.3843
AC105046.10	8p21.3	ENSG00000134020	4.15E-21	-29.9423
C19orf59	19p13.2	ENSG00000183019	3.44E-21	-29.0808
CACNA2D2	3p21.31	ENSG00000007402	2.45E-25	-28.0355
A2M	12p13.31	ENSG00000175899	1.18E-39	-27.0021
FOSB	19q13.32	ENSG00000125740	8.89E-22	-25.7972
PGC	6p21.1	ENSG00000096088	1.27E-24	-25.682
WISP2	20q13.12	ENSG00000064205	3.49E-37	-24.8654
ITLN2	1q23.3	ENSG00000158764	5.00E-19	-23.4193
MRC1	10p12.33	ENSG00000120586	1.51E-36	-22.8349
FXYD1	19q13.12	ENSG00000221857	1.55E-37	-22.0589
VSIG4	Xq12	ENSG00000155659	1.40E-29	-20.3516
HBB	11p15.4	ENSG00000223609	8.51E-27	-20.3464
TNNC1	3p21.1	ENSG00000114854	1.49E-25	-20.0629
DLC1	8p22	ENSG00000164741	8.38E-44	-19.5953
FCN1	9q34.3	ENSG00000085265	1.52E-34	-19.1559
ABCA8	17q24.2	ENSG00000141338	2.88E-46	-18.883
PGM5	9q21.11	ENSG00000154330	5.74E-44	-18.4629
SFTPA2	10q22.3	ENSG00000185303	4.16E-15	-18.4599
SFTA2	6p21.33	ENSG00000225454	9.37E-20	-18.445
CFD	19p13.3	ENSG00000197766	3.28E-27	-18.4153
GRINL1A	15q21.3	ENSG00000137878	1.17E-30	-17.7111
SGCA	17q21.33	ENSG00000108823	1.29E-29	-17.6202
CA4	17q23.1	ENSG00000167434	4.15E-25	-16.695
FABP4	8q21.13	ENSG00000170323	9.04E-10	-16.5943
C16orf89	16p13.3	ENSG00000153446	9.25E-24	-16.3112
NPR1	1q21.3	ENSG00000169418	1.27E-37	-16.2828
SDR	2q32.3	ENSG00000168497	1.21E-20	-15.9844
C4BPA	1q32.2	ENSG00000123838	2.12E-16	-15.971

adj.P.Val: adjusted P value; Lin FC: linear fold change; Mapping: Chromosomal gene location. Minus sign means down regulation

Table 5. Top upregulated genes in tumor invasion front compare to normal lung.

Symbol	Mapping	EnsEMBL.ID	adj.P.Val	Lin Fc
KRT6B	12q13.13	ENSG00000185479	4.30E-34	154.5645
KRT6A	12q13.13	ENSG00000205420	5.39E-31	137.1149
KRT17P1	17p11.2	ENSG00000186831	3.97E-25	118.3397
AC022596.6	17p11.2	ENSG00000226145	3.97E-20	113.5754
KRT17	17p11.2	ENSG00000231645	1.79E-25	108.6275
KRT17	17q21.2	ENSG00000128422	1.95E-24	97.00643
KRT16	17q21.2	ENSG00000186832	1.91E-25	84.18846
KRT15	17q21.2	ENSG00000171346	1.14E-23	70.93647
DSG3	18q12.1	ENSG00000134757	1.85E-24	60.50598
S100A2	1q21.3	ENSG00000196754	3.46E-21	53.6924
KRT14	17p11.2	ENSG00000226145	2.79E-14	49.67675
KRT5	12q13.13	ENSG00000186081	8.44E-25	46.63427
KRT16	17q21.2	ENSG00000214822	9.35E-17	44.66299
CKMT1B	15q15.3	ENSG00000237289	1.53E-35	44.03072
TRIM29	11q23.3	ENSG00000137699	1.95E-28	40.68923
KRT6C	12q13.13	ENSG00000170465	4.85E-17	39.26701
CALML3	10p15.1	ENSG00000178363	7.16E-22	38.40687
KRT13	17q21.2	ENSG00000171401	1.96E-17	38.1287
SPRR1A	1q21.3	ENSG00000169474	8.18E-16	36.85293
GPR87	3q25.1	ENSG00000138271	7.81E-27	36.34092
LGALS7B	19q13.2	ENSG00000178934	2.06E-15	35.20288
SERPINB5	18q21.33	ENSG00000206075	2.58E-27	28.43915
SOX2	3q26.33	ENSG00000181449	4.68E-20	28.00406
PTHLH	12p11.22	ENSG00000087494	2.73E-18	27.25168
AKR1B10	7q33	ENSG00000198074	2.53E-17	25.45017
SPRR2D	1q21.3	ENSG00000163216	9.56E-14	25.40704
DST	6p12.1	ENSG00000151914	1.75E-27	25.23768
FNTB	14q23.3	ENSG00000125954	2.03E-24	22.39549
SPRR2A	1q21.3	ENSG00000213166	8.45E-13	22.28788
VTCN1	1p13.1	ENSG00000134258	2.43E-18	21.21021
SPRR2A	1q21.3	ENSG00000213166	4.16E-13	20.66738
GJB5	1p34.3	ENSG00000189280	7.28E-29	20.16415
CLCA2	1p22.3	ENSG00000137975	1.29E-20	19.58683
ADH7	4q23	ENSG00000196344	3.21E-15	18.21506
COL17A1	10q25.1	ENSG00000065618	9.88E-14	18.13308
FAM83A	8q24.13	ENSG00000147689	3.37E-15	17.67467
AKR1C1	10p15.1	ENSG00000187134	7.47E-11	17.38196
ALDH3A1	17p11.2	ENSG00000108602	1.29E-11	17.09044

adj.P.Val: adjusted P value; Lin FC: linear fold change; Mapping: Chromosomal gene location.

Table 6. Top downregulated genes in tumor invasion front compare to normal lung.

Symbol	Mapping	EnsEMBL.ID	adj.P.Val	Lin Fc
AGER	6p21.32	ENSG00000204305	1.14E-29	-46.8989
MFAP4	17p11.2	ENSG00000166482	6.77E-43	-40.7799
INMT	7p14.3	ENSG00000106125	6.21E-37	-30.5934
FOSB	19q13.32	ENSG00000125740	6.9E-22	-23.7059
A2M	12p13.31	ENSG00000175899	6.2E-39	-22.6565
C7	5p13.1	ENSG00000112936	1.17E-30	-22.2781
WISP2	20q13.12	ENSG00000064205	8.79E-37	-21.3595
CLIC5	6p21.1	ENSG00000112782	7.64E-32	-21.1094
FXYD1	19q13.12	ENSG00000221857	5.37E-37	-18.9306
ITLN2	1q23.3	ENSG00000158764	3.66E-18	-18.7364
NR4A1	12q13.13	ENSG00000123358	1.83E-24	-17.2841
MRC1	10p12.33	ENSG00000120586	2.53E-34	-16.9544
PGC	6p21.1	ENSG00000096088	3.59E-21	-16.5795
DLC1	8p22	ENSG00000164741	6.77E-43	-16.3804
ICAM1	19p13.2	ENSG00000090339	5.51E-23	-16.3034
ABCA8	17q24.2	ENSG00000141338	5.64E-46	-16.2486
PGM5	9q21.11	ENSG00000154330	2.62E-43	-15.7244
FMO2	1q24.3	ENSG00000094963	5.32E-24	-15.5785
CA4	17q23.1	ENSG00000167434	2.89E-25	-15.5427
GRINL1A	15q21.3	ENSG00000137878	1.03E-29	-15.3252
HBB	11p15.4	ENSG00000223609	6.62E-25	-15.2867
C19orf59	19p13.2	ENSG00000183019	1.03E-16	-15.109
TNNC1	3p21.1	ENSG00000114854	1.34E-23	-14.9554
CXCL12	10q11.21	ENSG00000107562	1.75E-25	-14.8765
VSIG4	Xq12	ENSG00000155659	6.76E-27	-14.4312
CACNA2D2	3p21.31	ENSG00000007402	4.55E-20	-14.3696
ADH1B	4q23	ENSG00000196616	3.4E-13	-14.2711
SFTPC	8p21.3	ENSG00000168484	7.83E-10	-14.2423
FABP4	8q21.13	ENSG00000170323	2.21E-09	-14.2014
FBLN5	14q32.12	ENSG00000140092	3.12E-37	-13.9026
ZBTB16	11q23.2	ENSG00000109906	2E-26	-13.8517
DUSP1	5q35.1	ENSG00000120129	1.96E-30	-13.5759
F13A1	6p25.1	ENSG00000124491	6.15E-16	-13.3616
ANGPTL1	1q25.2	ENSG00000116194	1.27E-46	-13.1252
SFTA3	14q13.3	ENSG00000229415	1.69E-18	-12.8797
IL6	7p15.3	ENSG00000136244	1.21E-13	-12.8604
F13A1	6p25.1	ENSG00000124491	3.66E-23	-12.6628
SGCA	17q21.33	ENSG00000108823	1.44E-26	-12.348

adj.P.Val: adjusted P value; Lin FC: linear fold change; Mapping: Chromosomal gene location. Minus sign means down regulation

Table 7. Downregulated microRNAs in inner tumor cells.

microRNA	q.value	Fold Change
hsa-miR-190	0.009940101	-6.58953
hsa-miR-451	0.001457199	-6.17
hsa-let-7e	0.013974043	-5.62798
hsa-miR-135a	0.005724506	-4.29444
hsa-miR-194	0.045831708	-4.19197
hsa-miR-15a	0.020403062	-4.00488
hsa-miR-338	0.020538837	-3.9441
hsa-miR-125b	0.000988138	-3.89715
hsa-miR-143	0.002782112	-3.71458
hsa-miR-199b	0.011148548	-3.64453
hsa-miR-501	0.023413255	-3.56648
hsa-miR-30e-5p	0.001844947	-3.51801
hsa-miR-486	0.001457199	-3.3031
hsa-miR-565	0.020806392	-3.21053
hsa-miR-335	0.002511387	-3.0568
hsa-miR-133a	0.00168233	-2.79899
hsa-miR-195	0.001457199	-2.78938
hsa-miR-497	0.001599137	-2.54194
hsa-let-7c	0.001844947	-2.50758
hsa-miR-339	0.032638191	-2.49983
hsa-miR-23b	0.008995752	-2.49749
hsa-miR-101	0.002884265	-2.44876
hsa-miR-145	0.001457199	-2.37872
hsa-miR-134	0.045860635	-2.28879
hsa-miR-29a	0.001969757	-2.27967
hsa-miR-199a	0.019735528	-2.19765
hsa-miR-223	0.006086033	-2.18971
hsa-miR-142-5p	0.005133286	-2.18146
hsa-miR-199a	0.02429884	-2.12823
hsa-miR-99a	0.002515456	-2.09845
hsa-miR-30a-5p	0.005475354	-2.05929
hsa-miR-100	0.002511387	-2.03477
hsa-miR-192	0.013587897	-2.03461
hsa-miR-130a	0.009957273	-2.00025

Table 8. Downegulated microRNAs in tumor invasion front.

microRNA	q.value	Fold Change
hsa-let-7e	0.022512	-10.37096244
hsa-miR-190	0.043505	-8.052713881
hsa-miR-15a	0.02554	-7.045229688
hsa-miR-451	0.003718	-6.021546746
hsa-miR-501	0.023938	-5.52870941
hsa-miR-199b	0.017845	-5.351641225
hsa-miR-135a	0.011582	-5.331926504
hsa-miR-134	0.024891	-5.23701634
hsa-miR-125b	0.000332	-4.691462046
hsa-miR-143	0.009567	-3.78046963
hsa-miR-30e-5p	0.002753	-3.71462856
hsa-miR-199a	0.006856	-3.687690514
hsa-miR-486	0.001281	-3.23075016
hsa-miR-335	0.004593	-3.060529808
hsa-miR-23b	0.011016	-3.017293587
hsa-miR-195	0.000683	-2.964220227
hsa-let-7c	0.000566	-2.758378365
hsa-miR-145	0.000332	-2.707176583
hsa-miR-133a	0.002018	-2.70704494
hsa-miR-497	0.000631	-2.578576022
hsa-miR-130a	0.002018	-2.557047222
hsa-miR-101	0.002789	-2.522172459
hsa-miR-10a	0.002011	-2.472195003
hsa-miR-29a	0.000607	-2.417566908
hsa-miR-22	0.003202	-2.368991372
hsa-miR-99a	0.000332	-2.361222156
hsa-let-7f	0.024891	-2.263648988
hsa-miR-30a-5p	0.002819	-2.180092544
hsa-miR-99b	0.001078	-2.141361999
hsa-miR-125a	0.000332	-2.138887256
hsa-miR-100	0.000332	-2.127458597
hsa-miR-214	0.032308	-2.08985287
hsa-let-7a	0.006538	-2.058469683
hsa-miR-29c	0.002018	-2.039642777
hsa-let-7b	0.002011	-2.035463783
hsa-miR-218	0.003718	-2.018435681
hsa-miR-142-5p	0.026613	-2.017714222

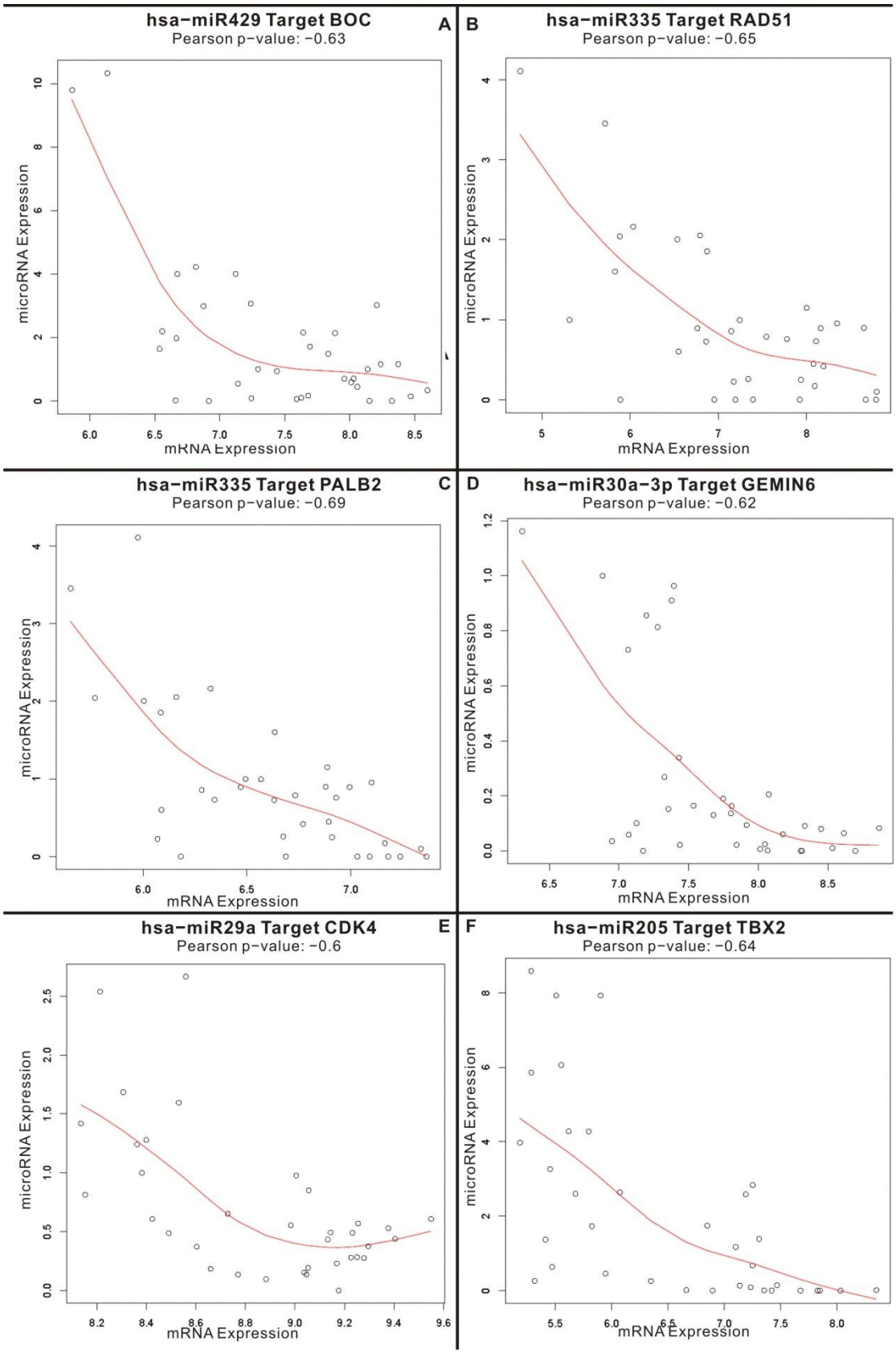
A
hsa−miR429 Target BOC
Pearson p−value: −0.63
microRNA Expression
mRNA Expression
B
hsa−miR335 Target RAD51
Pearson p−value: −0.65
microRNA Expression
mRNA Expression
C
hsa−miR335 Target PALB2
Pearson p−value: −0.69
microRNA Expression
mRNA Expression
D
hsa−miR30a−3p Target GEMIN6
Pearson p−value: −0.62
microRNA Expression
mRNA Expression
E
hsa−miR29a Target CDK4
Pearson p−value: −0.6
microRNA Expression
mRNA Expression
F
hsa−miR205 Target TBX2
Pearson p−value: −0.64
microRNA Expression
mRNA Expression

Figure 1.

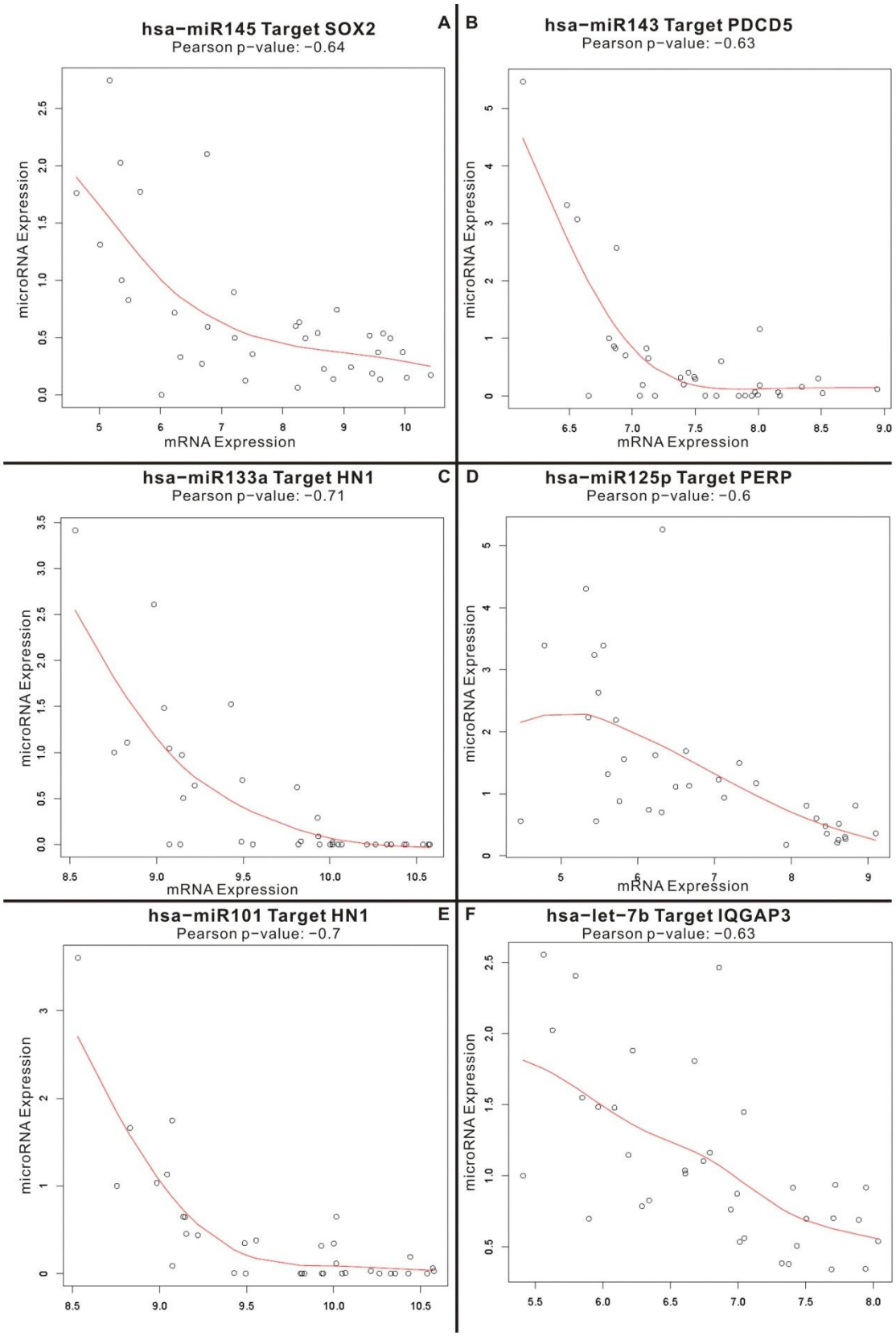
A
hsa-miR145 Target SOX2
Pearson p-value: -0.64
microRNA Expression
mRNA Expression
B
hsa-miR143 Target PDCD5
Pearson p-value: -0.63
microRNA Expression
mRNA Expression
C
hsa-miR133a Target HN1
Pearson p-value: -0.71
microRNA Expression
mRNA Expression
D
hsa-miR125p Target PERP
Pearson p-value: -0.6
microRNA Expression
mRNA Expression
E
hsa-miR101 Target HN1
Pearson p-value: -0.7
microRNA Expression
F
hsa-let-7b Target IQGAP3
Pearson p-value: -0.63
microRNA Expression

Publications

Article based on this dissertation

Wu H, Haag D, Muley T, Warth A, Zapatka M, Toedt G, Roger MA, Pscherer A, Joos S, Hahn M, Rieke RJ, Miester M, Schnabel P, Hoffmann H, Lichter P. Tumor-microenvironment interactions studied by zonal transcriptional profiling of squamous cell lung carcinoma. (In preparation)

Articles in addition to this dissertation

Liu HK, Belz T, Bock D, Takacs A, **Wu H**, Lichter P, Chai M, Schütz G. The nuclear receptor tailless is required for neurogenesis in the adult subventricular zone. *Genes Dev.* 2008;22(18):2473-8

Abba M, Laufs S, Aghajany M, **Wu H**, Korn B, Benner A, Allgayer H, Look who's talking: Decoding differentially regulated epithelial and stromal pathways in colorectal cancer. (In preparation)

Poster presentation and invited lecture

Wu H, Haag D, Muley T, Warth A, Zapatka M, Toedt G, Roger MA, Pscherer A, Joos S, Hahn M, Rieke RJ, Miester M, Schnabel P, Hoffmann H, Lichter P. Laser capture microdissection mediated expression analysis of tumour and tumour adjacent regions in squamous cell lung cancer. *Stem Cells, Tissue Homeostasis and Cancer,* EMBL Heidelberg, Germany, 12th-15th, May, 2010. (Poster presentation)

Wu H, Systems Study Lung Tumor Invasion by Novel Microgenomics Platform. *Carl Zeiss Workshop*, Bernried, Germany, 19th-20th, June, 2008. (Invited lecture)

Acknowledgements

I wish to thank Prof. Dr. Peter Lichter for the kind opportunity to perform my PhD project in his laboratory. I very much appreciated his thoughtful supervision and the continuous support during my PhD study. Without his nice invitation from Beijing in 2004, I would not have come to this beautiful country and city to pursue my PhD study.

I would like to thank Dr. Karsten Rippe and Prof. Dr. Peter Lichter for the evaluation of my thesis.

I would like to thank my supervisors Prof. Dr. Stefan Joos, Dr. Armin Pscherer and PD. Dr. Michael A. Rogers. Thanks for the detailed and outstanding supervision during my PhD research.

I would like to thank all members of the gene expression group. Daniel Haag for his full support on RNA amplification, microarray technique, bioinformatics and many beneficial discussions during my PhD study, and to Karin Pfleger for the excellent experimental support.

Especially, I would like to thank Dr. Marc Zapatka and Grischa Toedt for excellent bioinformatic support on mass microarray data analysis. In addition, I appreciated very much the technical support from Hsing Chen Bai on microRNA FISH and Frauke Devens on immunohisrochemisry.

Finally, I would like to thank to all B060ers!